Faculty of Bioscience Engineering

Academic year 2015 – 2016

Risk Analysis and Spatio-Temporal Modeling of Wildfires in Belgium

Arthur Depicker
Supervisors: Prof. dr. Bernard De Baets and dr. ir. Jan Baetens

Master thesis submitted in fulfillment of the requirements for the degree of
Master of Science in Bioscience engineering: Forest and Nature Conservation

Ghent, June 2016

The promoters, The author,

Prof. dr. Bernard De Baets dr. ir. Jan Baetens Arthur Depicker

Dankwoord

Het lijkt moeilijk te bevatten dat dit moment, waarnaar ik sinds het eerste bachelorjaar reikhalzend heb uitgekeken, aanbreekt. Alle blok- en buisvakken en maandenlange studeermarathons in winter of zomer zijn nog slechts vage herinneringen die de gedachten niet meer kunnen verontrusten. Tegenover deze 'kwellingen' stonden natuurlijk ook talrijke geneugten: beloftevolle vriendschappen, Afrikaanse avonturen maar ook tal van plezante uitstappen in de Belgische bossen, het eerste echte (en huidige!) lief en – laat ons eerlijk zijn – het totale gebrek aan al die verantwoordelijkheden waarvan het 'volwassen leven' gespijsd is.

Deze thesis is – of dat was toch de bedoeling – de bekroning van de vijf jaren aan het boerekot. De totstandkoming ervan is echter geen individuele verwezenlijking, maar het resultaat van een intensieve samenwerking met Dr. Jan Baetens en Prof. De Baets. Zoals de titel van dit stukje reeds verraden heeft, vallen hen dus enkele dankuitingen te beurt. Allereerst wil ik Dr. Baetens bedanken voor de wekelijkse samenkomsten, constructieve discussies, intellectuele hulp en ettelijke revisies die dit werk mee hebben helpen vormen. Mijn dank gaat ook uit naar Prof. De Baets, die met een nietsontziende blik de thesis in een definitieve plooi heeft gelegd.

Bedankt ook aan dat ene meisje dat op woensdag 14 november, 2012, aan het dansen was in de Cuba Libre (en haar oog op mij liet vallen).

Abstract

This thesis aims to gain a better understanding of the phenomenon of wildfires in Belgium. The impact of wildfires seems rather limited. Nevertheless, because of global warming and an increasing pressure on the withering nature, the Directorate-General of the Federal Public Service Internal Affairs expressed the need for a scientifically based wildfire risk map. This way, the available resources can be distributed more efficiently. In order to aid the fire suppression itself, several wildfire spread models are useful. Thus two objectives for this thesis are set. The first is to develop a wildfire risk map for the Belgian territory, using data on historical wildfire events. Several approaches are used to construct this risk map, leading to different results which are compared and discussed accordingly. The second goal is to enable simulations of the wildfire spread in the case of the vast wildfire in Baelen, Belgium, 2011. Two models are used for this purpose, the renowned Fire Area Simulator (FARSITE) and a cellular automaton.

Samenvatting

Deze masterproef heeft als doel meer inzicht te krijgen in natuurbranden die voorkomen in België. De impact van dit fenomeen lijkt in eerste instantie eerder beperkt, maar in het licht van de klimaatverandering en de stijgende druk op de slinkende natuur, ontstond vanuit het Crisiscentrum van de Federale Overheidsdienst Binnenlandse Zaken de behoefte naar een wetenschappelijk onderbouwde risicokaart. Aan de hand van deze kaart kunnen de beschikbare middelen op een meer efficiënte manier verdeeld worden over het hele land. Voor de bestrijding van de natuurbranden zelf, worden een aantal brandverspreidingsmodellen opgesteld. Samengevat heeft deze thesis dus twee objectieven. Ten eerste wordt er aan de hand van de data van historische branden een risicokaart ontworpen voor België. De constructie van deze kaart wordt op meerdere manieren aangepakt, waarna de verschillende resultaten vergeleken en besproken worden. Het tweede objectief is het simuleren van de natuurbrand te Baelen, België, 2011. Hiervoor werden twee modellen aangewend, het internationaal geprezen FARSITE (Fire Area Simulator) en een cellulaire automaat.

Contents

Glossary

α	parameter in the transition function of the model proposed by Alexandridis et al. (2008)
β_{op}	optimum packing ratio of the fuel bed
β_r	packing ratio of the fuel bed
β	weighing coefficient of the predictors in the logistic regression equation
C_i	event of encountering a certain environment, characterized by slope and vegetation
l_{crown}	crown bulk density
δ	perturbation
E_0	critical energy flux
E_1	height of a cell in a CA-based model
E_2	height of a neighboring cell in a CA-based model
E_{actual}	actual energy flux
E_{co}	relative number of false positives
E_i	fraction of the rate of spread in the direction of the fire propagation in the vertex and the rate of spread in the maximum spread direction
E_{om}	relative number of false negatives
ϵ_h	effective heating number
ϵ	number of time steps a cell can burn
F	transition function of a cellular automaton
F_t	fraction of trees that take part in the crown fire phase

Φ_s	dimensionless coefficient for slope
Φ_w	dimensionless coefficient for wind
γ	parameter in the transition function of the improved CA-based model
H	head-to-back ratio of the fire ellipse
h_{base}	crown base height
h_{crown}	crown height
I_0	fire line intensity threshold value for crown fire initiation
I_b	fire line intensity
I_c	active crown fire intensity
I_R	reaction intensity
I	event of an ignition
L	length-to-width ratio of the fire ellipse
l	width of a cell
M	crown foliar moisture content
N	neighborhood of a cell in a cellular automaton
ν_1	correction factor for the wind in the transition function of the improved CA-based model
ν_2	correction factor for the slope in the transition function of the improved CA-based model
O	output function of a simulation of the CA-based model with modified transition function
Ω	objective function of the hill climbing algorithm
P_i^T	the probability that a cell will burn during the next time step in the improved CA-based model
P_{ignition}	probability that a wildfire will occur, calculated with a logistic regression equation
$\tilde{P}$	the probability that a cell will be ignited by one of its neighbor cells in the improved CA-based model

p_{burn}	the probability that a cell will be ignited by one of its neighbor cells in the model proposed by Alexandridis et al. (2008)
p_d	fire propagation probability, depending on the vegetation density, in the model proposed by Alexandridis et al. (2008)
p_h	the probability that a burning cell will pass a wildfire onto an adjacent, unburning cell, given a certain type of vegetation and no wind or slope
p_s	fire propagation probability, depending on the slope, in the model proposed by Alexandridis et al. (2008)
p_{total}	the probability that a cell will burn during the next time step, in the model proposed by Alexandridis et al. (2008)
p_{veg}	correction factor for the vegetation in the transition function of the improved CA-based model
p_v	fire propagation probability, depending on the vegetation type, in the model proposed by Alexandridis et al. (2008)
p_w	fire propagation probability, depending on the wind, in the model proposed by Alexandridis et al. (2008)
Q_{ig}	heat of pre-ignition
R_0	critical surface fire spread rate
R_{10}	forward surface fire rate of spread from model 10 of Anderson's fuel model, using a 0.4 wind reduction factor
$\tilde{R}_{\text{active}}$	actual active crown fire spread rate
R_{active}	active crown fire spread rate
R_{max}	maximal rate of spread
ρ_b	oven dry bulk density
R	rate of spread
$\tilde{S}(c_i, t)$	the simulated state of cell c_i at time t
$\breve{S}$	backward finite difference
S_i	Sobol' index
$\dot{S}$	forward finite difference
S	state set of a cellular automaton
σ	surface area to volume ratio of the fuel bed
θ_s	slope (radians)

θ angle between the wind direction and subtracted from angle between the neighboring cells (radians)

$\tilde{U}$ virtual windspeed

U midflame windspeed

V windspeed

X multidimensional cellular automaton space

ξ propagation flux ratio

x predictor in the logistic regression equation

Acronyms

BUI	Buildup Index
CA	Cellular Automaton
CBFiM	Community-Based Fire Management
CFFP	Cooperative Forest Fire Prevention
DC	Drought Code
DMC	Duff Moisture Code
DTM	Digital Terrain Model
EFFIS	European Forest Fire Information System
FARSITE	Fire Area Simulator
FBP	Canadian Forest Fire Behavior Prediction
FDRS	Fire Danger Rating System
FFMC	Fine Fuel Moisture Code
FWI	Canadian Forest Fire Weather Index
Global EWS-Fire	Global Early Warning System for Wildfires
IdE	Integro-Difference Equation
ISI	Initial Spread Index
MAE	Mean Absolute Error
NGI	National Geographic Institute

ODE Ordinary Differential Equation

PAH Polycyclic Aromatic Hydrocarbon
PDE Partial Differential Equation
PdE Partial Difference equation

RIN Risico-Index Natuurbranden
RIW Risk Index for Wildfires
ROS Rate Of Spread

SA Sensitivity Analysis
STM Spatio-Temporal Model

WUI Wildland Urban Interface

List of Figures

List of Tables

CHAPTER 1

Introduction

Wildfires impact many regions in the world and can have devastating effects on humans and nature. Because of global warming and the accumulation of fuel due to aggressive fire suppression strategies, the occurrence of wildfires is rising. This accumulation is associated with higher damage costs, degradation of nature, and even the loss of human lives. Therefore, it is important to study this phenomenon and to combat the different underlying causes.

In 2011, a series of wildfires destroyed almost 2200 ha of nature in Belgium. A great deal of this area was located within protected NATURA 2000 sites. In order to avoid or limit the wildfire damage in the future, the Directorate-General of the Federal Public Service Internal Affairs proposed the National Action Plan Wildfires. One component of this plan concerns a wildfire risk analysis of the Belgium territory, in other words, the development of a scientifically underpinned wildfire risk map. Chapter 3 in this thesis aims to provide such a map by applying three different methods. Firstly, an expert system derived from the Dutch Risk Index for Wildfires is used to derive a score, proportional to the probability of a wildfire ignition. Secondly, Bayes' theorem is applied to construct a risk map. The theorem is used to calculate the probability that a wildfire ignition will take place on an area of 1 ha during one year. Thirdly, in agreement with Catry et al. (2009), a logistic regression equation is constructed to assess the wildfire ignition probability. In the final section of Chapter 3, the advantages and disadvantages of these three methods are compared to each other. Finally, some recommendations are given for future data collection.

Not only the risk assessment is an important aspect of wildfire management, but also the insight into wildfire dynamics. Through predictions thereof, emergency services are better prepared to the task of fire suppression. A commonly used method to gain such insight, is by means of simulations with dedicated spatio-temporal models. In this thesis, two models are used: FARSITE and a CA-based model. The former model is a renowned wildfire model, developed by Finney (2004) for the USDA Forestry Service. After a short introduction on the

mechanics behind this model, the predictive power of FARSITE is tested on a case study of the great wildfire in Baelen, Belgium, 2011. The latter model was proposed by Alexandridis et al. (2008). This model is used for the same case study. Yet, it turns out that this model contains several flaws. Hence, a new CA-based model is proposed and applied on the aforementioned case study. Finally, a sensitivity analysis is performed for this model, in order to gain insight in the relative importance of the model parameters and the model structure.

Figure 1.1: Wildfire in Yosemite National Park, September 8, 2014. Photo by Stuart Palley (Worland, 2015).

CHAPTER 2

The Concept of Wildfires

Although wildfires may have a negative connotation, they do not necessarily have a negative impact on the environment. In some regions, such as the Mediterranean, they occur frequently and help shape the ecosystems (Keeley et al., 2011). Because of their associated risk for humans and increasing frequency, however, it is necessary to understand and describe the physics behind wildfires in order to reduce the negative effects and anticipate disasters. In this section, the nature of wildfires will be discussed. Next, the impact and management of wildfires on a global, European and Belgian level will be elaborated upon. Finally, a short introduction on spatio-temporal models, which are frequently used for wildfire simulations, is given.

2.1 Description

Papadopoulos (2011) defines a wildfire as the complicated combination of energy released (in the form of heat) in the process of combustion and the transport of that energy to surrounding unburnt fuel and the subsequent ignition of that fuel. Combustion is a chemical process, transport of energy is a physical one. Whelan (1995) adds to this definition that a wildfire is beyond any human control. This is a relevant distinction since many fires are deliberately lit as a management practice and kept under control. In Africa, for example, fire is an indispensable tool for farmers to hold back the forest or for children to chase away spiders and snakes (Schmitz et al., 1996). In general, there are four major ignition causes: arsons (intentionally and illegally ignited fires), accidents, lightning and out-of-control management fires (Whelan, 1995).

2.1.1 Combustion

In wildfire events, the combustion of biomass (hence referred to as fuel) takes place. The combustion is a mass and energy conversion process during which chemical bond energy is

transformed into thermal energy. The fuel reacts with the oxygen in the air to form products, such as carbon dioxide and water, which have a lower enthalpy of formation or reference enthalpy than the reactants (Peters, 2010). Three stages can be distinguished in the process of combustion. First, the fuel is preheated, dried and partly pyrolysed. Pyrolysis is a chemical reaction that transforms the fuel into gases such as water vapor, carbon dioxide and combustable gases like methane, hydrogen and methanol. The second phase is the flaming combustion caused by the ignition of inflammable gases. Thirdly, glowing combustion takes place. This is the burning of the remaining charcoal, resulting in ash (Whelan, 1995). Wildfires burn with so-called diffusion flames that are sustained by a positive feedback mechanism (Figure 2.1). When the combustable gases ignite, heat is produced, which will increase pyrolysis and the emission of more combustable gases (Johnson and Miyanishi, 2001).

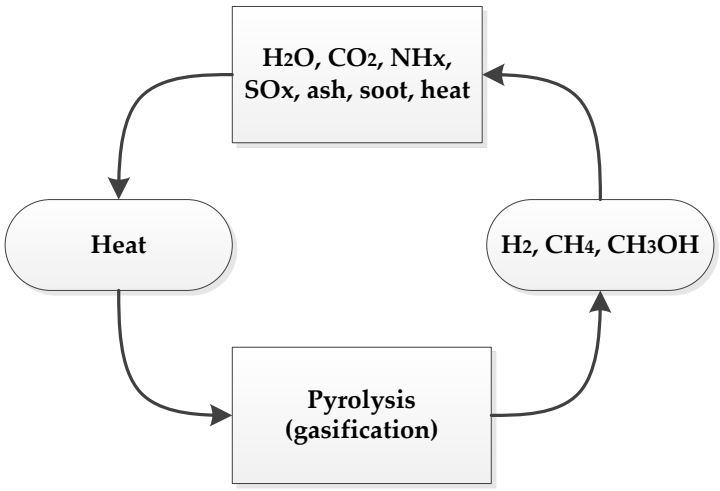

Figure 2.1: The positive feedback mechanism that sustains diffusion flames (Johnson and Miyanishi, 2001).

Biomass has a complex composition with lignin and cellulose as main components. Nonetheless, the proportion of carbon, hydrogen and oxygen in wood is approximately $C_6H_9O_4$. Overall, the combustion process can be described by Eq. 2.1 (Byram, 1959):

$$4\,C_6H_9O_4 + 25\,O_2 + [0.322M\,H_2O + 94.0\,N_2] \rightarrow 18\,H_2O + 24\,CO_2 + [0.322M\,H_2O + 94.0\,N_2] + 11.6\times10^9 J, \tag{2.1}$$

where M is the $\%_m$ of moisture in the Forrest fuel. This moisture is chemically inert, idem for the atmospheric N_2. These last two molecules are displayed between brackets because they do not take part in the reaction. The last term in the equation is the generated heat (Byram, 1959). Apart from the heat, the combustion also generates smoke and ash. The composition of the ash is dominated by SiO_2 and CaO, but also contains Mg, Al, K and P oxides (Nunes et al., 2016) while the smoke contains water, NO_x, SO_x and CO_2. If the combustion is

incomplete (if the O_2 supply is lacking), soot is formed, consisting of Polycyclic Aromatic Hydrocarbons (PAHs) and other hydrocarbons (de Bree, 2009). The soot influences human health and climate. The health hazard is caused by small particles ($< 2\,\mu m$) accompanied by phenols and other poly-aromatic compounds that are carcinogenic. The effects of soot on the climate are caused by the absorbtion of heat in the atmosphere and the reduction of the albedo of snow when deposited on the surface (Lea-Langton et al., 2015). The emission of CO_2 is also affecting global change, although it is part of the global carbon cycle, and will be partially reabsorbed by the biosphere (Andreae, 2004; Ehlers et al., 2006).

2.1.2 Phenomenology of Wildfires, after den Ouden et al. (2010)

Surface Fire

A surface or crawling fire is a fire that advances relatively slowly on ground level. It consumes grasses, herbs, mosses and humus. It can damage the stem base and roots of trees. In the presence of bushes and young trees, the fire can use these woody elements as a ladder to reach the canopy, as such initiating crown fires. A surface fire is relatively easy to extinguish, either at ground level or using aerial means.

Crown Fire

A crown fire is very intense and spreads rapidly throughout the canopy of the forest. In the temperate European climate, they only occur in coniferous forests and are very hard to suppress. The fire is not accessible from the ground and new fires can arise several meters ahead of the fire front. Airborne assistance is crucial to moisten the canopy and prevent ignition of the canopy. Because of the enormous heat release, fire fighters cannot approach, so the fire suppression is often concentrated to residential areas to restrict damage. Another way of fighting the flames is by removing the fuel by small, controlled fires. Spotting occurs if strong wind is present. Burning and glowing plant material is then blown away and can land hundreds of meters - even kilometers ahead of the fire front, causing new wildfires (Alexandridis et al., 2008).

Ground Fire

A ground fire spreads subterranean and consumes organic matter, mostly peat, but occasionally thick humus layers. The seed bank and underground plant parts are destroyed, allowing colonization by species that originate elsewhere. The peat ground fires are very hard to battle and can last for months. To suppress this fire, the soil must be moistened. Alternatively, the peat is dug up and removed to stop the fire front.

2.2 Prevalence

2.2.1 Global

Wildfires consume annually not less than 9200 million tons of biomass (Andreae, 2004), corresponding with hundreds of millions hectares of grass land, savannah, forests and other kinds of vegetation. The associated damage cost can run over billions of US dollar (US$). An example of the direct costs is the annual loss of US$0.5-1 billion of commercial wood in North East Asia (de Groot et al., 2006). A famous example of the devastating powers of wildfires are the Yellowstone fires in 1988. The flames consumed 0.524 million hectares and the suppression cost ran up to US$120 million (National Park Service, 2008). One can distinguish four types of costs: direct costs like suppression costs, rehabilitation costs to restore the vegetation, indirect costs like the decline of sales, and finally additional costs, for example the loss of civilian lives (Dale, 2009). As a consequence of the lack of an internationally accepted method to assess the damage, it is hard to determine the global cost accurately (Benndorf et al., 2007). It is anticipated that the damage and costs associated with wildfires will rise. In the United States, for instance, the annual wildfire appropriations have almost tripled in the last two decades, from an average US$1.39 billion per year for the period 1991 – 1999 to an average US$3.51billion per year for the period 2002 – 2012 (Gorte, 2013). Gorte (2013) also states that the increasing severity of wildfires is caused by two factors. First, the availability of fuel has risen, following the aggressive fire suppression policy that eliminates low-intensity fires that reduce the amount of biomass. Second, the changing climate is causing higher temperatures, droughts, and so on. The sensitivity for wildfires is expected to increase most in areas like the boreal forests of Canada and Siberia and the moist tropical forests in the Amazone basin and south of Indonesia (Bedia et al., 2015). As wildfires might occur more frequently, the soil hydrology and atmospheric moisture content can be altered. Also, the nutrient potential will decrease due to erosion and the burning of organic matter in the top soil. Finally, an increased wildfire frequency will contribute to global change (Goldammer, 1990), thus enforcing the driving factor that leads to more fires.

2.2.2 Europe

Every year, approximately 65 000 fires take place on the European continent, destroying on average 500 000 ha (San-Miguel-Ayanz et al., 2012). The fire season in Europe generally spurs from March to October when the atmospheric conditions are warm and dry (Schmuck et al., 2014). The Mediterranean region is by far the most vulnerable. Portugal, Spain, France, Italy and Greece are responsible for 85% of the recorded fires, which are arsons in most cases, though the number of fires due to negligence is increasing. (Ganteaume et al., 2013). Natural fires do not happen frequently, as they only represent 5% of all ignitions (San-

Miguel-Ayanz et al., 2012). Nevertheless, the ecosystem is shaped by the antropogeneous fire regime. Most fires take place in the Wildland Urban Interface (WUI), the borderline between urban areas and agricultural land and/or abandoned areas (Fiorucci et al., 2004). In the Fenno-Scandinavian region, dominated by coniferous forests, on the one hand, wildfires are considered a part of the forest dynamics, as the main driving force for succession (this is also the case for the forests in North America)(Goldammer, 1990). In Central Europe, on the other hand, the perception of wildfires is different and its ecological role is less accredited and less studied (Adámek et al., 2015). The reasons why coniferous forests are much more sensitive to forest fires than deciduous forests are the large amount of sap in the branches, the higher number of trees per hectare (Alberta Government, 2012) and the so called ladder-effect whereby dead branches provide a mean for ground fires to evolve to crown fires (Alexander, 1988).

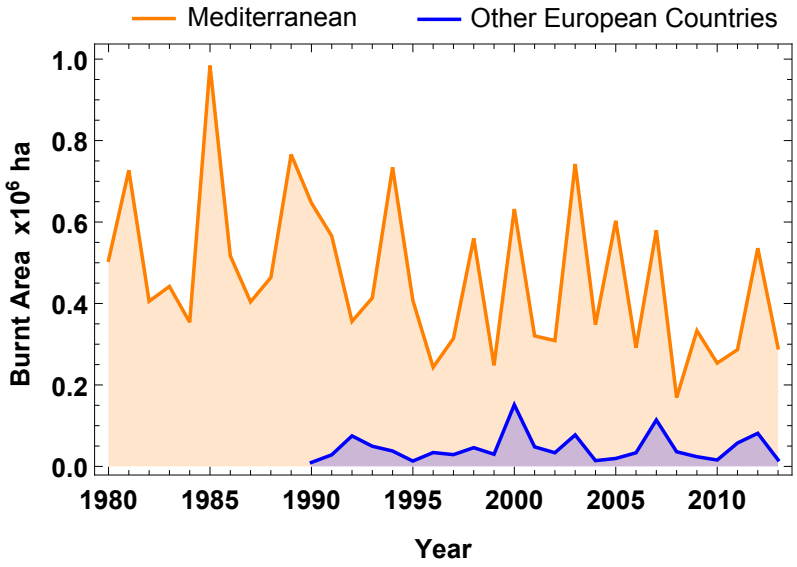

Figure 2.2: The total burnt area in the Mediterranean region (Portugal, Spain, France, Italy and Greece) and the rest of Europe (Austria, Bulgaria, Croatia, Cyprus, Czech Republic, Estonia, Finland, Germany, Hungary, Latvia, Lithuania, Macedonia, Poland, Romania, Slovakia, Sweden and Switzerland)(Schmuck et al., 2014).

2.3 Management

Considering the ongoing global warming and the vast impact of wildfires on human lives, property, and economy, it is clear that there is a growing need for cooperation on the national and international level to improve the prevention, detection and suppression of wildfires, but also the exchange of information (Global Fire Monitoring Center, 2006). In this section, a

number of these initiatives at global, European and national level are presented (Table 2.1). Since most of the systems are still under development, the year of initiation of the initiative is given in the table.

Table 2.1: Initiatives for the risk and damage assessment and prevention of wildfires on different scales.

Scale	Risk assessment	Year	Initiator
Global	Global EWS-Fire	2006	i.a. GOFC-GOLD
Europe	EFFIS Danger Forecast	1998	European Commission
National	Forest Fire Weather Index	1968	Canadian Forestry Service
	Damage assessment		
Europe	EFFIS Rapid Damage Assessment	1998	European Commission
	Prevention		
Global	Community-based fire management	2000	FAO
National	Cooperative Forest Fire Prevention	1942	USDA Forest Service

2.3.1 Risk Assessment

Two different types of risk assessments can be distinguished, namely *static* and *dynamic* hazard assessment. The first one is determined by means of topography, land use, climate, the average fuel condition, and data on prior wildfires in the region at stake. This type of assessment provides information for land use planning and the location of resources. Dynamic hazard assessment is based on real-time information, e.g. meteorological forecasts and the vegetation condition and is also referred to as a Fire Danger Rating System (FDRS). The goal of such an assessment is to identify the areas with the highest wildfire risk in order to send out patrols and take preemptive action, like alerting local authorities and prohibiting agricultural practices like stub burning (Fiorucci et al., 2004). Hence, three groups of parameters are proposed by the European Union's Joint Research Center (EU Joint Research Center, 2002; Adab et al., 2011):

1. *Structural or long-term parameters*: topography, vegetation type, land-cover and -use, slope, aspect, proximity of urban areas, population density, climate and soil.

2. *Dynamic or short-term parameters*: vegetation and weather condition.

3. *Integrated or Advanced parameters*: these indices combine both structural and dynamic parameters.

An FDRS integrates the effects of current and expected states of the involved parameters into one or more qualitative or numerical indices that reflect an area's protection needs. The three most important parameters are topography, fuel and weather. The rating can be done for the current period, but if predictions are available for the aforementioned parameters, a forecast of the wildfire risk can be made (National Wildfire Coordinating Group, 2002).

Many countries already developed a national fire danger rating system (de Groot et al., 2006) and the selected parameters differ across the systems. For example, the FDRS for the Netherlands, called the Risico-Index Natuurbranden (RIN) or Risk Index for Wildfires (RIW), does not only take topography, fuel, and weather into account, but also elements like the ecological value of the land and the presence of valuable objects (Verboom et al., 2013). This FDRS not only gives an indication of the ignition of wildfires, but also of the possible damage the fire can cause (see Section 3.1). In literature, different methods for conducting risk assessment can be found (Table 2.2). Examples are expert systems like the RIN and logistic regression equations, which will be explained in detail in Section 3.3. When large datasets are available, machine learning algorithms can be applied. Some examples are Random Forests, Maximum Entropy, Boosting Regression Trees, and Support Vector Machines (Massada et al., 2012; Rodrigues and de la Riva, 2014). Three initiatives to construct a risk map at the international, European and national level are discussed below.

Table 2.2: Methods for Risk Assessment

Technique	**Author**
Expert Systems	Verboom et al. (2013)
Logistic Regression	Preisler et al. (2004)
	Amatulli et al. (2006)
	Martinez et al. (2008)
	Catry et al. (2009)
	del Hoyo et al. (2011)
Machine Learning	Massada et al. (2012)
	Rodrigues and de la Riva (2014)

Global Early Warning System for Wildland Fire

The Global Early Warning System for Wildfires (Global EWS-Fire) is part of the *Strategy to Enhance International Cooperation in Fire Management* from the FAO (Global Fire Monitoring Center, 2006). It displays the fire danger accros the globe (Figure 2.3) and is based on the Canadian Forest Fire Weather Index (see Section 2.3.1). Forecasts of one month are possible

by relying on data that are provided by the NCEP Global Forecast System. The system is still under development in the sense that regional calibration concerning the real fire danger still has to be done (Global Fire Monitoring Center, 2015a). The objectives of the Global EWS-Fire are threefold. First, the goal is to obtain longer-term predictions for fire danger. Secondly, the predictions should encourage international fire management cooperation like resource-sharing, and finally the Global EWS-Fire provides a fire danger rating system for those countries that do not have their own national rating system (Global Fire Monitoring Center, 2015b).

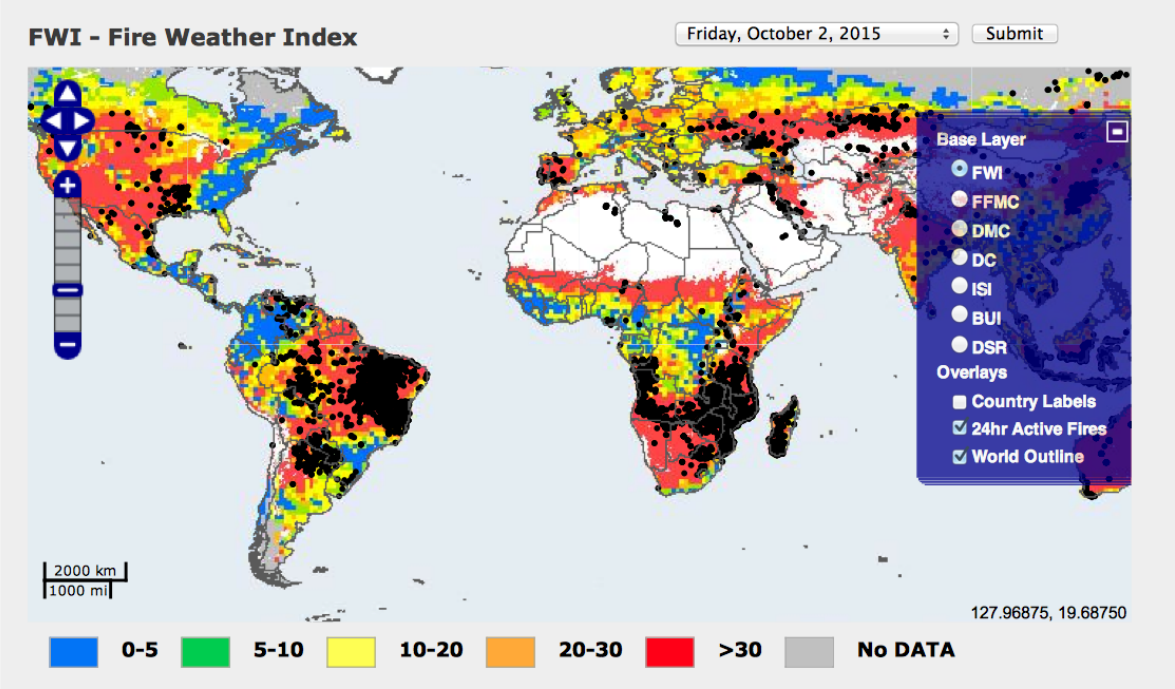

Figure 2.3: Screenshot from the Global EWS-Fire danger rating for the 2nd of October, 2015 (`http://www.fire.uni-freiburg.de/gwfews/forecast_ews.html`).

EFFIS Danger Forecast

The EFFIS Danger Forecast was has been under development by the European Forest Fire Information System (EFFIS) and was initiated in 1998. EFFIS was established by the European Commission, the EU Member States and other European countries. It aims at supporting national fire protecting services. Its Danger Forecast Module also uses the Canadian Fire Weather Index to predict ignition probability (Schmuck et al., 2014). Forecasts of six days are possible (San-Miguel-Ayanz and Camia, 2012).

Forest Fire Weather Index

The Canadian Forest Fire Weather Index (FWI) is Canada's national FDRS. It is one of the two current subsystems of the Canadian Forest Fire Danger Rating System that has been under developedment since 1968, mainly by the Canadian Forestry Service. The second subsystem is the Canadian Forest Fire Behavior Prediction (FBP) System (Van Wagner, 1987). The former subsystem deals with the influence of the weather on fuels and fires, while the latter accounts for the effects of topography and fuels. The FWI system calculates three fuel moisture codes, the Drought Code (DC), the Duff Moisture Code (DMC) and the Fine Fuel Moisture Code (FFMC). These fuel moisture codes are used to determine two fire behavioral indices, namely the Initial Spread Index (ISI) and the Buildup Index (BUI), which are on their turn used to determine the FWI (De Groot, 1998). The FBP System quantitatively estimates the fire spread rate, fuel consumption and fire intensity (Van Wagner, 1987).

2.3.2 Damage Assessment

EFFIS Rapid Damage Assessment

This module of EFFIS assesses the wildfire damage for all European countries. To determine the total burnt area, MODIS satellite imagery is used. Allas, only fires larger than 40 hectares are mapped, so many fires are not incorporated in the statistics. Historical data, however, have revealed that the burnt area from fires larger than 40 hectares accounts for 75% of the total burnt area (Schmuck et al., 2014).

2.3.3 Prevention

Community-Based Fire Management

Ganz et al. (2003) define Community-Based Fire Management (CBFiM) as a type of land and forest management in which a local resident community (with or without the collaboration of other stakeholders) is involved in deciding the objectives and practices for the prevention, control, or use of fires. The motivation for CBFiM is self-preservation, the restriction of economical damage. Such programs are very popular in developing countries as the social involvement is bigger in these regions. After all, the involved communities have a lot to lose and often cannot rely on stable governments when a disaster strikes (Benndorf et al., 2007; FAO, 2003).

Cooperative Forest Fire Prevention

Wildfires in the United States are responsible for burning approximately between 2.5 and 3 million ha annually (Ehlers et al., 2006). Nine out of ten of these wildfires are lit by humans. In 1942, after a Japanese shell attack near Los Padres National Forest in California, a growing awareness led the USDA Forest Service to initiate the campaign entitled Cooperative Forest Fire Prevention (CFFP). The symbol of this campaign, Smokey the Bear, was introduced in 1944. The CFFP mainly aims at instructing people how to pick a safe campfire spot, how to extinguish them safely and how to protect houses against wildfires (National Association of State Foresters, 2015).

2.4 Wildfires in Belgium

In this section, the history of wildfires is assessed. The earliest valuable records, i.e. those with an accurate description, date from 1911 and can be retrieved in digitized newspapers. Between 1950 and 1995, these newspapers were not available in digital format, therefore, no assessment of the wildfire events in this period could be made. From 1995 on, the news is published on the internet, facilitating the assessment. In this section, the Belgian wildfire seasons and management will also be discussed.

2.4.1 Wildfires between 1911 – 1950

The data for this period of time were collected through consultation of digitized newspapers in the Royal Library of Belgium, Brussels. The following newspapers were browsed: *L'Avenir du Luxembourgh* (1899 – 1950), *La Cité Nouvelle* (1937 – 1947), *Le Messager de Gand* (1832 – 1856), *L'Echo du Parlement* (1858 – 1885), *Le Bien Public* (1853 – 1914), *Le Courrier de l'Escaut* (1846 – 1950) and *Gazet van Antwerpen* (1911 – 1950). Thanks to these sources, it is possible to gain insight into the history of wildfires in Belgium.

In the beginning of the 20^{th} century, it was still common practice for farmers to burn heathland in order to increase the fertility of the soil (Anonymous, 1911). In some occasions, this could lead to enormous wildfires with long-lasting consequences. For instance, on April 9, 1909, a forester named Geebelen was ordered by the authorities to set fire on the heathland between Dilzen and Stokkem. The events had an unfortunate twist, as the wind direction suddenly changed, burning thousands of hectares of forests (Anonymous, 1913). Another cause of ignition were the embers produced by braking steam locomotives (Anonymous, 1927). Military exercises were also linked to a higher ignition risk due to exploding ammunition or hot shells (Anonymous, 1933). To this day, exercises of this kind still have a hand in enlighting wildfires on heathland. Besides these factors, negligence (mostly by careless smokers) and

malice were major ignition causes. In this time period, the suppression of the fire was not only done by firefighters, but also by the military and volunteers from the neighborhood. The costs could run up to several thousands of francs, for example 30 000 francs in the Geebelen case – the average annual salary for the working class was about 1000 francs (Scholliers and Zamagni, 1995).

In total, the date of 371 wildfires was registered. The geographical coordinates of these wildfires was not relevant since these data can not be used for the risk analysis. The reason for this is that the events took place a long time ago, and there have been many changes in land use and land cover since then.

2.4.2 Wildfires between 1995 – 2015

Data on wildfires during this period were gathered in two ways. Firstly, a list of all wildfires between 2010 and 2013 was provided by the Directorate-General of the Federal Public Service Internal Affairs. Secondly, the digital archives of the following newspapers were searched: *Gazet van Antwerpen*, *Het Belang van Limburg*, *Le Soir*, *L'Echo*, *La Dernière Heure*, *La Meuse*, *La Nouvelle Gazet*, *Metro* and *L'Avenir*. When possible, the exact location of each wildfire was recorded, so these data are useful for the static hazard assessment in chapter 3. The research learned that cigarettes, arsons and military exercises were again major drivers of ignition, but even pieces of glass can trigger a fire through redirection and focusing of sunlight (Timperman and Willekens, 1999). The practice of burning heathland nowadays aims to counteract atmospheric eutrophication due to farming and traffic exhaust gasses. It is, however, rarely done and solely on a small scale (< 1 ha) (Anonymous, 2011). An alternative to burning is the removal of dead branches and thicket (Coenen, 1999).

One of the most vulnerable regions is the *Kalmthoutse Heide*, a nature reserve at the Dutch border that is part of the transnational park *De Zoom-Kalmthoutse Heide* with a total area of 6000 hectares (ANB, 2015). It is part of the NATURA 2000 network and contains vegetation types like heathland, coniferous forests and fens (Van Eeckhoutte, 2012). The effect of wildfires on biodiversity is ambiguous. Species like the smooth snake (*Coronella austriaca*) are affected negatively because of habitat destruction, but a lot of pioneer species like the woodlark (*Lullula arborea*) thrive well in this regime (Wyckmans et al., 2011; Jacobs, 2013). Another fire-sensitive area is the *Hoge Venen* (the High Fens). This area is situated in the east of Belgium and covers 4600 hectares. Despite the relatively cool climate and high precipitation (1400 mm year^{-1}), there is a high risk of fires in spring and summer (Loos, 2011). In August 2004 and April 2011, wildfires consumed respectively thousand and hundreds of hectares of fen (Belga, 2011). The wildfire of 2011 took place on the territory of the municipality Baelen and is studied in Chapters 4 and 5. Finally, the military domains in

Leopoldsburg, Hechtel-Eksel, Meeuwen-Gruitrode and Wuustwezel are annually affected by wildfires due to the many military exercises in combination with the heath- and grassland.

The result of this research was a set of 261 ignition points (Figure 2.4), 80.5% of the ignitions took place in Flanders and 19.5% took place in Wallonia. An additional 113 ignitions were registered without geographical coordinates.

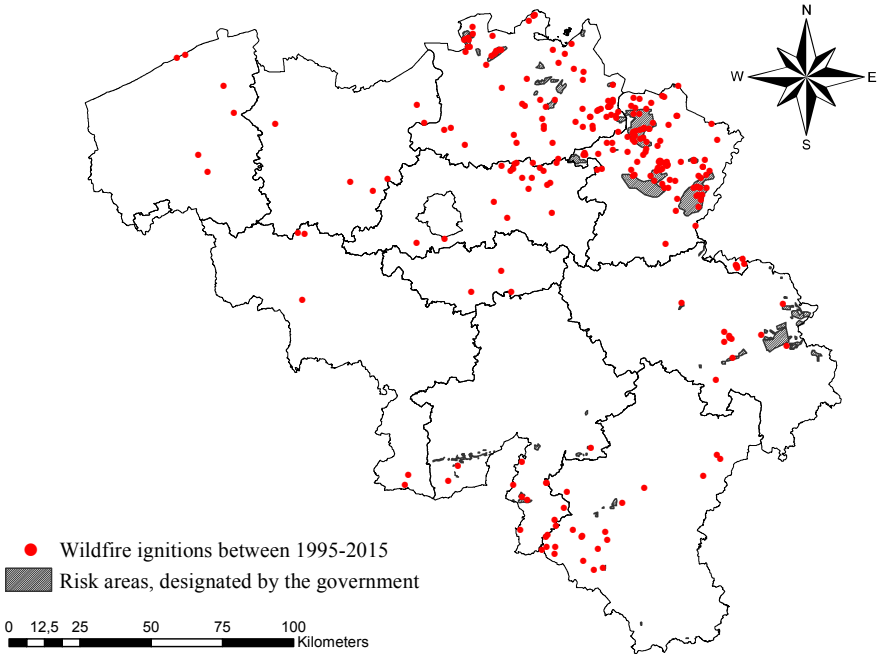

Figure 2.4: The ignitions that took place between 1995 and 2015. The government-designated risk areas are discussed in Section 2.4.4.

2.4.3 The Fire Season

Belgium has a temperate maritime climate that is characterized by four distinct seasons: spring, summer, fall and winter. Two critical periods for the occurrence of wildfires can be distinguished. One runs from the end of the winter until the beginning of spring (end of March). During this period, dry eastern continental winds reign, lowering the moisture content of the vegetation and the air humidity. The second period is the end of summer (August), again a period characterized by dry vegetation and low air humidity (Federal Public Service Internal Affairs, 2013). To illustrate this, Figure 2.5 displays the prevalence of wildfires between 1911 – 1950 and 1995 – 2015. The average annual number of ignitions is 41.25. This was calculated as the average number of ignitions between 2010 and 2013, since the list of all

wildfires provided by the Directorate-General of the Federal Public Service Internal Affairs is assumed to be complete.

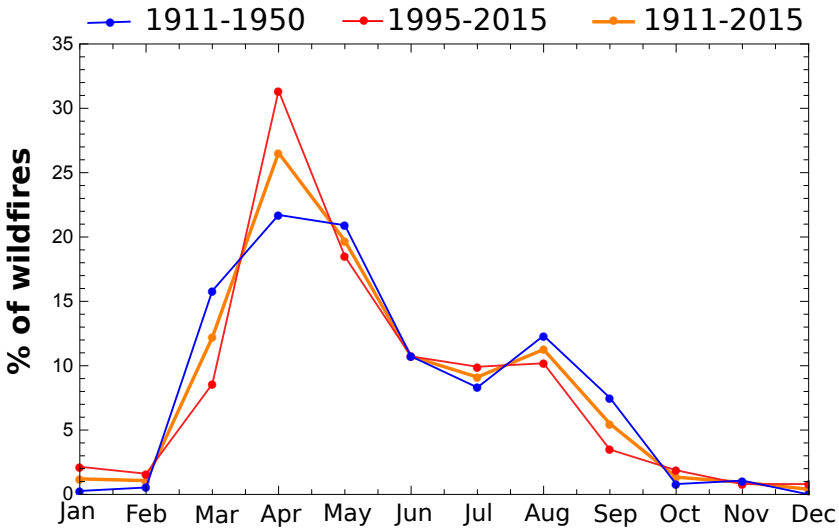

Figure 2.5: The relative frequency of the 744 wildfires ignitions between 1911–1950 and 1995–2015.

2.4.4 Wildfire Management in Belgium

In 2011, a series of wildfires raged through *de Hoge Venen* (the High Fens), *de Kalmthoutse Heide* (heathland) and the military domain in Meeuwen, destroying respectively 1000, 500 and 360 ha. In total, 2180.39 ha of land were burnt that year, mainly NATURA 2000 sites (Schmuck et al., 2012). The experience with the suppression of these fires learned that there was a lack of coherent operation procedures. Moreover, the fire fighting teams needed more specific training, procedures, material and a risk map. On July 5, 2011, the National Action Plan Wildfires was introduced by the Directorate-General of the Federal Public Service Internal Affairs in order to evaluate and improve the risk analysis and cartography, materials, procedures and training, emergency planning, and exercises. To each theme, a workgroup was dedicated, in order to solve the problems efficiently and coherently (Federal Public Service Internal Affairs, 2013).

Risk Analysis and Cartography

In 2011, the emergency planning services of the provincial governors compiled a risk map with 32 risk zones. The selection of risk areas was based on common sense and discussions between the participants in the dedicated working group. This approach resulted in a number of problems, among which the lack of uniformity that is needed for collaboration between intervention teams of different regions. In Chapter 3, more scientifically elaborated approaches

will be applied to construct such a risk map. From the 261 ignitions retrieved between 1995 – 2015, only 50 (19.2%) took place on the risk areas that were designated by the government (Figure 2.4). The total risk area is 1.41% of the total Belgian area and 68.03% of this risk area lays in Flanders, versus 31.97% in Wallonia. This also explains why more ignitions have been observed in Flanders. In the past, there were already attempts to construct maps that visualize only the necessary information to fight wildfires and enhance the coordination of different fire departments (Maes, 1999).

Materials

After the disastrous year 2011, it was clear that there was insufficient knowledge of the cost of materials, vehicles were outdated, the provision of the intervention teams was ill-regulated and the helicopters were used inefficiently. Based on an analysis of the issues during the 2011 campaign, the National Action Plan stated five objectives: making an inventory of damaged and destroyed material, making an inventory of the available means for each provincial governor, organizing the water and fuel provision, organizing the food supply of the intervention teams and organizing the use of helicopters. At present, there is international cooperation with Germany, France and the Netherlands for the use of helicopters (Belgian Federal Government, 2015).

Procedures and Training

This workgroup focused on the suppression of new fires and counteracting the evolution from controllable to uncontrollable fires rather than the prevention and rehabilitation of sites. To improve these actions, a limited number of employees were introduced to tactical and strategical training. They were selected in all the Belgian risk areas in such a way that they cover the whole national territory. The first training focused on Standard Operational Procedures that depend on the vegetation type, terrain, wind, and topography. Since 2013, this training is provided for three to four staff members of each fire brigade. The strategical training covers real-time management, prospective fire modeling, the relation with authorities, and so on (Directorate-General Civil Security, 2012).

Emergency Planning

Even though there are emergency and intervention plans for wildfires at a provincial and intercommunal level, there is no national approach for this type of emergency situation. The experience of 2011 learned there was a need for a more efficient declaration of the different phases. That year, the declaration of the appropriate phase happened too late, or stayed unnoticed by some instances. Even worse, there was no homogenous terminology for the different phases, leading to an unnecessary complexity (e.g. the communal, provincial and federal phases versus the operational phase, fire fighting phase,...). There was also a need

for more multidisciplinary coordination, a better flow of information and a better preparation of the evacuation. Based on the aforementioned problems, four objectives were stated by the workgroup, namely analyzing the debriefings of the events, analyzing the existing emergency plans, proposing a standard for the provincial emergency plans and developping practical tools for the management of wildfires.

2.5 Spatio-Temporal Modeling of Wildfires

A wildfire model consists of formulas that describe the spatial and/or temporal evolution of different variables like the Rate Of Spread (ROS), fire intensity, flame height, ignition risk and fuel consumption (Pastor et al., 2003). The majority of models attempts to predict the ROS for a certain vegetation type under varying climatic conditions. This is important to determine how long plants will be exposed to lethal temperatures. The fire intensity is strongly linked with the amount of heat that is produced during combustion. It determines the scorch height, and hence the amount of burnt canopy (Whelan, 1995; Papadopoulos, 2011). The models can be used for real-time decisions that aid the fire suppression (Kessel and Beck, 1991), for land use planning, designing suppression strategies and training of fire brigades (Green and Gill, 1989). In recent years, numerous authors developed so called faster-than-real-time simulations, providing both accurate data and a user-friendly visualization (Ghisu et al., 2015). An example of the latter is FLogA, an interactive web-based software tool that simulates wildfires in Europe and generates the required GIS layers automatically (Bogdos and Manolakos, 2013).

2.5.1 Mechanistic versus Empirical Models

Mechanistic or *phenomenological* models are based on mechanisms like mass and heat transfer. The underlying processes of wildfires are described. These models are sometimes referred to as *white box* models (Cameron and Hangos, 2001). This type of model is validated through observations. One of the advantages is that they can be extrapolated, since they capture the underlying physics. Some disadvantages are the necessary simplifications to deal with the huge complexity of the equations on the one hand, and their high computational demands on the other hand (Johnston et al., 2005). In contrast, an empirical model does not rely on the description of the underlying processes of a phenomenon (which are often poorly understood) (Cameron and Hangos, 2001), but attempts to derive a simple equation that relates the observations in the field and the phenomenon at stake, for instance wildfire spread (Johnston et al., 2005). An advantage of an empirical model is its straightforward implementation. Disadvantages are the high dependence on the conditions of the source data and the need for major approximations (Papadopoulos, 2011). They are often referred to as *black box* models. In practice, most models are mechanistic models with some empirical parts, for example Fire

Area Simulator (FARSITE), a model proposed by Finney (2004). These models are referred to as *grey box* models (Cameron and Hangos, 2001).

2.5.2 Continuous versus Discrete Models

Similar to the classification of spatially explicit models of population dynamics by Berec (2002), spatio-temporal models can be classified according to whether space, time and state are conceived in a discrete or continuous way (Table 2.3). When all three are treated as continuous entities, the model consists of Partial Differential Equations (PDEs). Relatively simple PDEs can sometimes be used to describe complex nonlinear and unsteady behavior, as illustrated by (Mandel et al., 2008). Nonetheless, PDEs have little success for describing wildfires due to their high computational demands and processing time (Perona and Brebbia, 2010). Cellular automata, introduced by von Neumann (1966), are built upon discretized time, space and state domains (Muzy et al., 2005). A CA can perform complex computations based on local information and suffers less from instabilities than PDEs (Ganguly et al., 2003). Moreover, they are computationally more efficient (Ghisu et al., 2015). Therefore, many examples of CAs for wildfire simulation can be found in literature (e.g. Karafyllidis and Thanailakis, 1997; Encinas et al., 2007; Alexandridis et al., 2008). A major disadvantage, however, is the distortion of the fire shape due to the restriction of the wildfire spread to its neighboring cells. The fire shape tends to be more angular, rather than rounded as would be expected. Several authors have already suggested methods to counter this problem (Trunfio et al., 2011; Ghisu et al., 2015; Encinas et al., 2007). As illustrated in Table 2.3, several Spatio-Temporal Models (STMs), intermediary to PDEs and CAs, can be distinguished, for instance Partial Difference equations (PdEs), Integro-Difference Equations (IdEs) and Ordinary Differential Equations (ODEs) (Berec, 2002). These models will not be further elaborated upon in this thesis.

Table 2.3: Classification of spatio-temporal models, based on the continuous or discrete nature of the space-time region and state-space (Berec, 2002).

Time	Space	State	Name	Constructs
C	C	C	PDE-based model	PDEs
C	D	C	Spatially implicit model	ODEs
D	C	C	Reaction-diffusion model	IdEs
D	D	C	Coupled-map lattice	PdEs
C	C	D	Spatial point model	Set of rules
D	C	D	Agent-based model	Set of rules
C	D	D	Interacting particle system	Set of rules
D	D	D	Cellular automata	Set of rules

CHAPTER 3

A Static Hazard Assessment of Belgium

In this chapter, several methods are applied to construct a static wildfire risk map for the Belgian territory. First of all, an expert system is used to assess the risk of ignition. Secondly, Bayes' theorem is applied to determine the probability an ignition takes place and thirdly, a logistic regression will be performed, following the methods presented in Catry et al. (2009). The chapter is concluded by comparing the results, advantages, and disadvantages of each model. The software packages used in this chapter are Mathematica (Version 10.0, Wolfram Research Inc., USA), ArcMap (Version 10.2.2, Esri, USA), and Matlab (Version 2015a, MathWorks, USA).

3.1 Belgian Risk Index for Wildfires

In this section, the methodology underlying the Dutch Risk Index for Wildfires (abbreviated as RIN, or in English: the Dutch RIW) will be adapted to construct a wildfire risk map for the Belgian territory. The Dutch RIW was developed in 2003 to gain insight into the wildfire risk in nature reserves and to stimulate the cooperation of fire fighters and site administrators. The Dutch RIW aims to provide a uniform and comparable risk analysis across the entire Dutch territory. It reflects the risk that a fire evolves to an uncontrollable wildfire once it has started, not the risk that a fire ignites. A wildfire is considered uncontrollable when (Verboom et al., 2013):

1. the affected area is too large to suppress the fire with the present regional firefighting teams, or
2. there are multiple casualties, or
3. there is the possibility of the loss of lives and a large-scale evacuation.

3.1.1 Methods

Three types of predictor are used to assess the wildfire risk, according to the Dutch RIW (Appendix A). The first type characterizes the terrain and identifies valuable objects and hazardous substances. The second type describes the presence of people and recreation in a region, while the last type reflects the measures taken for wildfire prevention and preparation for suppression, the distance to fire stations and the availability of suppression water. Every type encloses several categories that are scored (the higher the risk, the higher the score). The scores assigned to the different categories are based on expert knowledge. In the Dutch RIW, every nature area is subdivided into rectangular compartments of 1 km^2 and the sum of the scores for the different predictors gives the total risk.

In this thesis, the wildfire risk across the entire Belgian territory will be assessed, not limiting to nature reserves. A GIS will be used to calculate the score based on raster layers and on a resolution of 100m×100m. As the Belgian Risk Index for Wildfires (abbreviated as the Belgian RIW) should reflect only the risk that a wildfire will spread uncontrollably, many of the predictors in the Dutch case are discarded. Predictors such as recreation, prevention, distance to roads, proximity of water basins, etc., as taken into account in the Dutch RIW, will not be considered here because they hold no relation to the fire sensitivity of the terrain. The selected predictors are displayed in Table 3.1.

Flammability of Vegetation

The vegetation map of the Belgian territory with a resolution of 100m×100m was derived from the CORINE (Co-ORdinated INformation on the Environment) Land Cover Mapping which is developed by the European Environment Organization under the Copernicus land monitoring program since 2000 (Environmental Protection Agency, 2015). The 50 CORINE land cover types were reclassified according to the vegetation types in Table 3.1 and scored accordingly (Figure 3.2 (a)). Note that there are two types of grassland that were scored differently, namely agricultural and natural, which were assigned a score of 0 and 50, respectively.

Slope

The slope was calculated from the DTM that was provided by National Geographic Institute (NGI). The original resolution of the shape file was 20m×20m. The DTM was constructed through interpolation of altimetric data like altitude lines and points (National Geographic Institute, 2013). The resulting slope classes are depicted in Figure 3.2 (b).

Table 3.1: Predictors used in the assessment of the Belgian Risk Index for Wildfires.

Predictor	Category		Score
1. Flammability of Vegetation	Not inflammable	Water, pasture, farmland	0
		Land dunes	
		Artificial surfaces	
	Barely inflammable	Deciduous forest	20
	Slightly inflammable	Mixed forest	30
	Inflammable	Heathland	50
		Grassland	
		Fen	
		Reed land	
		Swamps	
	Extremely inflammable	Closed coniferous forest	100
2. Slope	0-1%		0
	1-5%		5
	5-10%		10
	$> 10\%$		40
3. Spreading capacity	Zero	$< 12.5\%$	0
	Low	$12.5\% <$ Spreading capacity $< 37.5\%$	10
	Intermediate	$37.5\% <$ Spreading capacity $< 62.5\%$	20
	High	$> 62.5\ \%$	40

Spreading Capacity

The spreading capacity is a measure for wildfires to disperse to a neighboring cell and ranges between 0 and 1, where '0' means that the cell is completely isolated and '1' that the wildfire can spread in every direction. To quantify it, the principles of heat dispersion are relied upon. The steady-state temperature of the central cell in a square grid can be computed iteratively as the weighted average of the temperature in its neighboring cells, as illustrated in Figure 3.1 (Schiff, 2008). Here, it was assumed that the ignition risk due to a neighboring cell is proportional to the transfer of heat from that cell. The spreading capacity (see Figure 3.2 (c)) is then calculated as:

$$\sum_{i=1}^{8} w_i \, F_i, \tag{3.1}$$

where F_i is '0' if the land cover type in the i-th neighboring cell is inflammable and '1' when the opposite is true.

1/20	1/5	1/20
1/5		1/5
1/20	1/5	1/20

Figure 3.1: Illustration of the Moore neighborhood and the weight of each neighbor (Schiff, 2008).

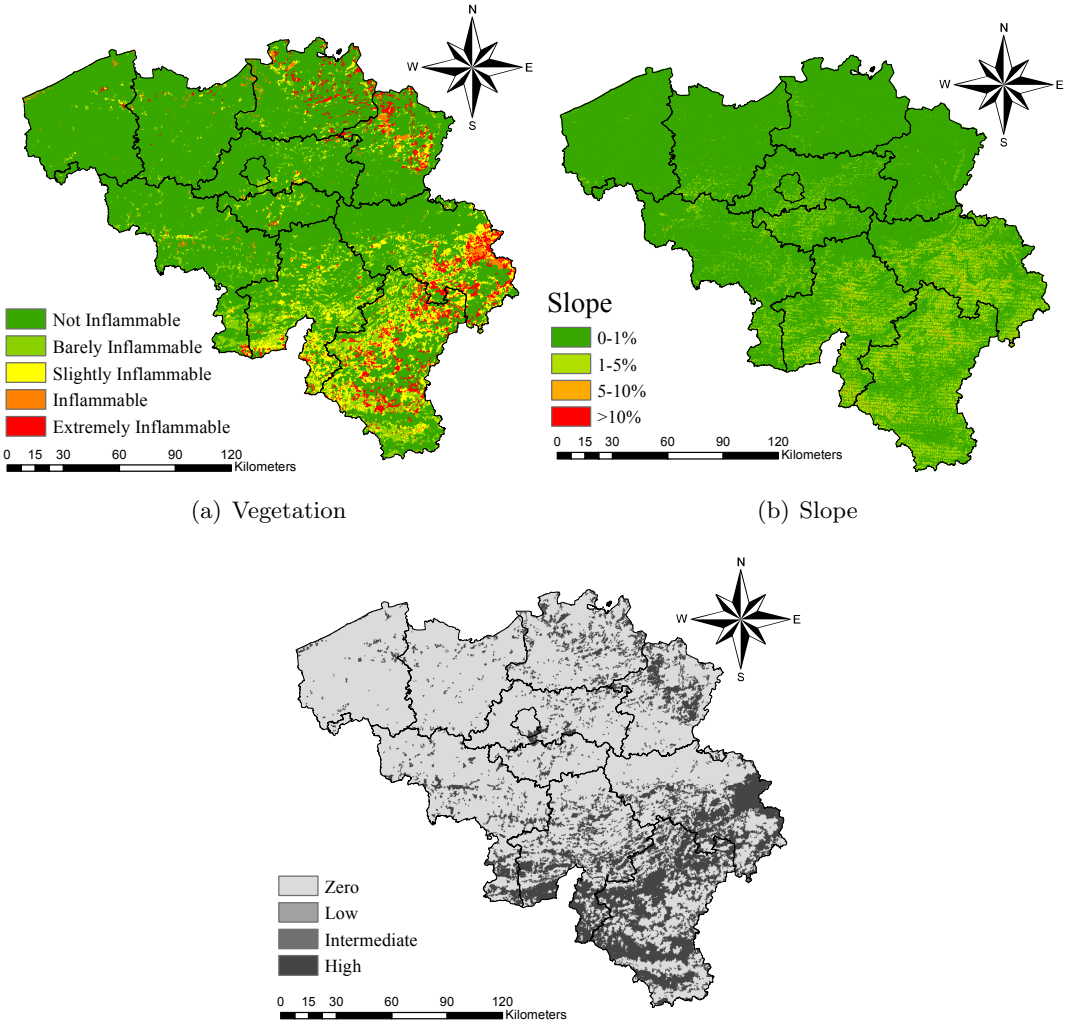

(a) Vegetation

(b) Slope

(c) Spreading capacity

Figure 3.2: Predictors of wildfire risk: the flammability of the vegetation (a), the slope of the terrain (b) and the spreading capacity (c).

3.1.2 Results

To calculate the Belgian RIW, the scores given to the three predictors (see Figure 3.2) were added in agreement with the methodology outlined for the Dutch RIW. Overall, scores between 0 and 180 were obtained, whereas a maximum of 750 was possible for the Dutch RIW (because it has more predictors). Hence, the score intervals corresponding to the different risk classes from the Belgian RIW were defined by a linear scaling of those of the Dutch RIW (see Table 3.2), hence the proportions of the risk intervals to the total range of scores is equal for the Belgian and Dutch RIW.

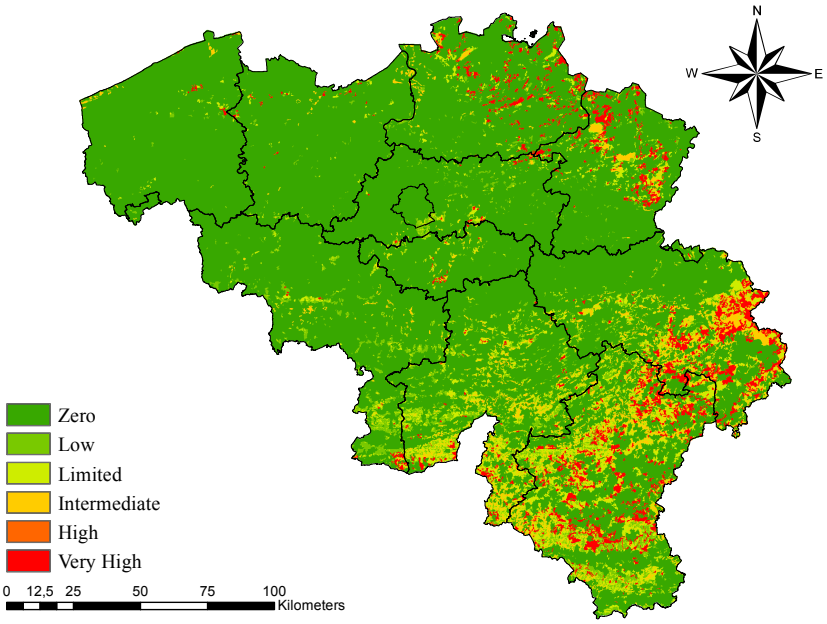

Figure 3.3: The Belgian Risk Index for Wildfires.

Table 3.2: The different risk classes according to the Belgian RIW. The relative area of these risk classes in the government-designated risk areas and the Belgian territory is given, as well as the relative frequency of all observed ignitions over these risk classes.

Risk Class	Score interval	Government (%)	Belgium (%)	Ignitions (%)
Zero	0 – 41	27.19	79.53	26.82
Low	41 – 60	3.49	5.40	8.81
Limited	60 – 72	13.47	6.75	21.84
Intermediate	72 – 96	27.27	3.70	16.48
High	96 – 120	3.00	0.50	1.15
Very High	120 – 180	25.75	4.13	24.90

The final wildfire risk map is displayed in Figure 3.3. Table 3.2 summarizes information that will allow to compare the Belgian RIW with risk maps that will be constructed in the subsequent sections. This table also shows the relative frequency of the risk classes over the government-designated areas (Figure 2.4) and the whole Belgian territory. Finally, the relative frequency of all observed ignitions over these risk classes is also given. Table 3.3 gives the percentage of the total area in every class per province and region.

Table 3.3: Prevalence of the different risk classes per region and province.

Region	Province	Wildfire Risk (% of total area)					
		Zero	**Low**	**Limited**	**Intmed.**	**High**	**Very High**
Flanders	West Flanders	98.04	0.63	0.59	0.45	0.06	0.22
	East Flanders	97.08	1.04	0.90	0.52	0.14	0.32
	Antwerp	85.98	2.84	3.43	1.23	1.63	4.98
	Limburg	81.75	2.93	5.06	2.66	1.28	6.34
	Flemish Brabant	93.02	3.94	1.95	0.44	0.10	0.54
	Total	**91.60**	**2.12**	**2.27**	**1.02**	**0.63**	**2.36**
Wallonia	Hainaut	88.87	7.09	2.76	0.81	0.04	0.43
	Walloon Brabant	93.53	2.36	2.25	1.14	0.09	0.63
	Liège	68.85	4.27	8.94	8.17	0.44	9.34
	Namur	67.89	10.91	13.01	6.23	0.16	1.80
	Luxembourg	49.69	11.12	18.04	9.14	0.91	11.10
	Total	**69.70**	**8.03**	**10.40**	**5.89**	**0.39**	**5.59**
Brussels		90.15	7.43	2.22	0.20	0.00	0.00
BELGIUM		**79.53**	**5.40**	**6.75**	**3.70**	**0.50**	**4.13**

3.1.3 Discussion

Two areas in Figure 3.3 stand out: the east of the Flemish Region and the east of the Walloon Region. This can be explained by the relatively large areas of forests and natural vegetation on the one hand, and the presence of coniferous forests, which are prone to wildfires, on the other hand (Wijdeven et al., 2006). In Flanders, the fundaments of the current land use were laid by the social, economical and technological shifts in the 19^{th} century, like the industrial revolution and agricultural innovations (Buis, 1985). The omnipresent heathland was afforested on the sandy soils in the east of Flanders (mainly with *Pinus sylvestris*, being ideal strut wood for the mines), while the forests on the rich soils in the west were cut (den Ouden et al., 2010). The inflammable heathland, a relict from the historical land use, is relatively more common in Limburg and Antwerp than in the rest of Flanders (Hermy et al., 2004), thus it makes sense that the wildfire risk in these two provinces is higher than the in the other provinces: 6.61% of the total area in Antwerp and 7.62% of the total area in

Limburg is assigned a high or very high risk score. In Wallonia, the relative forested area is three times as high as in Flanders, 32% versus 11.4% (Walloon Government and the European Commission, 2015; Stevens et al., 2015), though the forests are mainly concentrated in the provinces of Liège and Luxembourg. The typical tree species that is used for afforestation in this region is *Picea abies*, a coniferous species associated with a very high wildfire risk, which explains the relatively high risk in the latter two provinces. As expected, the nature reserve *the High Fens* and its surrounding area shows an elevated wildfire risk because of its fens. In the Brussels Capital Region, only the Sonian Forest presents a wildfire risk. Despite the deciduous nature of this forest (*Fagus sylvatica*, *Quercus spp.* and *Carpinus betulus* dominate the vegetation), the risk is still intermediate because of the high spreading capacity.
The results of the Belgian RIW can be compared to the risk map that was constructed in 2012 by the emergency planning service of the provincial governors (see Section 2.4.4 and Figure 2.4). As displayed in Table 3.2, a large portion of the area that has a high wildfire risk according to the latter map is assigned to risk class 'Zero' (27.19%). A possible explanation is that for the construction of this risk map in 2012, 'real' risk areas were connected to each other, so that the interstitial areas with no risk were classified as 'risk area'.

3.2 Bayes' Theorem

3.2.1 Methods

The drawback of the RIW is that it does not provide a link between the final score and the probability that an ignition will take place, during the course of one year, on a 100m×100m cell given a certain environment. To calculate this probability, Bayes' theorem was applied:

$$P(I|C_i) = \frac{P(I)\,P(C_i|I)}{P(C_i)}, \tag{3.2}$$

where I indicates an ignition event and C_i an environment that is defined by the vegetation (as presented in Table 3.1) and slope. The slope was first discretized in four classes, in such a way that each of them covered approximately 25% of the Belgian territory. Given that there were five vegetation classes, 20 different combinations of slope and vegetation were possible, referred to as C_i, $i \in [1, 20]$. The probability that a randomly selected cell belongs to class C_i is equal to

$$P(C_i) = \frac{\text{Area of } C_i}{\text{Total Belgian area}}. \tag{3.3}$$

$P(C_i|I)$ in Eq. (3.2) is the probability that, given an ignition took place in a cell, this cell belongs to class C_i, and was obtained from:

$$P(C_i|I) = \frac{\text{Average annual number of ignitions on } C_i}{\text{Average annual number of ignitions}}, \tag{3.4}$$

with the average annual number of ignitions being 41.25. The latter was obtained from the period 2010 - 2013 only because a complete ignition dataset was provided by the Directorate-General of the Federal Public Service Internal Affairs for this period . Hence, the average annual number of ignitions between 2010 and 2013 was considered representative for the average annual number of ignitions between 1995 and 2015. Finally, the probability an ignition occurs in a random cell within the time span of one year was calculated as

$$P(I) = \frac{\text{Average annual number ignitions}}{\text{Total number of cells}}. \tag{3.5}$$

Again, the wildfire dataset, discussed in Section 2.4 is used, so all registered ignitions between 1995 and 2015 were considered. The different $P(I|C_i)$'s were calculated a thousand times, each time using 234 randomly selected ignition points. The validation set consisted of the 27 remaining ignition points and 54 non-ignition points. These non-ignition points are randomly sampled points over the whole Belgian territory.

3.2.2 Results

The resulting $P(I|C_i)$ values were binarized using a cut-off value of 0.031×10^{-3}. The choice of this value is discussed in Section 3.4.1. The average model quality was 76.2% and was calculated as the ratio of the number of correctly classified ignition and non-ignition points over the total number of ignition and non-ignition points in the validation set. The greatest variance of $P(I|C_i)$ across the runs was 9.93×10^{-10}, indicating the result was consistent. The final model was constructed using all 261 ignition points. The resulting probabilities, ranging from 0 to 0.48×10^{-3}, were classified into five risk classes (Table 3.4 and Figure 3.5). The corresponding risk map is displayed in Figure 3.4. Table 3.4 also shows the relative frequency of the risk classes over the government-designated areas (Figure 2.4) and the whole Belgian territory. Finally, the relative frequency of all observed ignitions over these risk classes is also given.

Table 3.4: The different risk classes according to the risk map that was constructed using Bayes' theorem. The relative area of these risk classes in the government-designated risk areas and the Belgian territory is given, as well as the relative frequency of all observed ignitions across these risk classes.

Risk Class	**$P_{ignition}$ interval ($\times 10^{-3}$)**	**Government (%)**	**Belgium (%)**	**Ignitions (%)**
Very Low	0 – 0.015	35.36	81.31	28.35
Low	0.015 – 0.045	17.28	12.21	19.54
Intermediate	0.045 – 0.100	14.31	3.50	16.09
High	0.100 – 0.150	18.52	1.60	14.94
Very High	> 0.150	14.53	1.13	21.07

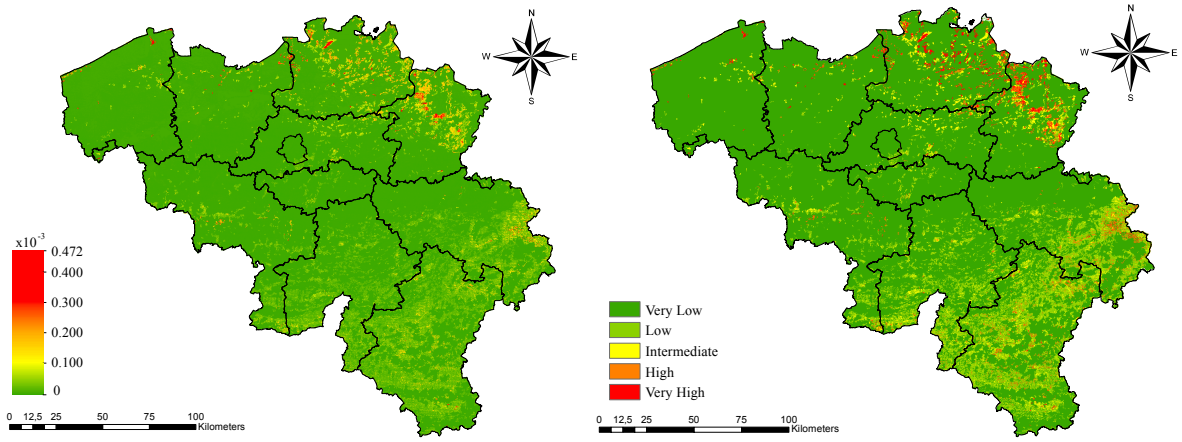

(a) (b)

Figure 3.4: The raw (a) and classified (b) wildfire risk map, calculated with Bayes' theorem.

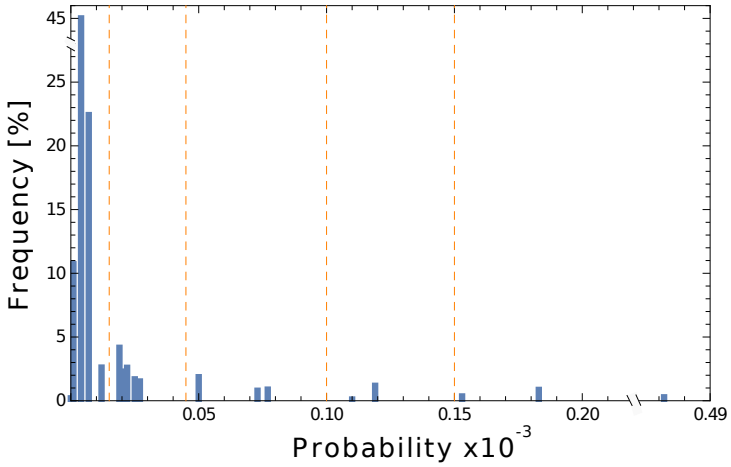

Figure 3.5: The frequency of the twenty calculated probabilities and the indication of the five intervals.

3.2.3 Discussion

The distribution of the five risk classes makes sense: the higher the probability that a wildfire will ignite, the lower the relative area this class covers. This is in contrast to the Belgian RIW since the latter did not establish such a relation. Flanders is better represented in the dataset than Wallonia, in the sense that 80.5% of the ignitions took place on Flemish soil. This is no surprise, since the governmental risk map (Figure 2.4) shows that the largest share of the fire sensitive area lies in Flanders. Taking into account that Wallonia is much more accidented, this explains why environments with a slope larger than 3% are assigned a low

ignition probability. After all, the probability $P(C_i|I)$ in Eq. (3.4) is directly proportional to the number of ignitions that took place on C_i. This implies that the magnitude of the resulting probabilities depends on the number of data points.

3.3 Logistic Regression

Here, the method presented by Catry et al. (2009) to obtain a static hazard assessment for Portugal, was followed. First, the original regression equation constructed for Portugal will be tested for the Belgian case, after which a new regression equation will be constructed for the Belgian setting with the same predictors as the ones used by Catry et al. (2009). Thirdly, an equation with additional predictors will be built.
The general form of a regression equation is:

$$P_{\text{ignition}} = \beta_0 + \beta x_1 + \beta x_2 + \ldots + \beta_p x_p, \tag{3.6}$$

where β_0 is a constant, β_p is the weighing factor of the independent predictor x_p and P_{ignition} is proportional to the probability of occurrence of a wildfire. As the latter is constrained to values between 0 and 1, whereas the right-hand side of Eq. (3.6) to values in the interval $[-\infty, +\infty]$. The logit transformation is used:

$$\log_e \left(\frac{P_{\text{ignition}}}{1 - P_{\text{ignition}}} \right) = \beta_0 + \beta_1 \, x_1 + \beta_2 \, x_2 + \ldots + \beta_p \, x_p, \tag{3.7}$$

so:

$$P_{\text{ignition}} = \left(1 + e^{-(\beta_0 + \beta_1 \, x_1 + \beta_2 \, x_2 + \ldots + \beta_p \, x_p)} \right)^{-1}, \tag{3.8}$$

whose right-hand side only take values between 0 and 1 (University of Freiburg, 2015).

3.3.1 Original Regression Equation (after Catry et al. (2009))

Methods

For the analysis of the Portuguese static hazard assessment, 127 490 ignitions during a five year period were analyzed. The study area is 90 000 km^2 and has a mediterranean climate. Approximately 48% of the land is used for agriculture, 27% is covered with forests and 19% with shrubland. The country has approximately 10 million inhabitants – comparable with Belgium ($\pm$ 11 million inhabitants), though the surface area of Belgium is much smaller ($\pm$ 30 000 km^2). The authors opted for logistic regression because of its usefulness to predict the presence/absence of an event. Another advantage is that both continuous and categorical predictors can be used (Hosmer and Lemeshow, 1989; Legendre and Legendre, 1998). The predictors selected by Catry et al. (2009) are considered independent. The predictors are:

1. *Population density*: The data used for the Belgian case were provided by Statistics Belgium and comes from a census in 2013 (Belgian Federal Government, 2013).

2. *Distance to roads*: The distance [m] to the main national and regional roads was calculated. For the Belgian case, the data of the primary and secondary highways were downloaded from `http://www.openstreetmap.org`.

3. *Land Cover*: For this predictor, the CORINE Land Cover database was reclassified into six different classes: agriculture, forests, shrublands, urban-rural interspersed areas, sparsely vegetated areas and wetlands.

4. *Elevation*: The same elevation model as discussed in Section 3.1.1 was used.

The first two predictors were taken into account because most fires are due to arsony or negligence (this is the case for Belgium too) and because roads were the best determinant of human access. Land cover was important because of the different levels of flammability. In Portugal, the land use on a different land cover is linked with a different ignition probability. Elevation was also important because human activities like pastoralism are frequent in a mountainous area. Pastoralism is linked with the burning of land to renovate pastures for livestock. In Belgium, however, burning as a management practice is very rare (as discussed in Section 2.4.2). All predictors x_p, except land cover, were transformed as $\log_e(x_p + 1)$ to reduce variance, turning Eq. (3.7) into:

$$\log_e\left(\frac{P_{\text{ignition}}}{1-P_{\text{ignition}}}\right) = -7.833 + 0.820\,x_1 - 0.166\,x_2 + 0.585\,x_3 + 2.455\,x_4 \\ +1.672\,x_5 + 0.388\,x_6 + 0.439\,x_7 + 0.426\,x_8, \tag{3.9}$$

with x_1 [people/km^2] the population density, x_2 [m] the distance to primary and secondary roads, x_3 [m] the elevation model. Predictors x_4 to x_8 are categorical (0/1) and represent the land cover classes. The resulting risk map is displayed in Figure 3.6. The risk classes were identified by dividing this range into six intervals, as proposed by Catry et al. (2009) (Table 3.5).

Results & Discussion

Figure 3.6 shows the wildfire risk map that corresponds to Eq. (3.9). As can be seen, the results for the Belgian territory are unrealistic. The risk areas that were designated by the government are not characterized by a (very) high ignition probability, as illustrated in Table 3.5. On the contrary, urban areas with a high population density are classified as areas with a very high wildfire risk. Also, only 3.45% of the locations where ignitions were observed were assigned to the (very) high risk class. Two reasons can explain the shortcomings of Eq. (3.9):

1. Belgium has a denser road network than Portugal. Because of this, almost every place is easily accessible by humans, who are also more abundantly present given the higher population density.

2. Agricultural land in Portugal is very different from the intensively cultivated acres in Belgium, which makes that ignitions often occur in agriculture areas in Portugal, whereas this is rare in Belgium.

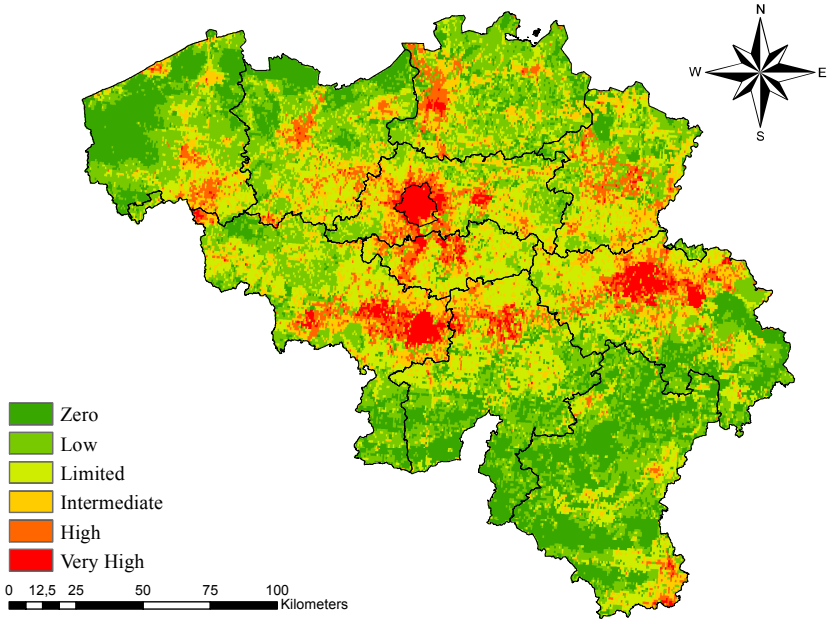

Figure 3.6: The wildfire risk, calculated with the logistic regression equation, constructed by Catry et al. (2009).

Table 3.5: The different risk classes according to the risk map obtained using the logistic regression equation by Catry et al. (2009). The relative area of these risk classes across the government-designated risk areas and the Belgian territory is given, as well as the relative frequency of the observed ignitions across these risk classes.

Risk Class	P_{ignition} **interval**	**Government** (%)	**Belgium** (%)	**Ignitions** (%)
Extr. Low	0 – 0.1	20.67	22.21	39.08
Very low	0.1 – 0.2	29.51	28.64	25.29
Low	0.2 – 0.4	28.47	24.16	13.03
Intmed.	0.4 – 0.6	11.14	13.79	18.39
High	0.6 – 0.8	9.53	7.97	2.68
Very High	0.8 – 1.0	0.69	3.24	0.77

3.3.2 Modified Regression Equation

Methods

The dataset consisted of 261 ignition points (as discussed in Section 2.4) and 522 non ignition points that were randomly generated. The examined predictors were the same ones as used by Catry et al. (2009), namely land cover, population density, height and distance to primary and secondary highways. Land cover was encoded using five categorical predictors, agriculture land not included. The variance explained by the latter categorical predictor was incorporated in the intercept of the regression equation. First, the non-parametric χ^2 homogeneity test was used to determine the predictor's significance, in other words, the test determines wether a predictor be used to explain the variance in the observed and expected ignition frequency. The level of significance was 0.001, in agreement with (Catry et al., 2009). Since the underlying distribution of the predictors was unknown, the non-parametric Spearman rank correlation test was used to assess mutual correlation (McDonald, 2014). When a predictor was significant and not correlated with others, it was retained as a predictor in the logistic regression equation. The training dataset consisted of 234 (90%) randomly selected ignition points and 468 randomly selected non-ignition points. The remaining data points were used to validate the regression equation (see Section 3.4). The regression equation was constructed ten times, each time from a new training and test dataset. To build the regression equation, it was ensured that each land cover class was represented in the non-ignition training data. Otherwise, the coefficients of corresponding categorical predictors had extremely wide confidence intervals, on the one hand, and were not significant on the other hand.

Results

Figure 3.7 shows the comparison between the observed and expected ignition frequencies. The expected ignition frequencies were calculated as the area of each class, divided by the total area of Belgium. Land cover clearly influenced the ignition probability ($\chi^2_{Belgium} = 197,\ p < 0.001$). In Portugal, ignitions occurred mainly in agriculture and urban-rural areas, while they were less frequent in forests, shrublands and sparsely vegetated areas. In Belgium, on the contrary, the agriculture and urban-rural areas show a lower ignition frequency than expected. Forests, shrubland and sparsely vegetated areas, on the other hand, show a higher frequency than expected. Despite being important for the Portuguese case, the distance to primary and secondary roads was not important for Belgium ($\chi^2_{Belgium} = 10.77,\ p = 0.112$), so it was not retained as a predictor. Population density significantly influenced ignition frequency ($\chi^2_{Belgium} = 43.27,\ p < 0.001$) and seemed positively correlated with the ignition frequency. Finally, also elevation significantly influenced the ignition frequency ($\chi^2_{Belgium} = 50.61,\ p < 0.001$).

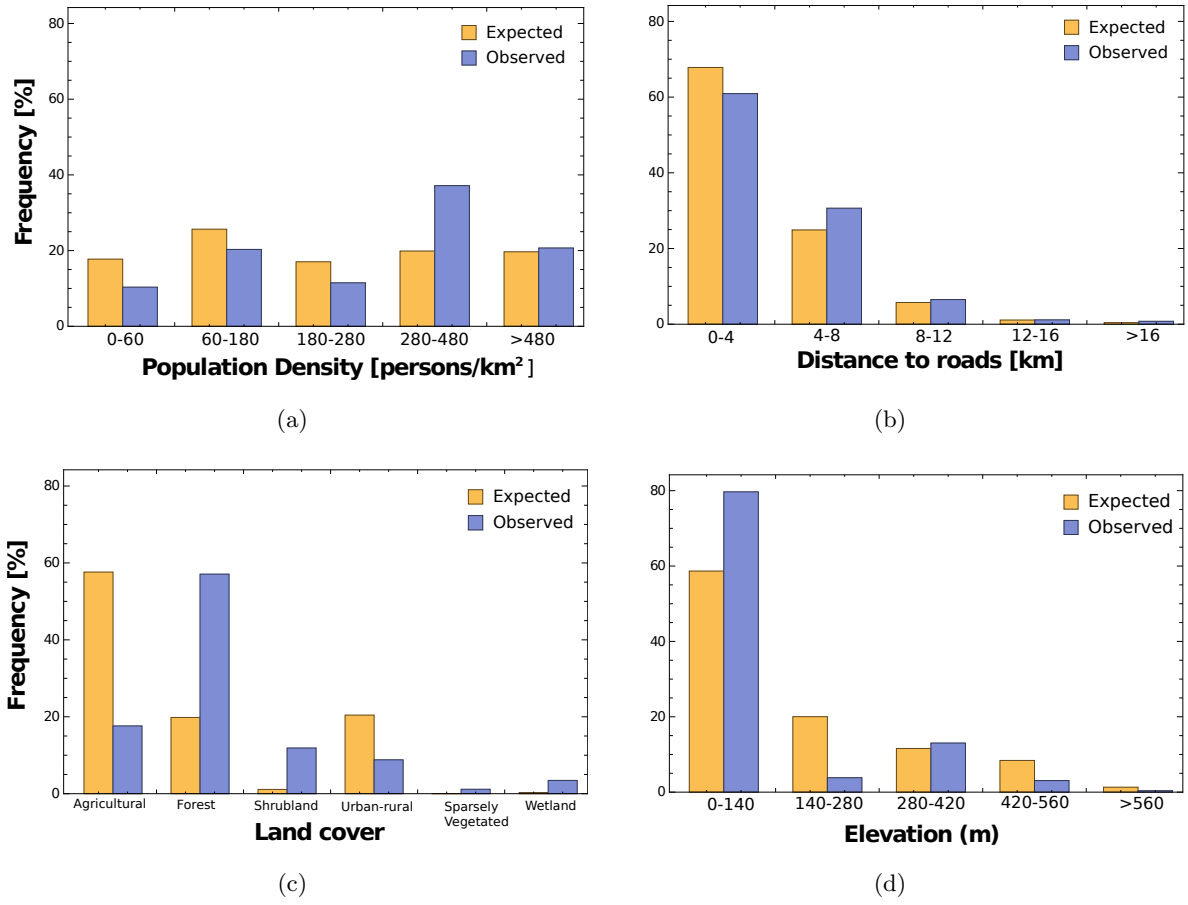

Figure 3.7: The expected and observed ignition frequency in relation to the distribution of population density (a), distance to roads (b), land cover (c) and elevation (d).

Since the predictors did not have a known, underlying distribution, the non-parametric Spearman rank correlation test was applied to verify the pairwise correlations between them. It appeared that the population density was correlated with elevation ($\rho = 0.694,\ \mathrm{p} < 0.01$), so only two predictors were retained ultimately: land cover and population density. The regression equation was constructed ten times, each time from a different, randomly generated training set. The average regression coefficients and their p-value are given in Table 3.6. This p-value is the result of a two-sided t-test to test the significance of a coefficient. Using these coefficients, the following regression equation was obtained:

$$P_{\text{ignition}} = \left(1 + e^{-(-5.301 + 0.621\,x_1 - 0.023\,x_2 + 2.622\,x_3 + 3.556\,x_4 + 2.986\,x_5 + 3.705\,x_6)}\right)^{-1}, \qquad (3.10)$$

where x_1 is the population density [people km^{-2}], predictors x_2 to x_6 are categorical, encoding the land cover classes. Table 3.7 summarizes the information needed to compare this risk map with others. This table also shows the relative area of the risk classes across the government-

designated areas (Figure 2.4) and the whole Belgian territory. Finally, the relative frequency of all observed ignitions across these risk classes is also given.

Table 3.6: The mean coefficients and p-values of the retained predictors

Predictor	**Coefficient**	**p-value**
Constant	-5.301	< 0.001
Population density	0.621	< 0.001
Land Cover		
Urban-Rural	-0.023	0.652
Shrublands	3.556	< 0.001
Sparsely vegetated	2.986	0.016
Forest	2.622	< 0.001
Wetland	3.705	< 0.001

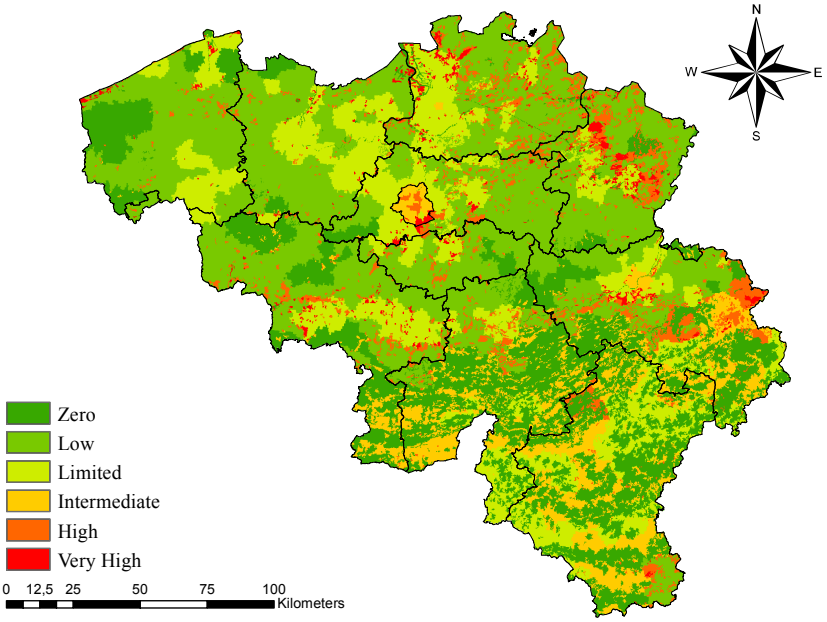

Figure 3.8: The wildfire risk, calculated with Eq. (3.10)

Discussion

The quality of the resulting risk map improved strongly using Eq. (3.10) (Table 3.7). The risk areas that were designated by the government are recognized as areas with a (very) high ignition probabilty in 56.95% of the cases, while only 7.83% of the Belgian territory was classified as such. Though 57.47% of all observed ignitions were designated a (very) high risk, a vast improvement compared to the risk map that corresponds to Eq. (3.9).

Table 3.7: The different risk classes according to the risk map corresponding to Eq. (3.10). The relative area of these risk classes across the government-designated risk areas and the Belgian territory is given, as well as the relative frequency of all observed ignitions across these risk classes.

Risk Class	P_{ignition} interval	Government (%)	Belgium (%)	Ignitions (%)
Extr. Low	0 – 0.1	12.04	22.86	1.53
Very low	0.1 – 0.2	16.97	40.87	17.62
Low	0.2 – 0.4	7.42	19.30	15.33
Intermediate	0.4 – 0.6	6.62	9.14	8.05
High	0.6 – 0.8	38.23	6.20	39.08
Very High	0.8 – 1.0	18.72	1.63	18.39

3.3.3 Modified Regression Equation with Additional Predictors

Methods

In this section, four new predictors were introduced: the distance to paths, coniferous and deciduous forests and soil texture. The distance to paths (footways, cycleways and bridleways) is relevant because paths enable intense contact between people and their environment. These paths include footways, cycle tracks and bridleways. The data were downloaded from `http://www.openstreetmap.org`. As opposed to the land cover classes used by Catry et al. (2009), a distinction between coniferous/mixed forests and broadleaved forests was made. The reason for this distinction is that coniferous trees are much more fire sensitive than deciduous trees. Soil texture was selected as a potential predictor because the soil particle size influences the soil humidity and hence the humidity of the vegetation. This predictor was incorporated using four categorical predictors: sand, loam, clay and fen. The variance explained by the categorical predictor 'antropogenic soils' was incorporated in the intercept of the regression equation. The χ^2 homogeneity test and the Spearman rank correlation test were used to assess significance of and correlation between predictors, respectively.

Results

Land cover is still an important predictor ($\chi^2 = 220.43,\ p < 0.001$). The distance to paths was not significant for the prediction of wildfire ignitions ($\chi^2 = 2.56,\ p = 0.46$), though it was correlated negatively with ignition frequency (Figure 3.9 (b)). A critical remark is that the data from Openstreetmap were probably incomplete, and that arsonists may avoid these paths in order not to be spotted by other people. For what concerns the soil texture, Figure 3.9 (c) shows a significant discrepancy between observed and expected frequencies ($\chi^2 = 186.90,\ p < 0.001$). Based on this analysis, the predictors soil, population density, and land cover were retained. The regression equation was constructed ten times, each time

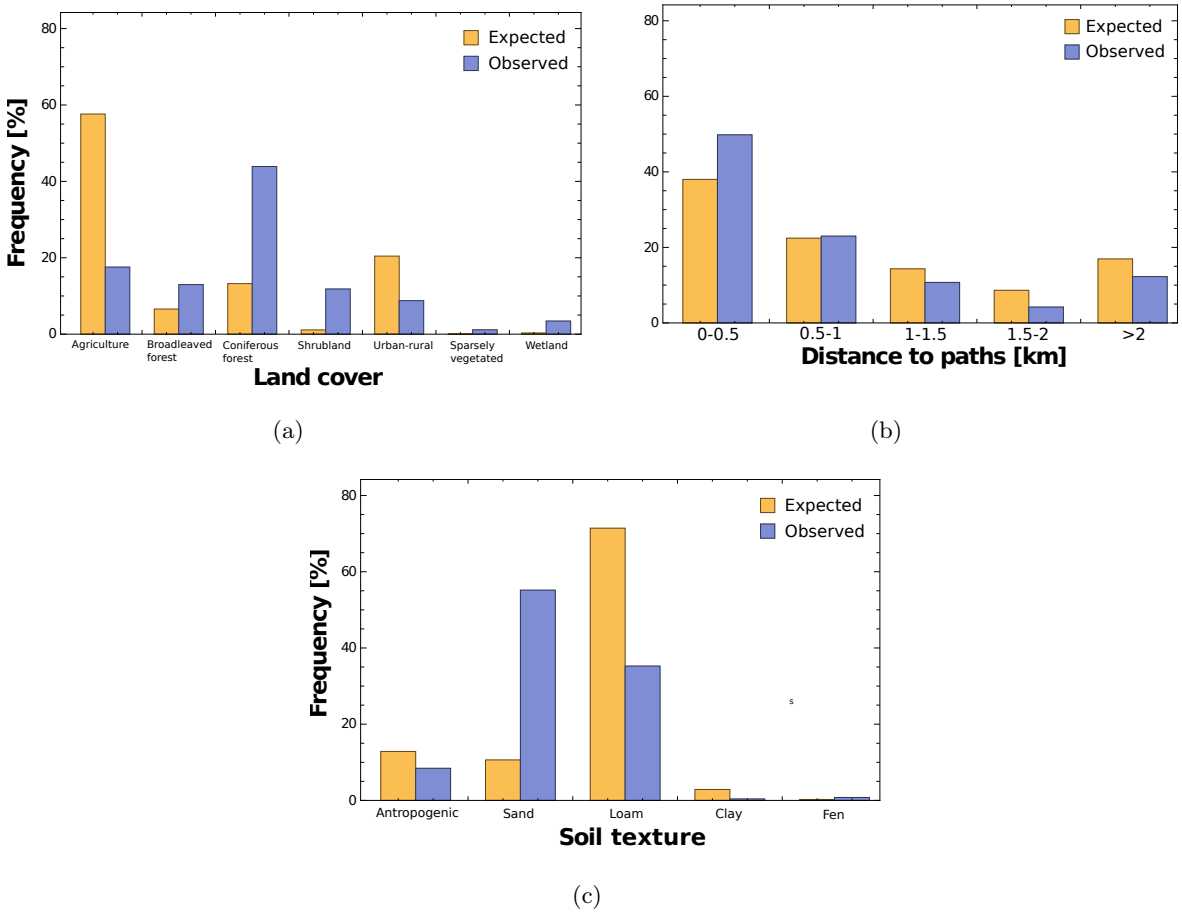

Figure 3.9: The expected and observed fire ignition frequency in relation to the distribution of land cover (a), distance to paths (b) and soil types (c).

with a randomly selected training dataset that consisted of 90% of the ignition points and 468 randomly selected locations. The remaining ignition points, together with 54 randomly selected locations, were used as a validation dataset. The average, significant coefficients are given in Table 3.8.

Using only the significant coefficients, the final regression equation becomes:

$$P_{\text{ignition}} = \left(1 + e^{-(-4.511+0.398\,x_1+2.601\,x_2+2.322\,x_3+2.553\,x_4+2.905\,x_5+1.939\,x_6)}\right)^{-1}, \qquad (3.11)$$

where x_1 is the population density [people km^{-2}]. Predictors x_2 to x_5 are categorical predictors, encoding the land cover classes. The categorical predictor x_6 encodes the sandy soil texture. The resulting wildfire risk map is displayed in Figure 3.10. Table 3.9 shows the relative area of the risk classes across the government-designated areas (Figure 2.4) and the whole Belgian territory. Finally, the relative frequency of all observed ignitions across these risk classes is also given.

Table 3.8: The average coefficients and p-values of the retained, significant predictors: soil, land cover and population density.

Predictor	Coefficient	p-value
Constant	−4.511	< 0.001
Population density	0.398	< 0.001
Land Cover		
Shrublands	2.601	< 0.001
Broadleaved Forest	2.322	< 0.001
Coniferous Forest	2.553	< 0.001
Wetland	2.940	0.013
Soil texture		
Sand	1.939	< 0.001

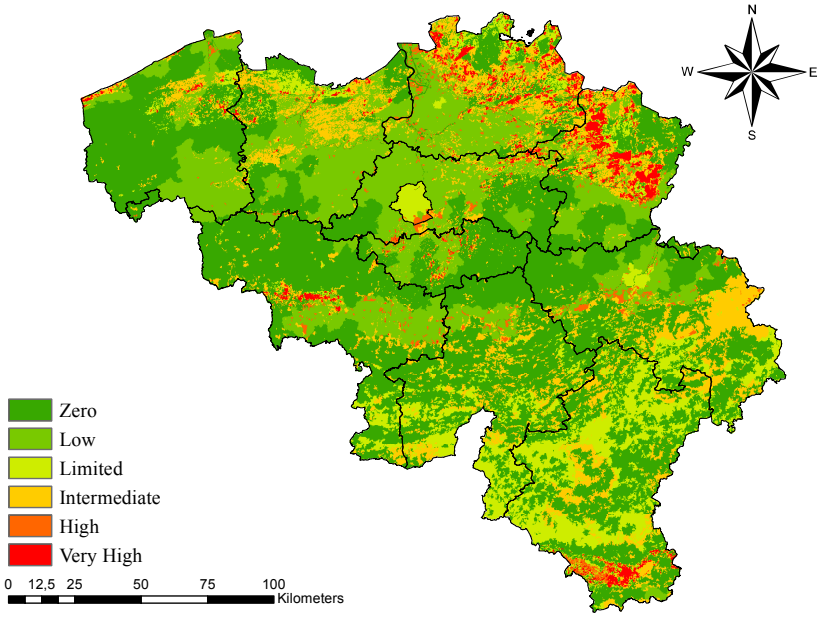

Figure 3.10: The wildfire risk, calculated with Eq. (3.11).

Discussion

The use of additional predictors affected the relative frequency of the risk classes across the government-designated risk areas and the Belgian territory, as compared to the risk map obtained using Eq. (3.10). The (very) high classified areas within the government-designated areas dropped from 56.95 to 38.85%, while the relative area of the (very) high risk class decreased (from 7.35 to 4.23%). This is good, since the total risk area should be kept as small as possible, without compromising the model accuracy, as discussed in Section 3.4. The

Table 3.9: The different risk classes according to the risk map corresponding to Eq. (3.11). The relative area of these risk classes across the government-designated risk areas and the Belgian territory is given, as well as the relative frequency of all observed ignitions across these risk classes.

Risk Class	P_{ignition} interval	Government (%)	Belgium (%)	Ignitions (%)
Extr. Low	0 – 0.1	8.66	47.20	7.28
Very low	0.1 – 0.2	4.66	22.70	8.05
Low	0.2 – 0.4	8.55	11.36	12.26
Intermediate	0.4 – 0.6	39.28	14.51	25.29
High	0.6 – 0.8	0.49	1.55	7.28
Very High	0.8 – 1.0	38.36	2.68	39.85

relative frequency of the ignitions assigned to the (very) high risk class also dropped from 57.47 to 47.13, which is not so drastic and can be explained by the decrease in size of the (very) high-risk designated areas.

3.4 Overview of the Different Techniques

In this chapter, five different wildfire risk maps for the Belgian territory were constructed. Three of them, the probability-based risk map (Section 3.2) and the two modified logistic regression equations (Section 3.3) were constructed using a training dataset, selected from the 261 ignition points. No such training set was needed for the construction of the Belgian RIW and the original equation because they were an expert system or already given, respectively. The Belgian RIW (Section 3.1) produced a score between 0 and 180 that is supposed to be proportional to the real probabilities, as opposed to the other methods that give rise to a qualification of the fire risk in terms of a probability.

3.4.1 Predictive Power

In order to enable comparisons between the five approaches, three measures were calculated for each of them. The first being the overall accuracy (Table 3.10). This was calculated by binarizing each risk map using a cut-off value. Every score higher than the cut-off value is replaced by '1' (fire prone), every lower score by '0' (non-fire prone). The accuracy was assessed by means of a validation dataset, consisting of 10% of the total number of observed ignition points and twice as many random locations, in agreement with the method outlined by Catry et al. (2009). In the case of the Belgian RIW and the original regression equation by Catry et al. (2009), all ignition points could be used (since there was no need for a training dataset). Ultimately, the accuracy was calculated as the number of ignition and non-ignition points, corresponding to '1' and '0' on the risk map, respectively, divided by the total number

of (non) ignition points in the validation dataset. For the Belgian RIW, areas with a score lower than 90 were considered non-fire prone and vice versa. The cut-off value for the method relying on Bayes' theorem was 0.031×10^{-3} in order to maximize the accuracy (Figure 3.11), while the cut-off value of the regression equations was $P_{\text{ignition}} = 0.50$.

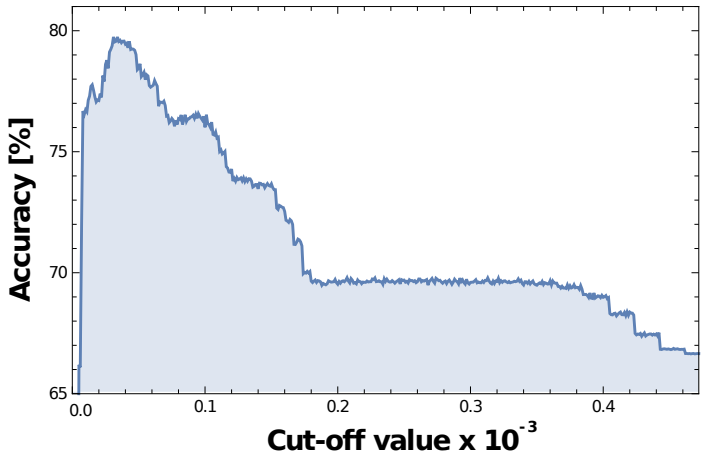

Figure 3.11: The mean accuracy of the risk map based on Bayes' theorem versus the cut-off value, used for its binarization.

The second statistic is the total risk area. This was equal to the area classified as '1' on the binarized risk map. The relative total risk area (Table 3.10) reflects also the relative number of commission errors or false positives (E_{co}), i.e. the percentage of random locations, wrongfully assigned the score '1'. The fact that the relative total risk area and the percentage of commission errors are equivalent can be explained by the manner in which the non-ignition points are generated. The underlying idea is that wildfires do not occur frequently. Hence, when a random point is generated, the odds are very small that this location is fire prone. The total risk area should be as small as possible, without compromising the model accuracy. This way, users of the risk map can spread their means over a smaller area.
The last measure is the relative number of omission errors or false negatives E_{om}, i.e. the percentage of ignition points, wrongfully assigned the score '0'. This statistic is heavily influenced by the total risk area. When, for example, the cut-off value used for the binarization would be 0, the relative total risk area would be 100% and E_{om} would be 0%. E_{co} would be 100%, yielding an overall accuracy of 33,3%, since one third of the validation points are ignition points. The impact of the chosen cut-off value on the overall accuracy is therefore very high. For example, when the total risk area diminishes, the number of ignition points that are classified as such, will lower as well. This is compensated by a decreasing commission error, since the non-ignition points are randomly selected and this error is expected to be the percentage of the area classified as fire prone. Choosing a cut-off value in the case of the

Bayes' theorem model of 0.100×10^{-3}, E_{om} increases from 47.51 to 73.99% with only a small decrease in risk area (from 6.24 to 2.73%), lowering the accuracy from 79.74 to 76.2%.

3.4.2 Advantages versus Disadvantages

An advantage of the original risk map (Figure 2.4) and the Belgian RIW (Figure 3.3) is that expert knowledge is needed to give an idea of the fire risk. The construction of these risk maps was based on the experience of fire fighters and other experts. Their disadvantage, however, is that no quantification was done of the risk that 'a fire will ignite and spread uncontrollably'. The approach using Bayes' theorem model and the regression equations do qualify this risk in terms of ignition probabilities between [0,1]. Allas, there were not enough ignition data present to incorporate more than two predictors in the approach with Bayes' theorem. Eqs. (3.10) and (3.11) incorporated at least four predictors, though some of them appeared to be not significant and were discarded. Table 3.10 summarizes the differences, strengths and weaknesses of the five approaches.

Table 3.10: An overview of the five different wildfire risk maps that were constructed in this chapter.

Approach	**Accuracy (%)**	**Total Risk Area (%)**	E_{om} (%)	**Advantages**	**Disadvantages**
Government	72.1	1.41	80.8	• Expert knowledge • Small total risk area	• No probabilities • No underlying data
Belgian RIW	76.3	13.47	60.15	• Expert knowledge	• No probabilities • High % omissions • No underlying data
Bayes	79.7	6.24	47.51	• Observed probabilities • Small total risk area	• Only 2 predictors • High % omissions
Equation by Catry et al. (2009)	58.5	25.22	77.4	• Multiple predictors • Calculates probability	• Inaccurate
Regression using LC & Population	80.3	10.70	39.08	• High accuracy • Calculates probability • Multiple predictors	• Large total risk area
Regression using LC, Population & Soil	81.0	8.46	45.2	• High accuracy • Calculates probability • Multiple predictors	• Large total risk area

The approach using Bayes' theorem appears to be the best one as it has the lowest total risk area and still a high accuracy. Furthermore, it is the only model that represents the real ignition probability.

3.4.3 Recommendations for Future Data Collection

The collection of the dataset was time consuming. None of the ignitions in the dataset provided by the Directorate-General of the Federal Public Service Internal Affairs was accompanied with geographical data, so these had still to be requested in order to do a geographical analysis. But even after this request, the provided geographical data were still not very accurate; in most cases only the address of the nearest house was given. In the future it should be possible for firefighters to register coordinates at the scene using a GPS and transmit them into a database. This would be more efficient, not only for wildfires, but also for all kinds of interventions. Every intervention, depending on its nature, is assigned a code by the involved commander. Allas, it occurs often that a wrong code is assigned to a wildfire, causing a loss of data. The opposite can also occur. for example an intervention for the controlled burning of biomass in some garden was sometimes assigned the code 1.6.2, indicating there was a wildfire.

CHAPTER 4

Simulating the Baelen Wildfire with FARSITE

The development of this wildfire model was initiated in 1994 by Mark A. Finney and funded by the USDA Forest Service and other organizations[1] (Finney, 2004). FARSITE is considered as one of the most accurate wildfire simulators worldwide. The reason for this is the detailed input and output, which distinguishes FARSITE from most other simulators. What is more, it supports data from geographic information systems (Papadopoulos, 2011). It incorporates five components: a surface fire spread model, a crown fire spread and initiation model, a spotting model, and a dead fuel moisture model. In this chapter, first the surface fire spread model and the crown fire spread and initiation model will be discussed. Secondly, the predictive power of FARSITE will be tested on the case of the wildfire in Baelen, Belgium, April 26 – May 1, 2011. (Finney, 1999). The software used in this chapter is FARSITE version 4.1.055 and is freely available[2]. This version was released in May 2008. The software package ArcMap (Version 10.2.2, Esri, USA) was used for the visualization of the results.

4.1 Surface Fire Spread Model

This model is based on Huygens' principle of wave propagation. This principle states that a disturbed medium (at $t_0 = 0$) will give rise to a spherical wave of disturbance at a distance which is the product of the speed of this wave, for example the speed of light in a particular medium, and the time elapsed at t_1 since t_0. Every affected point at t_1 is then a seed from which a new wave of disturbance originates (Baker and Copson, 2003). The same principle can be applied to the propagation of a fire front. Hence, every point along the fire front (these are referred to as a *vertex*) initiates a new spherical wave every time step (Figure 4.1). When

[1] the USDI National Park Service, the National Interagency Fire Center, the Intermountain Fire Sciences Laboratory, the Fire Behavior Research Work Unit (Cooperative Agreements INT-93854-RJVA and INT-95065-RJVA) and the Forest Service Washington Office Fire and Aviation Management

[2] at `http://www.firelab.org/document/farsite-software`

there is no effect of wind and slope, the fire front will be circular. Otherwise, the fire front is expected to be elliptical.

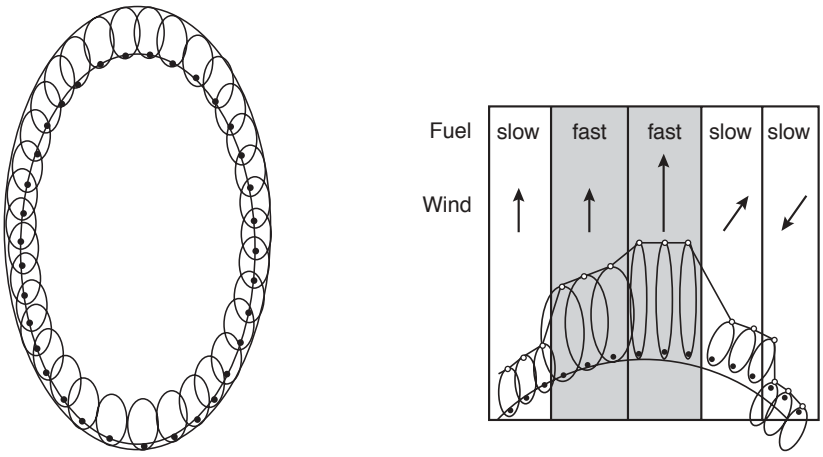

(a) (b)

Figure 4.1: Illustration of Huygens' principle in the setting of wildfires: with elliptical waves (a) and illustration when wind and fuel are nonuniform (b) (Finney, 2004).

Based on the principle of Huygens, Richards (1990) developed the following equations to compute the orthogonal spread rates x and y [m min^{-1}]:

$$\frac{dx}{dt} = \frac{a^2 \cos\theta(x_s \sin\theta + y_s \cos\theta) - b^2 \sin\theta(x_s \cos\theta - y_s \sin\theta)}{\sqrt{b^2(x_s \cos\theta + y_s \sin\theta)^2 - a^2(x_s \sin\theta - y_s \cos\theta)^2}} + c \sin\theta, \tag{4.1}$$

$$\frac{dy}{dt} = \frac{-a^2 \sin\theta(x_s \sin\theta + y_s \cos\theta) - b^2 \cos\theta(x_s \cos\theta - y_s \sin\theta)}{\sqrt{b^2 (x_s \cos\theta + y_s \sin\theta)^2 - a^2 (x_s \sin\theta - y_s \cos\theta)^2}} + c \cos\theta, \tag{4.2}$$

where x_s and y_s [m] encode the direction normal to the fire front, which is corrected in the case of a sloping terrain. The parameter θ ($0 < \theta < 2\pi$) is the direction of maximum fire spread and is governed by the wind and slope. The shape of the ellipse is determined by a, b and c (Figure 4.2), which depend on the ROS R [m min^{-1}] (Richards, 1990, 1995):

$$a = 0.5 \frac{R + \frac{R}{H}}{L}, \tag{4.3}$$

$$b = 0.5 \left(R + \frac{R}{H} \right), \tag{4.4}$$

$$c = b - \frac{R}{H}, \tag{4.5}$$

with L [-] the length-to-width ratio of the fire ellipse and H [-] the head-to-back ratio (Alexander, 1985), given by

$$L = 0.936\, e^{(0.2566\,\tilde{U})} + 0.461\, e^{(-0.1548\,\tilde{U})} - 0.397 \tag{4.6}$$

and

$$H = \frac{L + \sqrt{(L^2 - 1)}}{L - \sqrt{(L^2 - 1)}}, \tag{4.7}$$

respectively, where $\tilde{U}$ is the virtual windspeed [m s^{-1}], combining the effect of the wind and the slope.

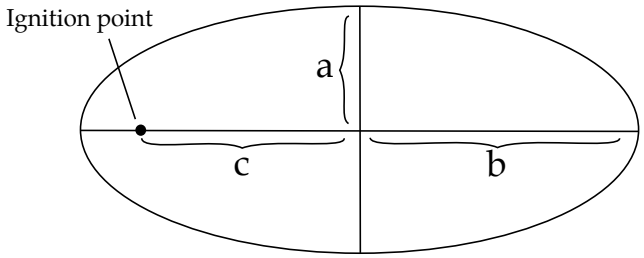

Figure 4.2: Meaning of the parameters *a, b* and *c* in Eqs. (4.1) and (4.2).

The ROS R [m min^{-1}] in Eqs. (4.3) – (4.5) is determined by the rate at which heat is transferred and accumulated in unburnt fuel (Johnson and Miyanishi, 2001). For surface fires, Rothermel (1972) proposes:

$$R = \frac{I_R\, \xi (1 + \Phi_s + \Phi_w)}{\rho_b\, \epsilon_h\, Q_{\text{ig}}}, \tag{4.8}$$

where I_R is the reaction intensity [kJ min^{-1}m^{-2}], ξ the propagating flux ratio [-], ρ_b the oven dry bulk density [kg m^{-3}], ϵ_h the effective heating number [-] and Q_{ig} the heat of pre-ignition [kJ kg^{-1}]. Finally, Φ_s and Φ_w are the dimensionless coefficients for slope and windspeed (Wilson, 1980; Rothermel, 1972):

$$\Phi_s = 5.275\, {\beta_r}^{-0.3} (\tan\theta_s)^2, \tag{4.9}$$

$$\Phi_w = C\, (3.281\, U)^B \left(\frac{\beta_r}{\beta_{\text{op}}}\right)^{-E}, \tag{4.10}$$

where θ_s [-] is the slope in radians, β_r is the packing ratio and β_{op} [-] the optimum packing ratio of the fuel bed, U [m s^{-1}] the midflame windspeed (defined by Rothermel (1991) as 1/2 speed of open wind) and C, B and E are functions of the fuel particle size (Burgan, 1987;

Rothermel, 1972). The fire line intensity I_b [kW m^{-1}] describes the rate of energy release per unit length of the fire front (Byram, 1959) and is calculated in FARSITE as (Wilson, 1980):

$$I_b = 0.21 \frac{I_R\, R}{\sigma}, \tag{4.11}$$

where σ [m^{-1}] is the characteristic surface area to volume ratio of the fuel bed.

4.2 Crown Fire Initiation and Spread Model

Equation (4.12) uses the crown base height h_{base} [m] and the crown foliar moisture content M [% on dry weight basis] to determine the threshold value I_0 [kW m^{-1}] for I_b, above which a crown fire starts:

$$I_0 = (0.010\, h_{\text{base}}\, (460 + 25.9\, M))^{\frac{3}{2}}. \tag{4.12}$$

A crown fire starts when $I_b > I_0$. Different types of crown fires can be distinguished: passive, active and independent crown fires. A passive crown fire means that individual trees or small groups of trees burn, but there is no solid fire in the canopy. During an active crown fire, the whole canopy is consumed by flames, but the combustion still depends on the heat released from surface fires. An independent crown fire produces enough heat to sustain itself (Scott and Reinhardt, 2001; Van Wagner, 1989). Alexander (1988) defines the active crown fire spread rate R_{active} as:

$$R_{\text{active}} = \frac{3}{l_{\text{crown}}}, \tag{4.13}$$

where l_{crown} is the crown bulk density [kg m^{-3}] and the factor 3 a dimensional constant [kg m^{-2} min^{-1}]. The R_{active} can be used to identify the crown fire type (Van Wagner, 1977), as indicated in Table 4.1.

Table 4.1: Classification of crown fires.

Type	ROS	Energy flux
Passive	$\tilde{R}_{\text{active}} < R_{\text{active}}$	
Active	$\tilde{R}_{\text{active}} \geq R_{\text{active}}$	$E_{\text{actual}} < E_0$
Independent	$\tilde{R}_{\text{active}} \geq R_{\text{active}}$	$E_{\text{actual}} > E_0$

In Table 4.1, E_{actual} and E_0 are the actual and critical energy flux, and $\tilde{R}_{\text{active}}$ the actual active crown fire spread rate. Independent crown fires are short lived and very rare, thus not incorporated in FARSITE. A passive crown fire has the same rate of spread as a surface fire, hence FARSITE only has a spread model dedicated to active crown fires. The actual active crown fire spread rate $\tilde{R}_{\text{active}}$ is determined as:

$$\tilde{R}_{\text{active}} = R + F_t\, (R_{\max} - R), \tag{4.14}$$

given $\tilde{R}_{\text{active}} \geq$, and

$$R_{\max} = 3.34\, R_{10}\, E_i, \tag{4.15}$$

where $3.34\, R_{10}$ [m min^{-1}] is the active crown fire spread rate, correlated with the forward surface fire spread rate ROS from model 10 of Anderson's fuel model, using a 0.4 wind reduction factor (Rothermel, 1991). The factor E_i [-] in Eq. (4.15) is the fraction of the ROS in the direction of the fire propagation in the vertex and the ROS in the maximum spread direction. The fraction of trees that take part in the crown fire phase is given by (Van Wagner, 1993; Forestry Canada Fire Danger Group, 1992):

$$F_t = 1 - e^{a_c\,(R - R_0)}, \tag{4.16}$$

with

$$a_c = \frac{-\log_e(0.1)}{0.9\,(R_{\text{active}} - R_0)}, \tag{4.17}$$

and

$$R_0 = I_0\,\frac{R}{I_b}. \tag{4.18}$$

Finally, the intensity of an active crown fire I_c is defined as:

$$I_c = 300\left(\frac{I_b}{300\,R} + F_t\, l_{\text{crown}}\,(h_{\text{crown}} - h_{\text{base}})\right)\tilde{R}_{\text{active}}, \tag{4.19}$$

where h_{crown} [m] is the crown height. For passive crown fires, $\tilde{R}_{\text{active}}$ is replaced by R.

4.3 Case Study on the Wildfire in Baelen, Belgium, 2011

In this section, the predictive power of FARSITE is tested on the case of the wildfire in Baelen, Belgium, 2011. The fire started on April 25, 5.30 p.m. The fire was reported to be under control on April 26, 5.30 p.m. in the High Fens (Belga, 2011), although the growing perimeter (see Figure 4.3), derived from MODIS satellite imagery, indicates the opposite. In total, an area of approximately 1400 ha burnt. No crown fires were reported, so only the surface fire spread model is enabled (see Section 4.1). The cause of the ignition remains unknown to this day, despite an inquiry of the firefighters. Hypotheses vary from lightening to careless smokers. The latter seems the most reasonable explanation, considering the proximity of walking trails. The location of the ignition point is believed to be in the north-east corner of the initial perimeter.

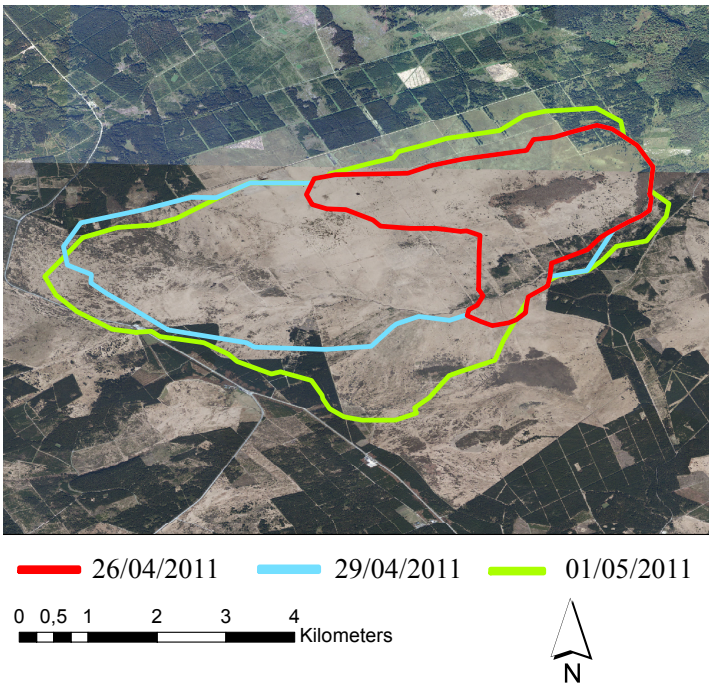

Figure 4.3: The observed perimeters, registered with MODIS, of the wildfire in Baelen on 26/04/2011 (415 ha), 29/04/2011 (1077 ha), and 1/05/2011 (1399 ha).

4.3.1 Study Area: The High Fens

The High Fens is a nature reserve in the east of Belgium, near the city of Eupen, in Baelen. The area consists of bogs and fens and is characterized by herbs like *Molinia caerulea* and *Erica spp.* (see Figure 4.4) and trees like *Betula spp.*, *Pinus sylvestris* and *Picea abies*.

(a) *Molinia caerulea* (b) *Erica spp.*

Figure 4.4: A tussock of *Molinia caerulea*, burnt during the wildfire in 2011 (a) and *Erica spp.* (b).

The aforementioned herbs are very prone to fire. However, *Molinia* can recover more quickly after wildfires and thus takes advantage of them. Despite the above average rainfall (1300 mm/year),

the vegetation dries out very easily because of the fast infiltration of rain water (Berendsen, 2008). During periods of drought, especially during April and May, the area is very sensitive to wildfires. The most recent, large wildfire took place in 2011. Five years after this event, the consequences are still visible on the terrain through burnt trees that remained standing. Figure 4.5 (a) shows the location of the final fire front. On the left side of this figure, there are many dead and burnt trees, while on the right, the vegetation looks perfectly healthy. The river Helle is displayed in Figure 4.5 (b).

(a) Fire front (b) Helle

Figure 4.5: The final fire front in the east on May 1, 2011 (a) and the river Helle (b).

This river corresponds more or less with the final wildfire perimeter in the east of the study area. This is no coincidence, as this river, in combination with a ridge created by the carving of the river in the landscape, formed an ideal place for fire suppression. The water and the downward slope of the ridge form natural barriers.

4.3.2 Methods

Landscape

In a first step, a virtual landscape had to be generated with the FARSITE *Landscape (LCP) File Generator*. This landscape required at least five data layers to simulate a ground fire: elevation, slope, aspect, fuel, and canopy cover. The elevation (the slope and aspect were derived from it), was provided by the Belgian NGI.
The vegetation was classified according to Anderson's Fuel Models (Table B.1) (Anderson, 1982; Rothermel, 1972; Albini, 1976) and derived from CORINE satellite imagery. Since there were no geographical data on the canopy cover, the following assumptions were made:

1. grass and grass-dominated fuel complexes: 0% canopy cover;
2. chaparral and shrub fields fuel complexes: 1 – 20% canopy cover;
3. timber litter fuel complexes: 50 – 80% canopy cover.

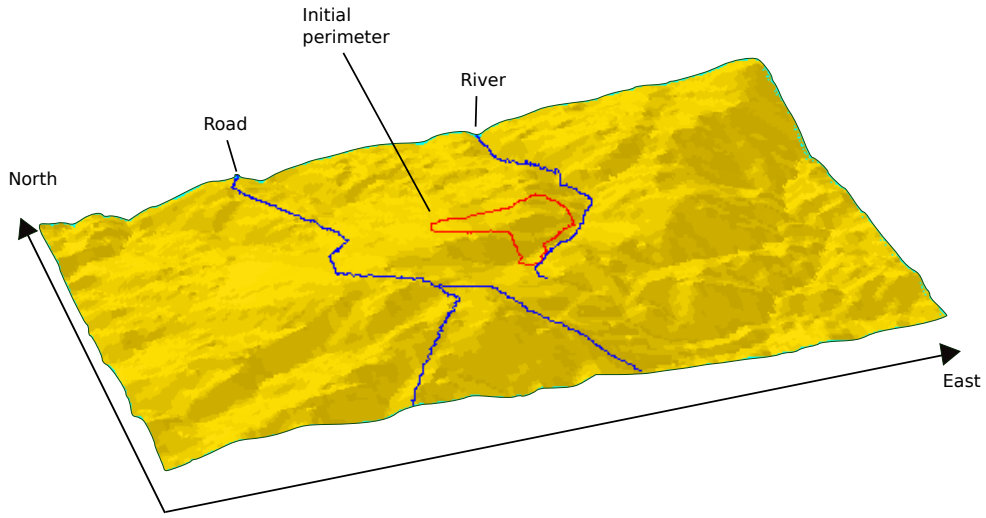

Figure 4.6: A DTM of the study area. The main road, the initial ignition polygon and the river Helle are also displayed.

The spatial resolution of the fuel map, one hectare, was lower than the actual distribution of the different fuel models. After all, in a raster cell on the fuel map, that was classified as coniferous forest, there could be still patches of grass or decidious trees in reality, associated with lower or higher values for the ROS (Eq. (4.8)). To compensate for this, the adjustment file was defined. For each fuel model, this file had to be assigned a value, greater than zero (Finney, 2004). An adjustment value of 0.7 for fuel model 1, for example, slowed down the ROS in this model by 30% during the simulations. As can be seen on Figure 4.6, there were two barriers that could halt the wildfire: a road and the river Helle, east and west of the initial perimeter, respectively.

After generating this virtual landscape, environmental data had to be supplied, namely temperature, rainfall, wind, and initial fuel moisture data (see Figure 4.7). The construction of the corresponding data files is explained and illustrated for the Baelen case in Appendix B. As the wind speed and direction fluctuated significantly over time, their low temporal resolution could cause over- or underestimations of the true ROS.

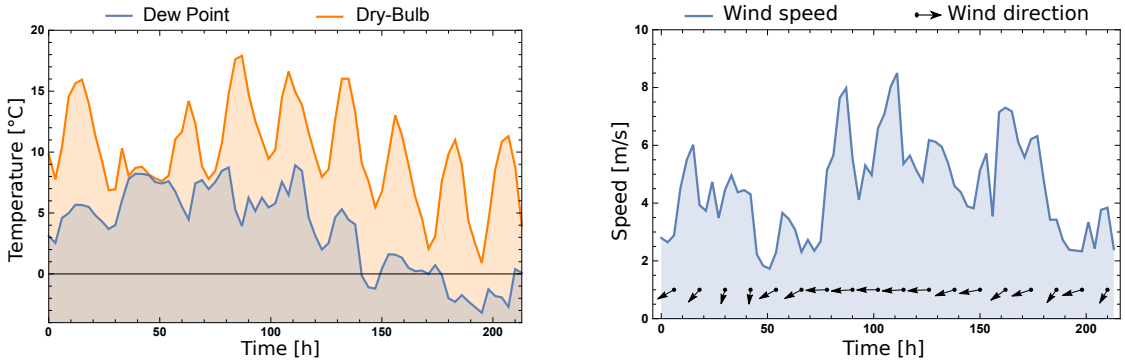

(a) (b)

Figure 4.7: The weather in Baelen from 26/4/2011 00:00 to 5/5/2011 00:00: the wind speed and wind direction (a) and the dry-bulb temperature and dew point temperature (b)

Settings

The time step for the simulation was set to two hours. The perimeter and distance resolution were both set to 30 meter. The crown fire simulation was disabled, since the wildfire of Baelen only consumed grass and shrubland. The simulation started on 26/04/2011 12.00 p.m. and ended on 01/05/2011 12.00 p.m. An adjustment factor of 0.7 for every fuel model was applied. This factor was set to optimize the agreement between the observed and simulated perimeters.

4.3.3 Results and Discussion

The simulated and observed perimeters on 26/04/2011 and 01/05/2011 are displayed in Figure 4.8. Table 4.2 summarizes the confusion matrices on these days. These matrices give the number of correctly classified cells within a radius of 3 km from the initial perimeter, as well as the false positives and negatives on 29/04/2011 and 01/05/2011.

Table 4.2: The false positives and negatives on 29/04/2011 and 01/05/2011, according to the FARSITE simulation. The columns show the relative number [%] of observed burnt and unburnt pixels, the rows the relative number [%] of simulated burnt and unburnt pixels.

(a) 29/04/2011

	observed	
simulated	**0**	**1**
0	76.35	7.10
1	6.07	10.48

(b) 01/05/2011

	observed	
simulated	**0**	**1**
0	68.76	2.79
1	8.41	20.04

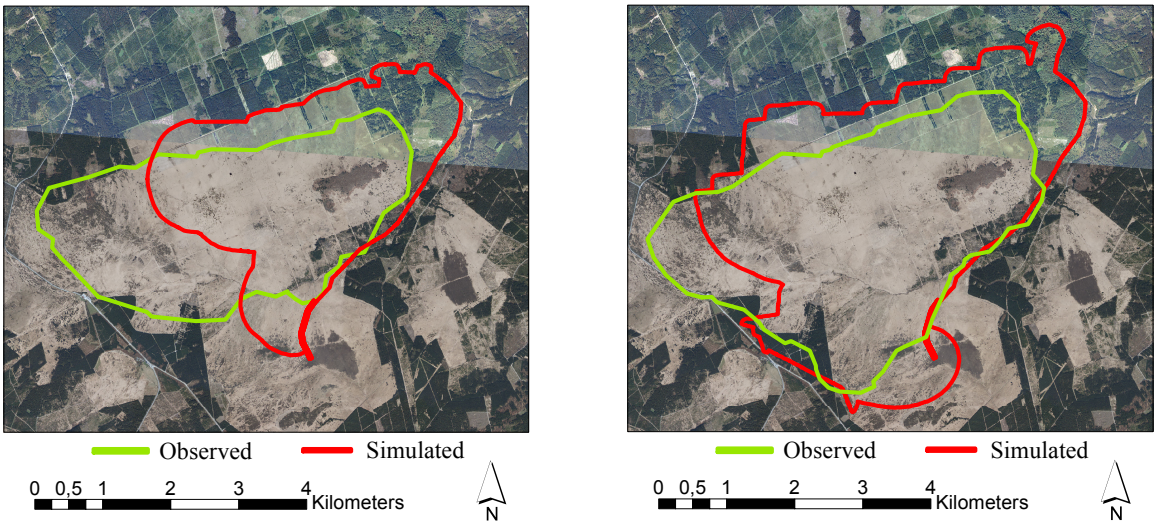

(a) 29/04/2011 (b) 01/05/2011

Figure 4.8: The observed and simulated wildfire perimeters on 29/4/2011 12:00 p.m. (a) and 01/5/2011 12:00 p.m. (b). The simulations were performed in FARSITE.

The percentage of correctly classified pixels within a radius of 3 km from the initial perimeter was 87.8%. The result depends on the adjustment factor which had to be set in agreement with the observed and simulated perimeters. Moreover, fire suppression activities had taken place since the ignition of the fire. In reality, the largest area (1000 ha) was burnt within the first 24 hours after ignition (Belga, 2011), and the fire probably did not expand much farther afterwards due to the actions of the firefighters. In fact, more than 300 firefighters were present (Belga, 2011). Unfortunately, no perimeter was registered at the moment the fire was under control (April 26, 5.30 p.m.).

The simulated perimeter on 29/04/2011 clearly underestimates the wildfire spread to the west. The percentage of false negatives is therefore high (7.10%). Between April 29 and May 1, there was a strong wind blowing towards the west, hence the simulated perimeter at 01/05/2011advanced strongly in this direction, while the observed perimeter shows that the fire had stopped spreading to the west on April 29. Probably, this is because of fire suppression activities. The result is that the simulated perimeter caught up with the observed perimeter, and on 01/05/2011, the percentage of false negatives is only 2.79%. Both on 29/04/2011 and 01/05/2011, the simulated perimeter overestimated the spread towards the north and the east.

Essentially, since in reality the largest expansion on the fire took place within the first 24 hours, one could argue that FARSITE modeled the ROS too slow, perhaps due to the use of the wrong fuel models. In the future, customized fuel models should be designed for the area,

in order to enable more realistic simulations of the ROS. The main disadvantage of FARSITE is that a vast amount of data have to be provided, contrary to some CA-based models which only need elevation and wind data (see Chapter 5). The computing time for a single run is less than 10 minutes, so this does not pose any problems for using FARSITE in real-time. Moreover, different scenarios can be implemented very easily and intuitively. The ignition point, for example, can be indicated manually on the map in the FARSITE GUI.

CHAPTER 5

Spatially explicit modeling of a wildfire in Belgium (Baelen, BE)

In the first section, an introduction to CA-based models is given. Next, the model, proposed by Alexandridis et al. (2008) is discussed in detail and used to simulate the wildfire in Baelen, Belgium, 2011. This model suffers from some drawbacks, hence, a novel CA-based model is proposed in Section 5.3. To conclude this chapter, a sensitivity analysis is performed for the latter model in order to determine the relative importance of the different parameters. The software packages used in this chapter are Mathematica (Version 10.0, Wolfram Research Inc., USA) and ArcMap (Version 10.2.2, Esri, USA).

5.1 CA-based models

Sun et al. (2013) characterize CA-based models by four aspects:

1. the neighborhood N_i of each cell c_i;
2. the state set S;
3. the multidimensional CA space X, consisting of cells c_i, and
4. the CA local rule or transition function F.

Typically, a Moore neighborhood is used, i.e. a cell, tesselated in a 2D square, has four adjacent and four diagonal neighbors (Moore, 1969). Encinas et al. (2007) propose a CA-based model with hexagonal cells, in order to overcome distortions of the fire shape.
The state set S is finite, i.e. $S =$ {burning, not burning}. When the state set S is infinite, for example in the models proposed by Yassemi et al. (2007), Encinas et al. (2007), and Sun et al. (2013), the model is not longer called a CA s.s., but a coupled-map lattice or continuous CA (see Table 2.3).

The CA space X consists of cells c_i that can be described by one or more features (e.g. wind speed and direction, slope, vegetation, ...). In the remainder, $S(c_i, t)$ denotes the state of a cell c_i at time step t.
The transition rule F is used to calculate the transition of a cell's state during a discrete time step Δt. A deterministic F will always give the same result, when started from the same initial conditions, whereas a stochastic F renders a different result for every run. Such a CA-based model was proposed by Alexandridis et al. (2008) and is discussed in the Section 5.2. A stochastic approach makes it possible to model spotting as well.
The duration of a time step Δt can be constant or adapted after each step. Examples of CA-based models with variable time step duration are proposed by Peterson et al. (2009) and Trunfio et al. (2011). Such an approach ensures that flames do not propagate beyond any of its neighbors during one time step.

5.2 Model by Alexandridis et al. (2008)

5.2.1 Model formulation

Alexandridis et al. (2008) propose a CA-based model using a square two-dimensional grid. Each cell can have one of a finite number of states:

State 1: the cell contains no forest fuel;

State 2: the cell contains forest fuel but is not ignited;

State 3: the cell contains forest fuel and is burning, and

State 4: the cell contains burnt forest fuel.

The transition function is given by:

$$S(c_i, t+1) = \begin{cases} 1\ , & \text{if } S(c_i,t) = 1, \\ 4\ , & \text{if } S(c_i,t) = 3, \\ 4\ , & \text{if } S(c_i,t) = 4, \\ 3\ , & \text{if } |\{j, j\neq i\,|S(c_j,t) = 3\}| = 1,\ S(c_i,t) = 2. \end{cases} \tag{5.1}$$

The first item in Eq. (5.1) implies that a cell with no fuel remains like that, while the second one learns that a cell can only burn during one time step, after that, no more fuel is left, and the third one that when a cell is completely burnt down, it cannot produce new fuel within the short time range that is modeled with the CA. The fourth item implies that a burning cell can pass the flames onto each of its eight neighboring cells with probability p_{burn}.

The probability p_{burn} is calculated as

$$p_{\text{burn}} = p_h\,(1 + p_v)\,(1 + p_d)\,p_w\,p_s, \tag{5.2}$$

where p_h is the probability that a burning cell will pass a wildfire onto an adjacent, unburning cell, given a certain type of vegetation in the absence of wind and slope. The parameters p_v and p_d are the fire propagation probabilities that depend on the vegetation type and density, respectively. The probabilities p_s and p_w depend on the slope and wind, respectively. The former is given by

$$p_s = e^{\alpha_1\,\theta_s}, \tag{5.3}$$

where α_1 [radian^{-1}] is a constant and θ_s [radian] is the slope:

$$\theta_s = \tan^{-1}\left(\frac{E_1 - E_2}{l}\right) \tag{5.4}$$

in the case of adjacent cells, and

$$\theta_s = \tan^{-1}\left(\frac{E_1 - E_2}{l\sqrt{2}}\right) \tag{5.5}$$

in the case of diagonal cells, where E_1 and E_2 [m] are the elevation of the cell and its neighboring cell, respectively, and l [m] is the width of one cell. Finally, p_w follows from

$$p_w = e^{V\,(\alpha_2 + \alpha_3\,(\cos\,(\theta) - 1))}, \tag{5.6}$$

where V is the wind speed [m s^{-1}], α_2 [s m^{-1}] and α_3 [s m^{-1}] are constants and θ [radian] is the difference between the angle of the wind direction and the angle between the neighboring cells. Every cell has eight neighbors, each of which can ignite this cell with a probability p_{burn}. Alexandridis et al. (2008) do not provide a method to combine these probabilities in order to obtain the overall probability p_{total} that this cell will ignite. Essentially, this probability is complementary to the probability that none of the eight neighbors will pass on the fire, or

$$p_{\text{total}} = 1 - \prod_{c_j \in N_i} (1 - p_{\text{burn},j}). \tag{5.7}$$

5.2.2 Simulation of the Wildfire in Baelen, Belgium, 2011

Calibration

The implementation of the CA-based model proposed by Alexandridis et al. (2008) (Section 5.2) required the calibration of six parameters: p_{h} [-], p_{veg} [-], p_{den} [-], α_1 [radian^{-1}], α_2 [s m^{-1}], and α_3 [-]. However, the factor $p_{\text{h}}\,(1 + p_{\text{veg}})\,(1 + p_{\text{den}})$ in Eq. (5.2) was replaced by a

single parameter α_0 [-], so assuming that the vegetation was homogeneous across the entire study area, so Eq. (5.2) collapses to:

$$p_{\text{burn}} = \alpha_0 \, e^{\alpha_1 \, \theta_s} \, e^{V \, (\alpha_2 + \alpha_3 (\cos(\theta) - 1))}, \tag{5.8}$$

Hence, only four constants were left to be determined: α_0, α_1, α_2 and α_3. In addition to these four parameters, a fifth one, ϵ [-], was introduced in order to reflect how long it takes before a cell is completely burnt after ignition. This parameter is an addition to the original model of (Alexandridis et al., 2008), where a cell could only burn during one time step (Eq. (5.1)). This is an important aspect, since the longer a cell can burn, the more time it has to ignite neighboring, unburnt cells. Because of this, the number of time steps elapsed since the ignition is stored for each cell and updated after each time step.

The following objective function was used to determine the parameter set that minimizes the differences between the observed and simulated perimeters:

$$\Omega = \sum_{t}^{n} \sum_{ij}^{m} 1 - |S(c_i, j) - \tilde{S}(c_i, t)|, \tag{5.9}$$

where $S(c_i, t)$ and $\tilde{S}(c_i, t)$ are, at a certain moment t, the observed and simulated state of cell c_i at time step t, respectively. The right-hand side of Eq. (5.9) equals the sum of all cells where $S(c_i, t)$ equals the state of cell $\tilde{S}(c_i, t)$. In silico, the number of states was reduced to two, for the sake of the calibration: '0' for unburnt or unburnable cells, and '1' for burning or burnt cells. Unfortunately, only two wildfire perimeters were observed, on 29/04/2011 12:00 p.m. and 01/05/2011 12:00 p.m. Both of them were needed for the calibration, hence, no perimeters are left for validation. In order to account for the stochasticity of the model, 15 simulations were run for each parameter set and Ω was averaged over these. The maximization of the objective function was achieved by means of a 'hill climbing' algorithm of which the pseudocode is given in Algorithm 1.

Algorithm 1: Hill climbing algorithm

Result: Parameter set that maximizes Ω, averaged over 15 runs

$k \leftarrow 0$, $s \leftarrow 0$;

$Q_r(1)$ = randomly generated set of parameters, within range of possible values;

$Q_r(2) = \Omega(Q_r(1))$;

Q_n = 2×25 zeros matrix;

while $s = 0$ *and* $k < 10$ **do**

  for $i = 1 : 25$ **do**

    $Q_n(1, i)$= new randomly generated parameters within range $Q_r(1) \pm \frac{1}{1+t}$;

    for $j = 1 : 15$ **do**

      $M(j)$= $\Omega(Q_n(1, i))$;

    end

    $Q_n(2, i)$=mean(M);

  end

  if $\max_j(Q_n(2, j)) > Q_r(2)$ **then**

    $Q_r(1)$= $Q_n(1, \arg\max_j(Q_n(2, j)))$;

    $Q_r(2)$=$\max_j(Q_n(2, j))$;

    k++;

  else

    s=1;

  end

end

Results

The hill climbing algorithm was aplied 10 times, each time starting from a different, random parameter set in order to avoid local maxima. The algorithm yielded the following parameter values: $\alpha_0 = 0.9148$, $\alpha_1 = 1.94856$, $\alpha_2 = -1.93421$, $\alpha_3 = -2.07873$ and $\epsilon = 18$, and the objective function value $\Omega = 38179.5$. One time step takes two hours, so a cell can burn a total of 36 hours. Figure 5.1 shows the simulated perimeters on April 29, 2011 and May 1, 2011, and the time elapsed since the ignition of each cell. The model overestimated the fire spread towards the south on April 29, 2011, while the spread to the east was underestimated. The simulated perimeter for May 1, 2011, fits reasonably well with the observed one. Table 5.1 gives the percentage of correctly classified cells, as well as the false positives and negatives on 29/04/2011 and 01/05/2011, within a radius of 3 km from the initial perimeter. The radius was set to 3 km, because this was estimated as the largest distance the fire could spread in the simulated time period.

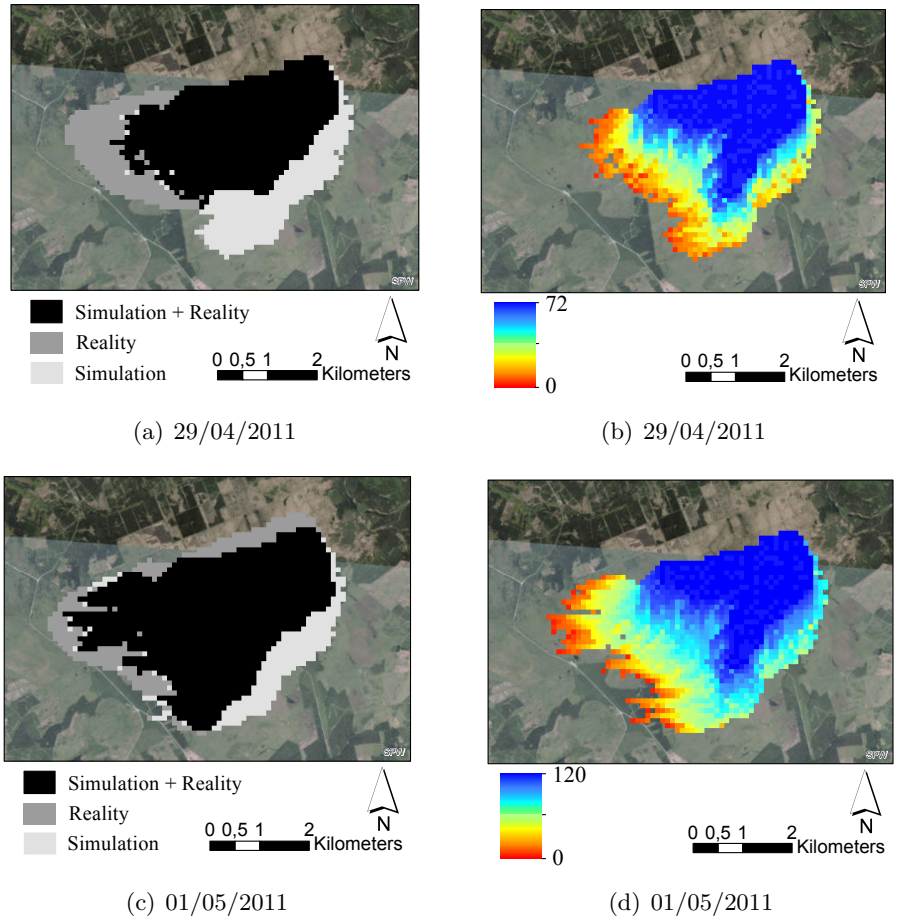

(a) 29/04/2011 (b) 29/04/2011

(c) 01/05/2011 (d) 01/05/2011

Figure 5.1: The simulated and observed wildfire perimeters (a, c) and the time [hours] elapsed since the cell's ignition (b, d), according to the CA-based model proposed by Alexandridis et al. (2008)

Table 5.1: Confusion matrices for the simulated perimeters on 29/04/2011 and on 01/05/2011 (Figure 5.1).

(a) 29/04/2011

	observed	
simulated	**0**	**1**
0	77.02	5.47
1	4.36	13.16

(b) 01/05/2011

	observed	
simulated	**0**	**1**
0	73.54	3.75
1	4.11	18.59

Discussion

The CA-based model provided accurate results. The average percentage of correctly classified cells on 29/04/2011 and 01/05/2011 for 15 runs of the model with the calibrated parameter

values, within a radius of 3 km from the initial perimeter, was 91.0%. Despite these good results, this model contains some flaws that are highlighted here.

First, the authors refer to five different probabilities in the right-hand side of Eq. (5.2), so their value should lie in the unit interval. Yet, this means that p_{burn} can take values in [0,4], which is meaningless since it is also a probability, and hence should take values between 0 and 1.

Furthermore, p_h is the probability that a burning cell will pass a wildfire to an adjacent, unburning cell, given a certain type of vegetation in the absence of wind and slope. In the case of a strong wind from a burning cell towards an unburning cell, it was expected that p_{burn} would be higher than p_h. But, since p_w lies between 0 and 1, p_{burn} will always have lower values than p_h, irrespective of the effects of the wind and slope.

A third weakness concerns the way the slope [radians], wind speed [m s^{-1}] and direction [radians] are converted to probabilities. Alexandridis et al. (2008) use the exponential function for this purpose (Eqs. (5.3) and (5.6)). The slope θ_s, however, varies between $-\frac{\pi}{4}$ and $\frac{\pi}{4}$. Hence, it is impossible to find a value of α_1 for which Eq. (5.3) would only yield values in [0,1]. To avoid this problem, the values of p_s had to be rescaled between 0 and 1. For what concerns Eq. (5.6), the problem was more complex. In order to get a value for p_w between 0 and 1, it has to hold that

$$\begin{aligned} V(\alpha_2 + \alpha_3 (\cos(\theta) - 1)) &\leq 0, \\ \alpha_3 (\cos(\theta) - 1) &\leq -\alpha_2, \end{aligned} \tag{5.10}$$

so, knowing that $\cos(\theta)$ takes values between -1 and 1 thus leads to the following system of inequalities:

$$\begin{cases} \alpha_2 \leq 0 \text{ and} \\ \alpha_2 \leq 2\,\alpha_3. \end{cases} \tag{5.11}$$

However, if α_2 was smaller than 0, problems would arise. For instance, suppose the wind blows from a neighboring cell towards the unburnt cell, i.e. $\theta = 0$. Then, Eq. (5.6) becomes

$$p_w = e^{-\alpha_2 V}, \tag{5.12}$$

so when the wind speed V increases, the probability p_w, and thus p_{burn} decreases, contradicting the basic physics of wildfire behavior. In Section 5.3, a new transition function is proposed, in order to avoid these flaws.

5.3 Improved CA-based model

5.3.1 Methods

A new model, similar to the model by Alexandridis et al. (2008) was proposed. The rationale behind this model is that if there is a very strong wind from a burning cell towards an unburnt cell on the one hand, and a very steep slope, on the other hand, the probability that this unburnt cell ignites should approach 1. The probability that a cell will burn in the next time step is

$$P_i^T = p_{\text{veg}} \left(1 - \prod_{c_j \in N_i} (1 - \tilde{P}_j) \right), \tag{5.13}$$

$$\tilde{P}_j = \nu_1 \, \nu_2, \tag{5.14}$$

$$\nu_1 = \frac{1}{1 + \gamma_1 \, e^{-\gamma_2 \, V_j \, \cos(\theta^j)}}, \text{ and} \tag{5.15}$$

$$\nu_2 = \frac{1}{1 + \gamma_3 \, e^{-\gamma_4 \, {\theta_s}^j}}, \tag{5.16}$$

where $\tilde{P}_j$ is the probability that the neighboring cell c_j will pass on a wildfire to the unburning cell c_i, regardless of the type of vegetation, ${\theta_s}^j$ is the slope of neighbor j, and θ^j is the difference between the angle of the wind direction and the angle between the cell and its neighbor j. The parameter p_{veg} accounts for the effect of the vegetation and lies between 0 and 1. Further, γ_1 [-], γ_2 [s m^{-1}], γ_3 [-] and γ_4 [radian^{-1}] are model parameters that need to be calibrated, and ν_1 and ν_2 are parametric functions that depend on these parameters and account for the wind and slope, respectively. Both ν_1 and ν_2 take values between 0 and 1. The effect of these parameters is illustrated in Figure 5.2. This plot shows that γ_2 and γ_4 influence the 'steepness' of the sigmoid curve, while γ_1 and γ_3 influence the intercept of the logit function.

A logistic regression equation, constructed with vegetation and soil texture as predictors for the dataset discussed in Section 2.4.2, is used to determine p_{veg}. In addition, there is still the parameter ϵ [-], the number of time steps a cell can burn.

5.3.2 Results

The logistic regression equation only includes categorical predictors 'vegetation' and 'soil texture' and is given by:

$$p_{\text{veg}} = \left(1 + \mathrm{e}^{-(-2.283 + 2.413\,x_1 + 1.884\,x_2 + 2.020\,x_3 + 2.545\,x_4 + 2.143\,x_5)} \right)^{-1}, \tag{5.17}$$

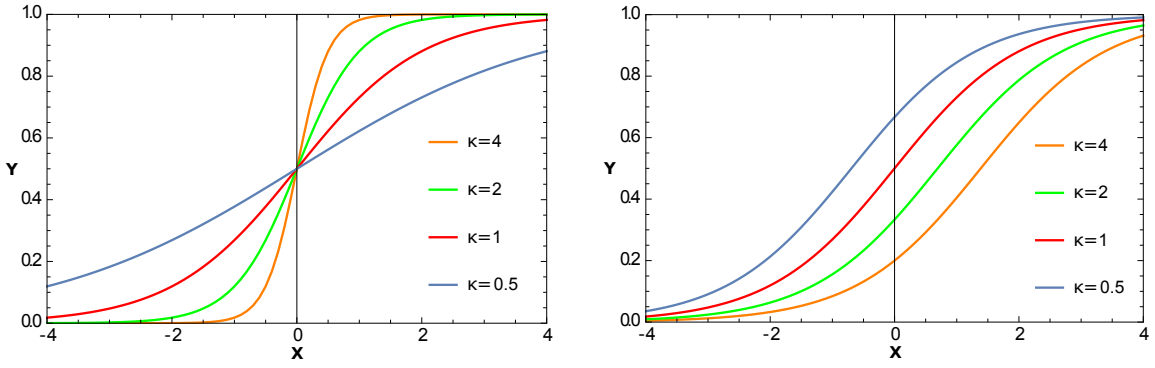

(a) $y = \left(1 + e^{-\kappa\, x}\right)^{-1}$ (b) $y = \left(1 + \kappa\, e^{-x}\right)^{-1}$

Figure 5.2: Effect of parameters γ_2 and γ_4 on the steepness of the logit function (a) and the effect of γ_1 and γ_3 on the intercept of the logit function(b)

where x_1 to x_4 are categorical variables, encoding the land cover classes shrubland, broadleaved forest, coniferous forest, and wetland, respectively. The variable x_5 encodes the sandy soil texture.

Through calibration using Algorithm 1 and the observed perimeters on April 29, 2011 and May 1, 2011, the following parameter values were found: $\gamma_1 = 9.28103$, $\gamma_2 = 7.9311$, $\gamma_3 = 6.60188$, $\gamma_4 = 5.65268$, and $\epsilon = 15$, and the objective function $\Omega = 38028.0$. Figure 5.3 shows the simulated perimeters on April 29, 2011 and May 1, 2011, and the elapsed time since ignition for each cell. Table 5.2 gives the percentage of correctly classified cells, as well as the false positives and negatives on 29/04/2011 and 01/05/2011, within a 3 km radius from the initial perimeter.

Table 5.2: Confusion matrices for the simulated perimeters on 29/04/2011 and on 01/05/2011 (Figure 5.3).

(a) 29/04/2011

	observed	
simulated	**0**	**1**
0	78.39	3.93
1	10.77	6.90

(b) 01/05/2011

	observed	
simulated	**0**	**1**
0	72.61	4.59
1	6.20	16.60

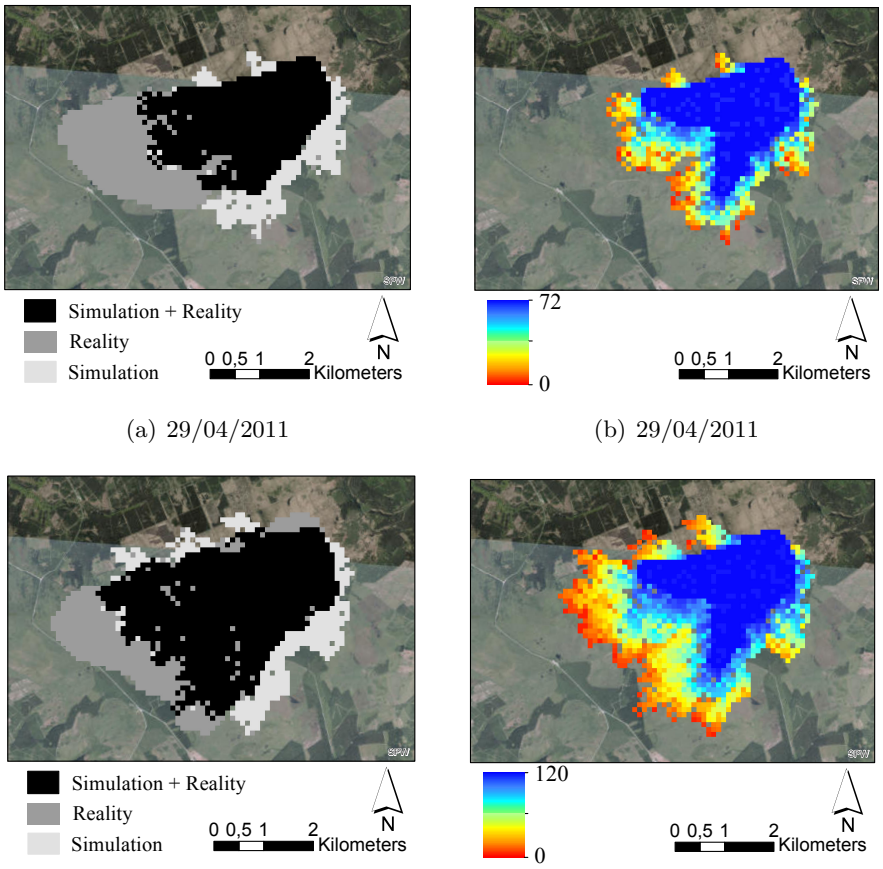

(a) 29/04/2011 (b) 29/04/2011

(c) 01/05/2011 (d) 01/05/2011

Figure 5.3: The simulated and observed wildfire perimeters (a, c) and the time [hours] elapsed since the cell's ignition (b, d), according to the CA-based model with the modified stochastic transition function.

5.3.3 Discussion

The average % of correctly classified cells on 29/04/2011 and 01/05/2011 within a 3 km radius from the initial perimeter, was 90.1%. The CA-based model clearly underestimated the observed perimeter, especially on April 29, just as the model by Alexandridis et al. (2008). Overall, its accuracy is slightly lower than the one reached with the model by Alexandridis et al. (2008). But it comes with the major advantage that the model structure and parameters are meaningful. The parameters have a positive value, despite of the sign of the slope and wind direction. For what concerns the underestimation of the perimeter, this can probably be attributed to the parameter p_{veg}, which was generally low with values between 0.093 and 0.565. Thus, one way to improve this model is to have better (higher) estimations of p_{veg}.

5.4 Sensitivity Analysis of the Improved CA-based Model

Saltelli et al. (2004) define a Sensitivity Analysis (SA) as the study of the attribution of the uncertainty in the inputs/parameters of a model, to the uncertainty in the outputs of this model. Hence, an SA can be used to enhance or simplify the model structure, to determine the minimum requirements for the data quality, and to identify critical regions in the space of model inputs/parameters. Two types of sensitivity analysis can be distinguished. The first is the local SA, used to quantify the effect of small variations of one particular model input/parameter on the output of this model. The second type, the global SA, considers all inputs/parameters simultaneously. A global SA can be applied to determine the hierarchy of the different inputs/parameters, according to their relative importance, i.e. their impact on the output of the model (Lilburne and Tarantola, 2009).

5.4.1 Global Sensitivity Analysis

In this section, a global SA was used to determine the relative importance of the five parameters in the CA-based model presented in Section 5.3. The relative importance was assessed by quantifying the impact of each parameter on a number of macroscopic quantities, derived from the model simulations. These quantities were the total burnt area, the circumference of the final perimeter, the ratio of the total area versus the circumference of the final perimeter, the average probability that a cell will burn during the next time step P_i^T across the study area at the end of the simulation, the maximum ROS, approximated as the largest distance between the terminal fire front and the initial perimeter, and finally, the horizontal and vertical coordinate of the centroid of the burnt area.
There is a wide variety of global SA techniques. Here, the global SA method, proposed by Sobol' (1993) was used. Some advantages of this approach are the fact that it does not require assumptions about the model structure, the exploration of the entire input/parameter space and the robust sensitivity rankings (Saltelli et al., 2004; Tarantola et al., 2006).

Methods

The method of Sobol' is used to decompose the variation in the tracked, simulated quantities. In a first step, two matrices Q and R, each consisting of 450 random parameter sets, were generated. This was achieved using Latin-Hypercube Sampling (McKay et al., 1979). For practical considerations, the sampling range of each parameter was set from 0 to twice its calibrated value (see Table 5.3).
Thus, both matrices Q and R have dimensions 450×5. In a second step, an auxiliary matrix R_i was constructed for each of the five parameters. This matrix was constructed by taking all columns of R, except for the i-th column, which was replaced by the i-th column of Q. The third step consisted of computing the matrices y_Q and y_{R_i}, where each row consisted of the

Table 5.3: The different parameters of the CA-based model presented in Section 5.3.

Parameter	Description	Range	Units
γ_1	Intercept in Eq. (5.15)	[0, 18.56]	[-]
γ_2	Steepness of Eq. (5.15)	[0, 15.86]	[s m^{-1}]
γ_3	Intercept in Eq. (5.16)	[0, 13.20]	[-]
γ_4	Steepness of Eq. (5.16)	[0, 11.31]	[radian^{-1}]
ϵ	Burning time of one cell	[1, 120]	[hours]

simulated quantities corresponding with the parameter sets in Q and R_i, respectively. In the final step, the Sobol' index S_i of each parameter for a certain quantity was estimated using following formula:

$$\widehat{S}_i = \frac{y_Q \cdot y_{R_i} - \widehat{f}_0^2}{y_Q \cdot y_Q - \widehat{f}_0^2} = \frac{\frac{1}{N}\sum_{j=1}^{N} y_Q^{(j)}\, y_{R_i}^{(j)} - \widehat{f}_0^2}{\frac{1}{N}\sum_{j=1}^{N}\left(y_Q^{(j)}\right)^2 - \widehat{f}_0^2}, \tag{5.18}$$

where

$$\widehat{f}_0^2 = \left(\frac{1}{N}\sum_{j=1}^{N} y_Q^{(j)}\right)^2. \tag{5.19}$$

The higher S_i, the more impact the parameter has on the model outcome.

Results and Discussion

Table 5.4: Sobol' indices of the five different parameters for the improved CA-based model presented in Section 5.3 for different quantities.

Measure	Sobol' indices				
	γ_1	γ_2	γ_3	γ_4	ϵ
Average P_i^T	-0.0541	0.0433	**0.5976**	-0.0629	-0.0067
Total burnt area	-0.0324	-0.0492	**0.8423**	-0.0528	0.0141
Circumference of the final perimeter	0.0539	-0.0030	**0.3896**	0.0461	0.0668
$\frac{\text{Circumference}}{\text{Area}}$ of the final perimeter	0.1179	0.1424	0.3027	0.1400	**0.4938**
ROS	-0.0089	-0.0109	**0.7635**	-0.0175	0.0663
Centroid (Horizontal)	0.5340	0.4465	**0.5421**	0.5006	0.4369
Centroid (Vertical)	0.0175	0.0790	**0.9279**	-0.0497	0.0156

Table 5.4 displays the Sobol' indices of each parameter for every quantity. The parameter that impacts a certain quantity the most, is the parameter that has the largest Sobol' index. Here, the parameter γ_3 which determines the intercept in Eq. (5.16), is most likely very decisive for the model output. It has the largest impact on almost every model output, except for the ratio of the cirumference and the area of the simulated perimeter. The latter measure is impacted the most by parameter ϵ. The least important parameters appear to be γ_1 and γ_4.

5.4.2 Local Sensitivity Analysis

The local SA is a tool to assess the impact of a single parameter on the model outcome at different points in time (Sumner, 2010). A main disadvantage of a local SA is that only the impact of one parameter at a time is assessed, thus ignoring the interactions between between different parameters. To investigate these interactions, global SA techniques can be used (Sumner, 2010; van Riel, 2006). The local SA, however, can be useful to assess the effect of small variations of the model inputs/parameters on the model output.

Methods

Here, a local SA will only be done for the most important parameter in the CA-based model presented in Section 5.3, being γ_3 (See Section 5.4.1). According to Sumner (2010), the simplest approach for a local SA is the finite-difference method, which estimates the first-order local sensitivity coefficients using a forward difference approximation:

$$\dot{S}^t_{\gamma_3} = \frac{O(\gamma_3 + \delta\,\gamma_3, t) - O(\gamma_3, t)}{\delta\,\gamma_3}, \tag{5.20}$$

where $O(x, t)$ returns the model output at time t, for a parameter x. The most difficult part of this approach may well be the determination of the given step size δ. The finite-difference approximation is based on the assumption of linearity around the considered point in the parameter space. If δ is too large, this assumption does not hold, but if δ is too small, the difference between the original and perturbated solutions becomes so small that numerical errors can not be ignored. The optimal δ is determined by trial and error (Saltelli et al., 2000), namely where the MAE between the forward and backward difference approximation reaches a minimum (Nopens, 2014):

$$\text{MAE} = \sum_{t=1}^{60} |\dot{S}^t - \breve{S}^t|, \tag{5.21}$$

where

$$\breve{S}^t_{\gamma_3} = \frac{O(\gamma_3, t) - O(\gamma_3 - \delta\,\gamma_3, t)}{\delta\,\gamma_3}, \tag{5.22}$$

where $\breve{S}$ is the backward difference. Here, there is also the issue of stochasticity because the CA-based model has a stochastic transition function, and hence there is already variability

between the outcomes of different simulations with the same parameter values. To decrease the corresponding variance, i runs for every set of parameter values were considered. The more runs, the smaller the variance becomes. However, a trade-off with the running time has to be made. Here, i is chosen in such a way that 99% of the simulations differed less than 5% of the overall mean outcome. The number of iterations i was determined by Algorithm 2.

Algorithm 2: Determining the number of iterations i

Result: The number of iterations i

$s \leftarrow 0$, $i \leftarrow 1$;

$p \leftarrow [9.28103, 7.9311, 6.60188, 5.65268, 15]$;

$T = 1 \times 10000$ zeros matrix ;

while $s = 0$ **do**

  for $j = 1 : 10000$ **do**

    O_1= average burnt area (for every time step) of i simulations with parameter set p;

    O_2= average burnt area (for every time step) of i simulations with parameter set p;

    if $\max(|O_1 - O_2|) \geq 0.05 \frac{O_1+O_2}{2}$ **then**

      $T(j) = 0$

    else

      $T(j) = 1$

    end

  end

  if average$(T) \geq 0.99$ **then**

    $s = 1$

  else

    $i = i + 1$

  end

end

Results and Discussion

The number of iterations, needed per parameter set, was 17. The MAE was calculated for δ ranging from 10^0 to 10^{-10} in steps of 0.1. The result is displayed in Figure 5.4. The value of δ for which the MAE reaches a minimum is probably $10^{-1.6}$, although it is not very clear at which point the variability across simulations starts dominating the MAE. This value of δ was then used to calculate the local sensitivity indices (Eq. (5.20)) at each time step. Both $O(\gamma_3 + \delta\,\gamma_3, t)$ and $O(\gamma_3, t)$ were evaluated on the basis of 100 runs and their means were used to calculate $\dot{S}^t_{\gamma_3}$.

As shown in Figure 5.5, the sensitivity to γ_3 increases with the duration of the simulation. Thus, on the one hand, the longer the required simulated period, the more important an ac-

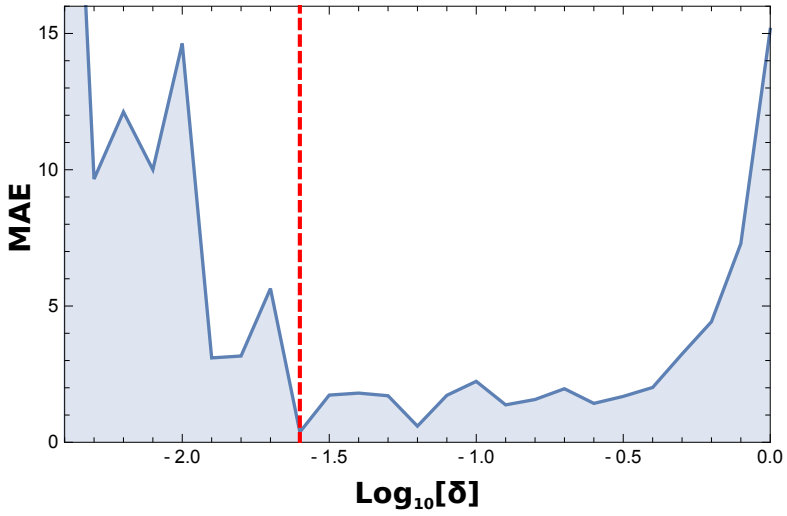

Figure 5.4: The MAE as a function of δ in Eq. (5.20), for the total burnt area. The minimum MAE is indicated by the red vertical line.

curate estimation of the parameter becomes. On the other hand, because of the stochasticity of the model, there is already a considerable variability of the model outcomes for the same parameter set. This gives rise to uncertainty which is then propagated over time.

A small decrease in the sensitivity of γ_3 for P_i^T is observed at 28 hours. This is due to the fact that after this moment, the initial perimeter is completely and instantaneously burn, significantly lowering the total number of burning cells and hence the average P_i^T.

The sensitivity of γ_3 for what concerns the burnt area seems to increase exponentially over time, and this can be explained by the fact that together with the burnt area, also the fire perimeter increases. A larger (burning) perimeter means there is a longer fire front, and hence more cells are able to propagate the wildfire. But, since the cell-to-cell propagation is governed by a certain probability (depending on γ_3), the impact, and hence the sensitivity, to γ_3 will also grow.

The sensitivity to γ_3 for the horizontal and vertical centroids show an awkward curve. It seems that the sensitivity does not only depend on time, but also on the wind speed V. Figure 4.7 (b) shows that 45 hours after the start of the fire, the wind direction changed rapidly from south to west. Thus before this, only the vertical centroid is affected by γ_3 because the wildfire travels south, and afterwards, when the wind blows from the west, only the horizontal centroid is affected.

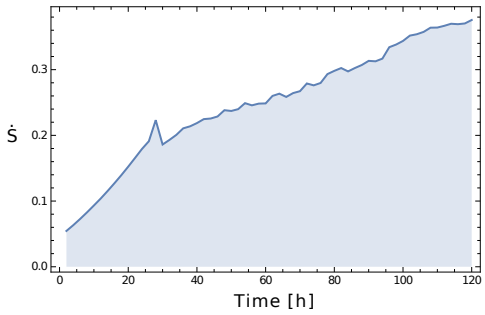

(a) Average P_i^T

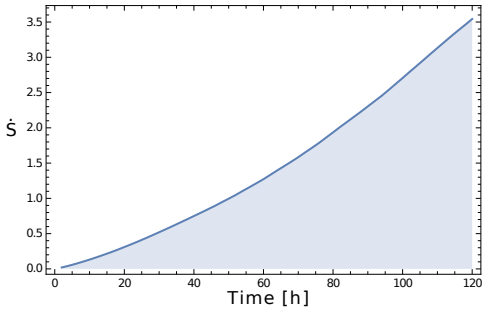

(b) Total Burnt Area

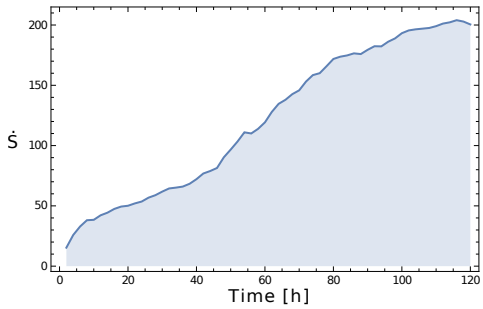

(c) Circumference

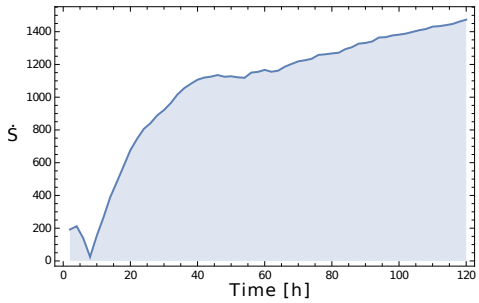

(d) $\frac{\text{Area}}{\text{Circumference}}$

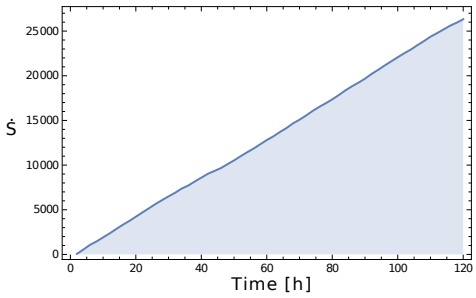

(e) ROS

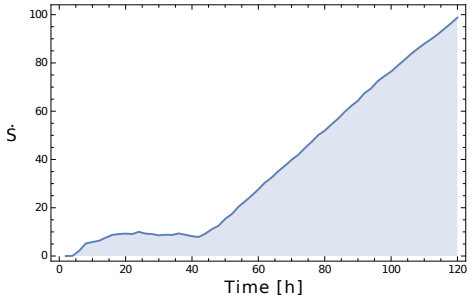

(f) Horizontal centroid

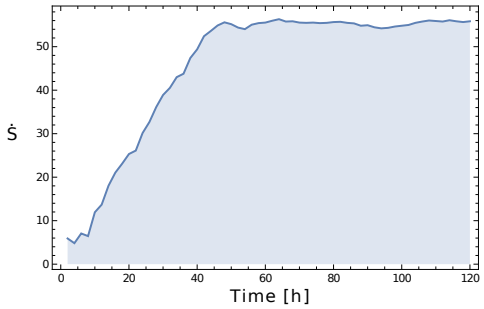

(g) Vertical centroid

Figure 5.5: The local sensitivity indices over time for different model outputs.

CHAPTER 6

Conclusion

In Chapter 3, three simple methods were used to construct wildfire risk maps for the Belgian territory. Although the data were limited – only 261 ignition points were available – several risk maps were consistent with the risk areas, designated by the Directorate-General of the Federal Public Service Internal Affairs in 2011. The most valuable method seems to be the one relying on Bayes' theorem. Although this method did not yield the highest accuracy, it is preferred because of the very small total risk area (6.24%) and the fact that it gives a clear meaning to 'risk'. A small total risk area is preferred, because this allows a more efficient and effective distribution of the available means for wildfire management.

In Chapter 4, FARSITE was successfully used to simulate the wildfire in Baelen, Belgium, 2011. The software proved its capacity for accurate simulations, without any calibration of the model, which was needed for the CA-based models discussed in Chapter 5. In addition to the accuracy, the GUI of FARSITE is very useful to explore different wildfire scenarios with varying weather conditions, ignition locations and firefighting activities. A disadvantage is its high data demand. The time needed for one simulation of five days is about five minutes. Thus, if the necessary data are already available in the correct format, FARSITE can be used for real-time decisions that aid the fire suppression. In the case of Belgium, it is also recommended to design new fuel models for the wildfire sensitive regions, such as the High Fens. In this chapter, the fuel models of Anderson were used, but none of these actually correspond to the vegetation in this area, which consists mainly of bogs and fens.

In Chapter 5, a CA-based model, proposed by Alexandridis et al. (2008), was tested for the wildfire in Baelen, Belgium, 2011. Although the results were quite accurate (91.0%), the model contained inconsistencies in the meaning and definition of the model parameters and structure. A model that overcame these flaws was proposed and tested on the basis of the same case study. The accuracy was slightly lower (90.1%) than the original model, but is compensated by a more consistent model structure. The major disadvantage of both CA-

based models was the time-consuming calibration. A single run of a CA-based model took 75 seconds, while for the sake of a proper model calibration, 30 000 simulations were required. As is the case for FARSITE, these CA-based models also have potential as a tool for real-time decision-making concerning fire suppression. The computing time to simulate five days is very short and the data requirements are low. However, the implementation of different scenarios is rather time-consuming.

Next, both a global and local SA were carried out for the proposed CA-based model. The global SA identified the most and least important parameters. It became clear, for example, that the CA-based model could be simplified by reducing the number of parameters, without compromising the model quality. Such a reduction would also enhance the calibration. The local SA provided other insights in the model, of which the most notable was that the importance of the parameter accuracy increases with the simulation time.

Finally, to enhance the simulations of both FARSITE and the CA-based model, additional data on fire suppression activities are required. This way, the wildfire behavior can be modeled more accurately. This information can be obtained from the local fire fighting corpses that participated in the suppression activities.

Bibliography

Adab, H., Kanniah, K., and Solaimani, K. (2011). GIS-based probability assessment of fire risk in grassland and forested landscapes of Golestan Province, Iran. *International Proceedings of Chemical, Biological and Environmental Engineering*, 19.

Adámek, M., Bobek, P., Hadincová, V., Wild, J., and Kopecký, M. (2015). Forest fires within a temperate landscape: A decadal and millennial perspective from a sandstone region in Central Europe. *Forest Ecology and Management*, 336:81–90.

Alberta Government (2012). How different tree species impact the spread of wildfire. Alberta, Canada.

Albini, F. (1976). Estimating Wildfire Behavior and Effects. General Technical Report INT-30, United States Department of Agriculture Forest Service, Washington, D.C., United States.

Alexander, M. (1985). Estimating the length-to-breadth ratio of elliptical forest fire patterns. In *Proceedings of the 8^{th} Conference on Fire and Forest Meteorology*, pages 278–304, Montana, United States. American Meteorological Society.

Alexander, M. (1988). Help with making crown fire hazard assessments. In: Fischer, W.C. and S.F. Arno (compilers), Protecting people and homes from wildfire in the Interior West. General Technical Report INT-251, United States Department of Agriculture Forest Service, Washington, D.C., United States.

Alexandridis, A., Vakalis, D., Siettos, C., and Bafas, G. (2008). A cellular automata model for forest fire spread prediction: The case of the wildfire that swept through Spetses Island in 1990. *Applied Mathematics and Computation*, 204:191–201.

Amatulli, G., Rodrigues, M., Trombetti, M., and Lovreglio, R. (2006). Assessing long-term fire risk at local scale by means of decision tree technique. *Journal of Geophysical Research*, 111:G04–S05.

ANB (2015). Kalmthoutse Heide. World Wide Web (consulted on October 10, 2015). (http://www.natuurenbos.be/kalmthoutseheide).

Anderson, H. (1982). Aids to Determining Fuel Models for Estimating Fire Behavior. General Technical Report INT-122, United States Department of Agriculture Forest Service, Intermountain Forest and Range Experiment Station, Ogden, United States.

Andreae, M. (2004). Assessment of global emissions from vegetation fires. *International Forest Fire News*, 31:112–121.

Anonymous (1911). Limburg. *Gazet van Antwerpen*. (March 19, 1911).

Anonymous (1913). Dilzen – De Bosbrand. *Gazet van Antwerpen*. (May 4, 1913).

Anonymous (1927). Rothem–Boschbrand. *Gazet van Antwerpen*. (May 12, 1927).

Anonymous (1933). Boschbrand te Elzenborn tengevolge van maneuvers. *Gazet van Antwerpen*. (April 27, 1933).

Anonymous (2011). Hoe snel herstelt heide zich van brand? *Het Belang van Limburg*. (May 27, 2011).

Baker, B. and Copson, E. (2003). *The Mathematical Theory of Huygens' Principle*. American Mathematical Society, Providence, United States. 193pp.

Bedia, J., Herrera, S., Gutiérrez, J. M., Benali, A., Brands, S., Mota, B., and Moreno, J. M. (2015). Global patterns in the sensitivity of burned area to fire-weather: Implications for climate change. *Agricultural and Forest Meteorology*, 214:369 – 379.

Belga (2011). Brand op Hoge Venen onder controle. *Het Nieuwsblad*. (April 26, 2011).

Belgian Federal Government (2013). Statistics Belgium. World Wide Web (consulted on October 28, 2015). (http://statbel.fgov.be/en/statistics/figures/).

Belgian Federal Government (2015). Minister Binnenlandse Zaken & Veiligheid ondertekent samenwerkingsakkoord met Nederland over uitlening blushelikopters. World Wide Web (consulted on October 14, 2015). (http://jambon.belgium.be/nl/minister-binnenlandse-zaken-veiligheid-ondertekent-samenwerkingsakkoord-met-nederland-over-uitlening).

Benndorf, A., Dimitrakopoulos, A., Ganz, D., Goldammer, J., A., H., Kondrashov, L., Manta Nolasco, M., Martínez, R., Mitsopoulos, I., Moore, P., Nikolov, N., Robbins, A., Shields, B., Smith, R., Stocks, B., Truesdale, D., and Vanha-Majamaa, I. (2007). Fire management - global assessment 2006. FAO Forestry Paper 151, Food and agriculture organisation of the United Nations, Rome, Italy.

Berec, L. (2002). Techniques of spatially explicit individual-based models: construction, simulation and mean-field analysis. *Ecological Modelling*, 150:55–81.

Berendsen, H. (2008). *Landschap in Delen: Overzicht van de Geofactoren*. Perspectef Uitgevers.

Bogdos, N. and Manolakos, E. (2013). A tool for simulation and geo-animation of wildfires with fuel editing and hotspot monitoring capabilities. *Environmental Modelling & Software*, 46:182–195.

Boyer, L. (2006). *De wetenschap van het vuur*. de Wetenschappelijke Bibliotheek van Natuurwetenschap & Techniek.

Buis, J. (1985). *Historia Forest: Nederlandse bosgeschiedenis*. HES Uitgevers, 't Goy, the Netherlands.

Burgan, R. (1987). Concepts and interpreted examples in advanced fuel modeling. general Technical Report INT-238, United States Department of Agriculture Forest Service, Washington, D.C., United States.

Byram, G. (1959). Combustion of Forest Fuels. Pages 61-89 In: Davis, K. P., editor. Forest fire: control and use. New York, United States.

Cameron, I. and Hangos, K. (2001). *Process Modelling and Model Analysis*. Academic Press, San Diego, United States. 543pp.

Catry, F., Rego, F., Bacao, F., and Moreira, F. (2009). Modeling and mapping wildfire ignition risk in Portugal. *International Journal of Wildland Fire*, 18:1–11.

Coenen, L. (1999). Natuurreservaten staan droog - Burgemeester waarschuwt voor brandgevaar op Kruiskensberg en Kesselse Heide. *Gazet van Antwerpen*. (July 31, 1999).

Dale, L. (2009). The True Cost of Wildfire in the Western U.S. Western Forestry Leadership Coalition. Colorado, United States.

de Bree, F. (2009). Effecten luchtemissies houtkachels sfeerhaarden en vuurkorven. Buro Blauw B.V. Luchthygiëne, onderzoek en advies, Wageningen, The Netherlands.

De Groot, W. (1998). Interpreting the Canadian Forest Fire Weather Index (FWI) System. In Proceeding of the Fourth Central Region Fire Weather Committee Scientific and Technical Seminar, Edmonton, Alberta, Canada.

de Groot, W., Goldammer, J., Keenan, T., Brady, M., Lynham, T., Justice, C., Csiszar, I., and O'Loughlin, K. (2006). Developing Global Early Warning System for Wildland Fire. In D.X.Viegas, editor, *Proceedings of the 5th International Conference on Forest Fire Research*, Coimbra, Portugal.

del Hoyo, L., Isabel, M., and Vega, F. (2011). Logistic regression models for human-caused wildfire risk estimation: analysing the effect of the spatial accuracy in fire occurrence data. *European Journal of Forest Research*, 130(6):983–996.

den Ouden, J., Muys, B., Mohren, F., and Verheyen, K., editors (2010). *Bosecologie en Bosbeheer*. Acco, Leuven, Belgium.

Directorate-General Civil Security (2012). Brevetten opleiding "natuurbranden" voor Belgische bevelvoerders. World Wide Web (consulted on October 10, 2015). (`http://www.civieleveiligheid.be/nl/news/protection-civile/brevetten-opleiding-natuurbranden-voor-belgische-bevelvoerders`).

Ehlers, E., Moss, C., and Kraft, T. (2006). *Earth System Science in the Anthropocene: Emerging Issues and Problems*. Springer Science & Business Media, New York, United States. 284pp.

Encinas, H., White, S., del Rey, A., and Sánchez, G. (2007). Modelling forest fire spread using hexagonal cellular automata. *Applied Mathematical Modelling*, 31:1213–1227.

Environmental Protection Agency (2015). Corine Land Cover Mapping. World Wide Web (consulted on October 16, 2015). (`http://www.epa.ie/soilandbiodiversity/soils/land/corine/#.ViY55kvDpTB`).

EU Joint Research Center (2002). Pilot projects on forest fires. World Wide Web (consulted October 20, 2015). (`http://natural-hazards.aris.sai.jrc.it/fires/`).

FAO (2003). Outcomes of the International Wildland Fire Summit Sydney, Australia, 8 October 2003. *International Forest Fire News*, 29.

Federal Public Service Internal Affairs (2013). Nationaal Actieplan Natuurbranden. Brussels, Belgium.

Finney, M. (1999). Spatial Modeling of Post-Frontal Fire Behavior. Final Report RMRS-99557-RJVA. Systems for Environmental Management, Missoula, United States.

Finney, M. (2004). FARSITE: Fire Area Simulator - Model Development and Evaluation. Research Paper RMRS-RP-4, United States Department of Agriculture, Forest Service, Rocky Mountain Research Station, Fort Collins, United States.

Fiorucci, P., Gaetani, F., and Minciardi, R. (2004). An integrated system for static and dynamic risk evaluation at a national level. In *Proceedings of the 2nd International Symposium on Fire Economics, Planning and Policy: A Global View*, Perugia, Italy.

Forestry Canada Fire Danger Group (1992). Development and structure of the Canadian Forest Fire Behavior Prediction System. Information report ST-X-3, Forestry Canada: Science and Sustainable Development Directorate, Hull, Canada.

Ganguly, N., Sikdar, B. K., Deutsch, A., Canright, G., and Chaudhuri, P. P. (2003). A Survey on Cellular Automata. Technical report, Centre for High Performance Computing, Dresden University of Technology, Dresden, Germany.

Ganteaume, A., Camia, A., Jappiot, M., San-Miguel-Ayanz, J., Long-Fournel, M., and Lampin, C. (2013). A review of the main driving factors of forest fire ignition over Europe. *Environmental Management*, 51:651–662.

Ganz, D., Fisher, R., and Moore, P. (2003). Further defining community-based fire management: Critical elements and rapid appraisal tools. In *3rd International Wildland Fire Conference, October*, Sydney, Australia.

Ghisu, T., Bachisio, A., Pellizzaro, G., and Pierpaolo, D. (2015). An optimal cellular automata algorithm for simulating wildfire spread. *Environmental Modelling & Software*, 71:1–14.

Global Fire Monitoring Center (2006). Fire management: Review of international cooperation. Technical report, Food and Agriculture Organization of the United Nations, Rome, Italy.

Global Fire Monitoring Center (2015a). Outline of fire danger products in the global early warning system for wildland fire. World Wide Web (consulted on October 2, 2015). (`http://www.fire.uni-freiburg.de/gwfews/index.html`).

Global Fire Monitoring Center (2015b). Overview of the global fire early warning system. World Wide Web (consulted on October 2, 2015). (`http://www.fire.uni-freiburg.de/gwfews/overview.html`).

Goldammer, J., editor (1990). *Fire in the Tropical Biota*. Springer-Verlag Berlin Heidelberg, New York, United States.

Gorte, R. (2013). The rising cost of wildfire protection. Published Online. Headwater Economics,Bozeman,United States.

Green, D. and Gill, A. (1989). Interactive bushfire simulation. In Green, D. and Gill, A., editors, *Proceedings of the 8th Biennal Conference and Bushfire Dynamics Workshop*, pages 573–578.

Hermy, M., de Blust, G., and Slootmaekers, M. (2004). *Natuurbeheer*. Davidsfonds (in cooperation with Argus vzw, Natuurpunt vzw), Leuven, Belgium.

Hosmer, D. and Lemeshow, S. (1989). *Applied Logistic Regression*. John Wiley & Sons, New York, United States.

Jacobs, A. (2013). Kolonisatie van afgebrande heide door grondbroedende vogels: Een studie op de Kalmthoutse Heide. Antwerp, Belgium.

Johnson, E. and Miyanishi, K., editors (2001). *Forest Fires: Behavior and Ecological Effects*. Academic Press, San Diego, United States.

Johnston, P., Milne, G., and Klemitz, D. (2005). Overview of bushfire spread simulation systems. Project progress report, School of Computer Science and Software Engineering, The University of Western Australia, Nedlands, Australia.

Karafyllidis, I. and Thanailakis, A. (1997). A model for predicting forest fire spread using cellullar automata. *Ecological Modelling*, 99:87–97.

Keeley, J., Pausas, J., Rundel, P., Bond, W., and Bradstock, R. (2011). Fire as an evolutionary pressure shaping plant traits. *Trends in Plant Science*, 16:406–411.

Kessel, S. and Beck, J., editors (1991). *Development and implementation of forest fire modeling and decision support systems in Australia. GIS/LIS*, volume 2, Atlanta, United States.

Lea-Langton, A., Baeza-Romero, M., Boman, G., Brooks, B., Wilson, A., Atika, F., Bartle, K., Jones, J., and Williams, A. (2015). A study of smoke formation from wood combustion. *Fuel Processing Technology*, 137:327–332.

Legendre, P. and Legendre, L. (1998). *Numerical Ecology*. Elsevier Science BV, Amsterdam, The Netherlands, 2nd edition.

Lilburne, L. and Tarantola, S. (2009). Sensitivity analysis of spatial models. *International Journal of Geographical Information Science*, 23(2):151–168.

Loos, J. (2011). Oernatuur tussen Ardennen en Eifel: De Hoge Venen. Boutersem, Belgium.

Maes, M. (1999). Nieuwe plannen bosbrand getest. *Het Belang van Limburg*. (April 24, 1999).

Mandel, J., L.S., B., Beezley, J., Coen, J., C.C., D., Kim, M., and Vodacek (2008). A wildland fire model with data assimilation. *Mathematics and Computers in Simulation*, 79(3):584–606.

Martinez, J., Chuvieco, E., Martiín, P., and González-Cabán, A. (2008). Proceedings of the Second International Symposium on Fire Economics, Planning and Policy: A Global View: Estimation of Risk Factors of Human Ignition of Fires in Spain by Means of Logistic Regression. General technical Report PSW-GTR-208, United States Department of Agriculture, Forest Service, Pacific Southwest Research Station, Albany, United States.

Massada, A., Syphard, A., Stewart, S., and Radeloff, V. (2012). Wildfire ignition-distribution modelling: A comparative study in the Huron-Manistee National Forest, Michigan, USA. *International Journal of Wildland Fire*, 22(2):174–183.

McDonald, J. (2014). *Handbook of Biological Statistics*. Sparky House Publishing, Baltimore, Maryland, 3rd edition.

McKay, M., Beckman, R., and Conover, W. (1979). A comparison of three methods for selecting values of input variables in the analysis of output from a computer code. *Technometrics*, 21(2):239–245.

Moore, G. (1969). Automatic scanning and computer processes for the quantitative analysis of micrographs and equivalent subjects. *Pattern Recognition: Pictorial Pattern Recognition*, 1:275–326.

Moritz, M. (2012). Wildfire ignite debate on global warming. *Nature*, 487:273.

Muzy, A., Innocenti, E., Aiello, A., and Santucci, J. (2005). Specification of Discrete Event Models for Fire Spreading. *Simulation*, 81(2):103–117.

National Association of State Foresters (2015). Wildfire Prevention. World Wide Web (consulted on October 6, 2015). (`http://stateforesters.org/smokey-bear/wildfire-prevention`).

National Geographic Institute (2013). Digitale gegevens: digitaal terreinmodel. World Wide Web (consulted on October 28, 2015). (`http://www.ngi.be/NL/NL1-5-5.shtm`).

National Park Service (2008). The Yellowstone fires of 1988. United States Department of the Interior.

National Wildfire Coordinating Group (2002). *Gaining A Basic Understanding of the National Fire Danger Rating System*. National Office of Fire and Aviation, Bureau of Land Management, National Interagency Fire Center, Boise, United States.

Nopens, I. (2014). *Modelleren en Simuleren van Biosystemen*. Ghent University, Gent, Belgium.

Nunes, L., Matias, J., and Catalão, J. (2016). Biomass combustion systems: A review on the physical and chemical properties of the ashes. *Renewable and Sustainable Energy Reviews*, 53:235–242.

Papadopoulos, G. (2011). A Comparative Review on Wildfire Simulators. *IEEE Systems Journal*, 5(2):233–243.

Pastor, E., Zárate, L., Planas, E., and Arnaldos, J. (2003). Mathematical models and calculation systems for the study of wildland fire behaviour. *Progress in Energy and Combustion Science*, 29:139–153.

Perona, G. and Brebbia, C., editors (2010). *Modelling, Monitoring and Management of Forest Fires II*. WIT Press, Southampton, United Kingdom.

Peters, N. (2010). Combustion Theory. Rheinisch-Westfälische Technische Hochschule Aachen, Aachen, Germany.

Peterson, S., Morais, M., Carlson, J., Dennison, P., Roberts, D., Moritz, M., and Weise, D. (2009). Using HFire for Spatial ModeModel of Fire in Shrublands. General Technical Report PSW-RP-259, United States Department of Agriculture Forest Service. Pacific Southwest Research Station, Fresno, United States.

Preisler, H., Brillinger, D., Burgan, R., and Benoit, J. (2004). Probability based models for estimation of wildfire risk. *International Journal of Wildland Fire*, 13:133–142.

Richards, G. (1990). An elliptical growth model of forest fire fronts and its numerical solution. *International Journal for Numerical Methods in Engineering*, 30:1163–1179.

Richards, G. (1995). A general mathematical framework for modeling two-dimensional wildland fire spread. *International Journal of Wildland Fire*, 5(2):63–72.

Rodrigues, M. and de la Riva, J. (2014). An insight into machine-learning algorithms to model human-caused wildfire occurence. *Environmental Modelling & Software*, 57:192–201.

Rothermel, R. (1972). A mathematical model for predicting fire spread in wildland fuels. Research Paper INT-115, United States Department of Agriculture Forest Service, Intermountain Forest and Range Experiment Station, Fort Collins, United States.

Rothermel, R. (1991). Predicting behavior and size of crown fires in the north Rocky Mountains. Research Paper INT-483, United States Department of Agriculture, Washington, D.C., United States.

Saltelli, A., Chan, K., and Scott, E. (2000). *Sensitivity Analysis*. Wiley, Chichester, United Kingdom.

Saltelli, A., Tarantola, S., Campologno, F., and Ratto, M. (2004). *Sensitivity Analysis in Practice. A guide to Assessing Scientific Models*. John Wiley, Chichester, United Kingdom.

San-Miguel-Ayanz, J. and Camia, A. (2012). The European Forest Fire Information System (EFFIS): Towards a Global Wildfire Information System (GWIS). European Union Joint Research Center, Ispra, Italy.

San-Miguel-Ayanz, J., Schulte, E., Schmuck, G., Camia, A., Strobl, P., Liberta, G., Giovando, C., Boca, R., Sedano, F., Kempeneers, P., McInerney, D., Withmore, C., Santos de Oliveira, S., Rodrigues, M., Durrant, T., Corti, P., Oehler, F., Vilar, L., and Amatulli, G. (2012). Comprehensive Monitoring of Wildfires in Europe: The European Forest Fire Information System (EFFIS). Technical report, European Commission, Joint Research Centre, Ispra, Italy.

Schiff, J. (2008). *Cellular Automata. A Discrete View of the World*. John Wiley & Sons, Hoboken, United States.

Schmitz, A., Oumara Fall, A., and Rouchiche, S. (1996). *Contrôle et utilisation du feu en zones arides et subhumides africaines*. Food and Agriculture Organization of the United Nations, Rome, Italy.

Schmuck, G., San-Miguel-Ayanz, J., Camia, A., Durrant, T., Boca, R., Libertà, G., Petroliagkis, T., Di Leo, M., Rodrigues, D., Boccacci, F., and Schulte, E. (2014). Forest Fires in Europe Middle East and North Africa 2013. Technical report, European Comission, Joint Research Centre Institute for Environment and Sustainability, Ispra, Italy. 107pp.

Schmuck, G., San-Miguel-Ayanz, J., Camia, A., Durrant, T., Boca, R., Withmore, C., Libertà, G., Corti, P., and Schulte, E. (2012). Forest Fires in Europe, Middle East and North Africa 2011. Technical report, European Comission, Joint Research Centre Institute for Environment and Sustainability, Ispra, Italy. 108pp.

Scholliers, P. and Zamagni, V., editors (1995). *Labour's Reward: Real Wages and Economic Change in 19^{th}- and 20^{th}-century Europe*. Edwar Elgar Publishing, Cheltenham, United Kingdom.

Scott, J. and Reinhardt, E. (2001). Assessing crown fire potential by linking model of surface and crown fire behavior. Research Paper RMRS-RP-29, United States Department of Agriculture Forest Service, Rocky Mountain Research Station, Fort Collins, United States.

Sobol', I. (1993). Sensitivity estimates for nonlinear mathematical models. *Mathematical Modeling and Computational Experiment*, 1:407–414.

Stevens, M., Demolder, H., Jacobs, S., Michels, Schneiders, A., Simoens, I., Spanhove, T., Van Gossum, P., Van Reeth, W., and Peymen (2015). Flanders regional ecosystem assessment: State and trends of ecosystems and their services in flanders. synthesis. communications of the research institute for nature and forest. M.2015.7842756, Research Institute for Nature and Forest, Anderlecht, Belgium.

Sumner, T. (2010). *Sensitivity Analysis in System Biology Modelling and its Application to a Multi-scale Model of Blood Glucose Homeostasis*. PhD thesis, Centre for Mathematics and Physics in the Life Sciences and Experimental Biology, University College London.

Sun, T., L., Z., Chen, W., Tang, X., and Qin, Q. (2013). Mountains forest fire spread simulator based on geo-cellular automaton combined with wang zhengfei velocity model. *IEEE Journal of Selected Topics in Applied Earth Observations and Remote Sensing*, 6(4):1971–1987.

Tarantola, S., Nardo, M., Saisana, M., and Gatelli, D. (2006). A new estimator for sensitivity analysis of model output: an application to the e-business readiness composite indicator. *Reliability Engineering and System Safety*, 91:1135–1141.

Timperman, B. and Willekens, G. (1999). Brandgevaar dreigt in bossen - Snel ingrijpen van Geelse, Molse en Grobbendonkse spuitgasten voorkomt erger. *Gazet van Antwerpen.* (July 30, 1999).

Trunfio, G., D'Ambrosio, D., Rongo, R., Spataro, W., and Di Gregorio, S. (2011). A new algorithm for simulating wildfire spread through cellular automata. *ACM Transactions on Modelling and Computer Simulation*, 22(1).

University of Freiburg (2015). Regression Models as a Tool in Medical Research - International School of Quantitative Research. World Wide Web (consulted on January 14, 2016). (`http://www.isqr.uni-freiburg.de/reginmed2011/logistic.pdf`).

Van Eeckhoutte, B. (2012). Jaarverslag 2011. Transnational Park De Zoom-Kalmthoutse Heide, Kalmthout, Belgium.

van Riel (2006). Dynamic modelling and analysis of biochemical networks: mechanism-based models and model-based experiments. *Briefings in Bioinformatics*, 7(4):364–374.

Van Wagner, C. (1977). Conditions for the start and spread of crownfire. *Canadian Journal of Forest Research*, 7:23–34.

Van Wagner, C. (1987). Development and Structure of the Canadian Forest Fire Weather Index System. Technical Report 35, Petawawa National Forestry Institute, Buchanan, Canada.

Van Wagner, C. (1989). Prediction of crown fire behaviour in conifer stands. In *Proceedings of the 10th Conference on Fire and Forest Meteorology.*, Ottawa, Canada.

Van Wagner, C. (1993). Prediction of crown fire behaviour in two stands of jack pine. *Canadian Journal of Forest Research*, 23:442–449.

Verboom, W., Mulder, M., Bruijnooge, M., R., H., van Baardwijk, M., and Verhoogt, M. (2013). *Landelijke Risico Index Natuurbranden.* Landelijk Informatieknooppunt Natuurbranden, Arnhem, The Netherlands, 2nd edition.

von Neumann, J. (1966). *Theory of Self-Reproducing Automata*. University of Illinois Press, Urbana, United States.

Walloon Government and the European Commission (2015). Programme Wallon de Développement Rural 2007-2013.

Whelan, R. (1995). *The Ecology of Fire*. Cambridge University Press, New York, United States. 343pp.

Wijdeven, S., Schelhaas, M., Olsthoorn, A., Bijlsma, R., and Kramer, K. (2006). Bosbrand en terreinbeheer - een verkenning. Technical report, Alterra, Wageningen, the Netherlands.

Wilson, R. (1980). Reformulation of forest fire spread equations in SI units. Research Note INT-292, United States Department of Agriculture Forest Service, Intermountain Forest & Range Experiment Station, Ogden, United States.

Worland, J. (2015). This technology could help predict where wildfires strike next. World Wide Web (consulted on April 17, 2016). (`http://time.com/3992447/technology-wildfire-predictions/`).

Wyckmans, M., Van Eeckhoutte, B., de Blust, G., Vandamme, I., Vermeersch, G., Verpraet, P., Willaert, E., and Lambeets, K. (2011). Zwarte dagen voor het Grenspark: de vuurzee in ons Grenspark. *Wissels*, 49.

Yassemi, S., Dragićević, S., and Schmidt, M. (2007). Design and implementation of an integrated GIS-based cellular automata model to characyerize forest fire behaviour. *Ecological Modelling*, 210:71–84.

Ziel, R. (2014). Fire Behavior Field Reference Guide. World Wide Web (consulted November 4, 2015). (`http://www.fbfrg.org/fuel-moisture/1-hour-moisture-content`).

APPENDIX A

Dutch Risk Index for Wildfires

Table A.1: Parameters used in the Dutch Risk Index for Wildfires (RIN).

TERRAIN CHARACTERISTICS			
Parameter	**Category**		**Indexation**
1. Vegetation	Not inflammable	Water, pasture, farmland Land dunes	0
	Barely inflammable	Deciduous forest	20
	Slightly inflammable	Mixed forest	30
	Inflammable	Heathland Grassland & *Rumex spp.* Fen Reed land *Molinia caerulea* Swamps *Ammophila arenaria* Lichenes	50
	Highly inflammable	Mixed coniferous forest and heathland	60
	Very highly inflammable	Open coniferous forest *Hippophae rhamnoides*	80
	Extremely inflammable	Closed coniferous forest *Rhododendron spp.* *Juniperus communis* shrubs	100
2. Slope		0%	0
		1-5%	5
		5-10%	10
		>10%	40
3. Spreading capacity	Zero	< 12.5%	0
	Low	12.5% < Spreading capacity < 37.5%	10
	Intermediate	37.5% < Spreading capacity < 62.5%	20
	High	> 62.5%	40
4. Proximity of Valuable Objects & Vulnerable Infrastructure		>2km	0
		1-2km	5
		<1km	10
5. Proximity of Hazardous Substances		>2km	0
		1-2km	5
		<1km	20

TERRAIN CHARACTERISTICS (continued)			
Parameter	**Category**		**Indexation**
6. Ecological Value	Low		-40
	Moderate		0
	High		40
PRESENCE OF VISITORS/INHABITANTS			
7. Visitors/Permanent Inhabitants	None	0 inh/km^2	0
	Scarce	1-100 inh/km^2	10
	Intermediate	100-500 inh/km^2	20
	Abundant	>500 inh/km^2	40
8. Camping guests within	None	0	0
radius of 1km	Scarce	0-200	40
	Intermediate	200-1000	60
	Abundant	>1000	100
9. Day Trippers & Beach	None	0 inh/km^2	0
Guests	Scarce	<100 inh/km^2	5
	Intermediate	100-500 inh/km^2	10
	Abundant	>500 inh/km^2	20
WILDFIRE PREVENTION & PREPARATIONS			
10. Distance to Primary Water		<1km	20
Extraction		1-2km	40
		>2km	60
11. Distance to Secondary/Tertiary		<1km	10
Water Extraction		1-3km	20
		>3km	40
12. Arrival Time 1st		<10min	20
Suppression Vehicle		10-15min	40
		>15min	80
13. Arrival Time 1st Peleton of		<20min	40
Suppression Vehicle		20-25min	20
		>25min	40
14. Probability of Fast Detection	High		5
	Intermediate		10
	Low		20
15. Escape Routes		Area not accessible for public	0
		>2	5
		2	10
		1	20
16. Knowledge of Terrain of Fire	Good		10
Fighting Teams	Intermediate		20
	Bad		40
17. Road Quality	Optimal	Paved	-40
	Sufficient	Partially paved	0
	Mediocre	Not paved	20
	Bad	No roads	40

APPENDIX B

FARSITE (Baelen, BE)

Table B.1: Fuel models of Anderson (Anderson, 1982; Rothermel, 1972; Albini, 1976)

Fuel Model	Typical Fuel Complex	Description
Group 1	***Grass and Grass-Dominated***	
1	Short grass	Fire spread through grasses and herbaceous fuels, low prevalence of shrub or timber. Typically grassland, savanna and tundra.
2	Timber (grass and understory)	surface fire, spread through fine, herbaceous fuels, litter and dead wood contribute to intensity. Occurs in open shrub lands, pine stands and scrub oak stands.
3	Tall grass	Most intense fire of the group. Wind causes high rate of spread. More or less one third of the plants are dead.
Group 2	***Chaparral and Shrub Fields***	
4	Chaparral	Almost continuous secondary over story, fire spreads fast through foliage and living and dead crown material.
5	Brush	generally surface fire that consume shrubs, grasses and forbs. young shrubs and little dead biomass, hence low fire intensity.
6	Dormant brush hardwood slash	Shrub layer more flammable than model 5. Fire drops through the ground if U<=3.6m s^{-1}.
7	Southern rough	Fire burns shrub and surface layers. Also occurs at higher dead fuel moisture because of flammable foliage.
Group 3	***Timber Litter***	
8	Closed timber litter	Low intensity ground fire under severe weather conditions. Typically closed, short needled conifer or hardwood stands.
9	Hardwood litter	Faster and higher fire than model 8. In long-needled conifer. and hardwood stands
10	Timber (litter and understory)	Larger intensity than models 8 and 9, ground and surface fires. Lots of dead material on forest floor. For example in insect infested stands.
Group 4	***Slash***	
11	Light logging slash	Fires consume herbaceous material and slash from exploitation. Typically in conifer stands where thinning or partial cuts took place.
12	Medium logging slash	Fire spreads rapidly through slash. Slash diameter <7.6cm and mass <35 tons per acre. Typically in heavily thinned or partially cut stands.
13	Heavy logging slash	Fire spreads rapidly, continuous slash layer that may exceed 200 tons per acre. Typically in clear cuts and partial cuts in mature stands.

`M` and `D` refer to the month and day. `P` is the daily amount of precipitation [mm]. `Hr1` and `Hr2` (hour 1 & 2) [0-2400] correspond respectively to the time of the minimum and maximum

Table B.2: The FARSITE Weather file (.WRT)

M	D	P	Hr1	Hr2	T1	T2	Hu1	Hu2	E	rt1	rt2
METRIC											
04	26	0	0312	1512	8	16	75	55	600		
04	27	0	0312	0912	7	10	80	78	600		
04	28	0	0312	1512	8	14	99	55	600		
04	29	0	0012	1512	8	18	95	40	600		
04	30	0	0312	1212	10	17	78	45	600		
05	01	0	0312	1512	8	16	68	50	600		
05	02	0	0312	1212	6	13	63	45	600		
05	03	0	0312	1512	2	11	95	43	600		
05	04	0	0312	1512	1	11	70	40	600		

recorded temperature (T1 & T2 in °C). Hu1 and Hu2 are the minimum and maximum recorded humidity [%]. E, the elevation, is the average height above sea level [m] and the perception duration is indicated by r1 (beginning of the rain) and r2 (ending). Note that the software can only handle one period of rain per day. The last two columns are blank as a consequence of the absence of rain in the period between April 26 and May 4, 2011.

Table B.3: The FARSITE Wind file (.WND)

M	D	Hr	v	D	CC
METRIC					
04	26	0012	3	173	0
04	26	1212	5	235	0
04	27	0012	5	260	0
04	27	1212	4	289	0
04	28	0012	2	282	0
04	28	1212	3	176	0
04	29	0012	2	193	0
04	29	1212	8	182	0
04	30	0012	5	178	0
04	30	1212	8	184	0
05	01	0012	5	185	0
05	01	1212	6	183	0
05	02	0012	4	180	0
05	02	1212	4	217	0
05	03	0012	6	220	0
05	03	1212	5	212	0
05	04	0012	2	192	0
05	04	1212	2	276	0

This file specifies the Speed v [km/h] and Direction D [degree] and cloud cover CC [%] at a certain moment. For the entire region, only one value for each parameter is provided.
FM refers to the fuel model that is specified. 1H, 10H and 100H refer to the moisture content after 1, 10 and 100 hours. The moisture content can be estimated with Table B.5. LH is the

Table B.4: The FARSITE Initial Fuel Moisture file (.FMS)

FM	1H	10H	100H	LH	LW
METRIC					
1	9	7	10	50	75
5	9	7	10	75	100
6	9	7	10	50	100
8	9	7	10	75	100
9	9	7	10	50	75

moisture content of 'live herbaceous' fuels, `LW` of 'live woody' fuels. They are assumed to be constant (according to the FARSITE4 online help).

Table B.5: Reference Fuel Moisture. The dry-bulb temperature is the temperature of the air, measured with a thermometer that is shielded from solar radiation (Ziel, 2014).

Dry Bulb	Relative Humidity (%)																			
Temp (°C)	<4	<9	<14	<19	<24	<29	<34	<39	<44	<49	<54	<59	<64	<69	<74	<79	<84	<89	<94	<99	<100
-12 – -2	1	2	2	3	4	5	5	6	7	8	8	8	9	9	10	11	12	12	13	13	14
-1 – 9	1	2	2	3	4	5	5	6	7	7	7	8	9	9	10	10	11	12	13	13	13
10 – 20	1	2	2	3	4	5	5	6	6	7	7	8	8	9	9	10	11	12	12	12	13
21 – 31	1	1	2	2	3	4	5	5	6	7	7	8	8	8	9	10	10	11	12	12	13
32 – 43	1	1	2	2	3	4	4	5	6	7	7	8	8	8	9	10	10	11	12	12	13
>43	1	1	2	2	3	4	4	5	6	7	7	8	8	8	9	10	10	11	12	12	12

The initial air temperature was 10°C and the initial relative air humidity was 60%, thus according to Table B.5, the moisture after 1 hour is more or less 9%. The temperature after 10 hours was 15°C and the air humidity at that moment was 50%, so the fuel moisture is 7%. The temperature after 100 hours was 10°C and the air humidity at this moment was 78%, hence the fuel moisture is 10%